

Aus dem Zentrum für Infektiologie der Universität Heidelberg  
(Zentrumssprecher: Prof. Dr. med. Dr. h. c. Hans-Georg Kräusslich)

Abteilung für Virologie

## Imaging of MLV cDNA dynamics and replication in living cells

Inauguraldissertation

Zur Erlangung des *Doctor scientiarum humanarum* (*Dr. sc. hum.*)

an der

Medizinischen Fakultät Heidelberg

der

Ruprecht-Karls-Universität

vorgelegt von

Tamara Naumoska

aus

Tetovo, Nordmazedonien

2023

Dekan: Herr Prof. Dr. med. Dr. h.c. Hans-Georg Kräusslich

Doktorvater: Herr Prof. Dr. med. Dr. h.c. Hans-Georg Kräusslich

# Contents

<b>I</b>	<b>List of Abbreviation</b>	<b>VII</b>
<b>II</b>	<b>List of Figures</b>	<b>XI</b>
<b>III</b>	<b>List of Tables</b>	<b>XIII</b>
<b>1</b>	<b>Introduction</b>	<b>1</b>
1.1	MLV biology	1
1.2	The genome and production process of MLV particles	2
1.3	The architecture of MLV and HIV-1 capsids	5
1.4	MLV replication cycle	7
1.4.1	Cell entry and transport	9
1.4.2	Reverse transcription	11
1.4.3	Nuclear entry	15
1.4.4	Uncoating	17
1.4.5	Integration	20
1.5	Host cell protein interaction with viral DNA and capsid	23
1.6	Experimental systems for visualization of retroviral DNA	25
1.7	Aim of the thesis	28
<b>2</b>	<b>Materials and Methods</b>	<b>30</b>
2.1	Generation of Plasmids	37
2.1.1	pNCA ANCH and derivatives	37
2.1.2	pMLVgag-pol-IN.SNAP	37
2.1.3	pWPI eBFP.mLMNB1	38
2.2	Cell and tissue culture	38
2.2.1	Isolation of MEF cells and their immortalization	38
2.2.2	Lentiviral vector transduction	39
2.3	Virus particle production and quantification of titer	39
2.3.1	Viral production	39
2.3.2	SG-PERT assay	40

2.3.3	Infectivity assays	40
2.3.4	Immunoblotting	41
2.4	Endogenous reverse transcription (ERT) reaction	41
2.5	Infection, treatment and staining of cells	42
2.5.1	Infection of MEFs and SC-1 with wild-type and minus glycoGag variant	42
2.5.2	Infection of eGFP.OR3 eBFP2.mLMNB1 expressing cells with ANCH viruses	42
2.5.3	Cell division, RT, and integration inhibitors	43
2.5.4	Fixation, extraction and IF staining	43
2.5.5	Labeling of viral cDNA with modified nucleosides in cells	43
2.5.6	DNA FISH staining	44
2.6	Imaging systems	45
2.6.1	Spinning disk confocal microscopy	45
2.6.2	Live imaging	45
2.7	Image analysis and visualization	46
2.7.1	Noise filter, deconvolution, and signal restoration software application in image processing	46
2.7.2	Manual analysis of eGFP.OR3 signals with Fiji	46
2.7.3	Labeling efficiency of viral DNA with EdUTP on immobilized particles with Icy	47
2.7.4	Semi-automated 3D quantification with Imaris	47
2.7.5	Data visualization and statistical analysis	48
2.8	Quantification of RT products using ddPCR	48
<b>3</b>	<b>Results</b>	<b>49</b>
3.1	Experimental system establishment for characterization of infection with MLV wild-type and destabilized capsid variants	49
3.1.1	Assay establishment for virus production, characterization of viral titer and infectivity of MLV	49
3.1.2	GlycoGag is an infectivity factor conditional on the target cell type	54
3.2	Establishment of experimental systems for visualization of MLV DNA	55
3.2.1	Visualization of MLV DNA using hybridizing fluorescently labeled probes	56
3.2.2	Visualization of MLV DNA using metabolic labeling with cell-permeable modified nucleosides	58

3.2.3	Adapting a genetically encoded DNA-binding protein labeling system for visualization of MLV DNA	61
3.2.4	Validation of the ANCHOR system as a suitable tool for MLV DNA visualization in murine infected cells	62
3.3	Visualization of MLV cDNA and interactions with viral and host cell proteins in fixed and living conditions	65
3.3.1	Visualization of MLV cDNA using the ANCHOR system in murine cells	65
3.3.2	Visualization of cytoplasmic OR3 signals in infected MLV cells	66
3.3.3	Comparison of lentiviral and retroviral location of OR3 signals in infected murine cells	67
3.3.4	Nuclear entry of MLV cDNA is blocked upon aphidicolin treatment	68
3.3.5	MLV cDNA accessible for protein-binding does not associate with CA and/or p12 proteins in the nucleus	72
3.3.6	IN. FP is associated with a subset of MLV cDNA foci in the nucleus	76
3.3.7	Real-time visualization of MLV DNA in infected living cells	79
3.3.8	Tracking up to three generations of infected living daughter cells with eBFP2.mLMNB1 as a division marker	82
3.3.9	Cellular division is necessary for visualization of viral cDNA in the nucleus of MLV ANCHOR infected cells	84
3.3.10	Characterization of nuclear OR3 foci dynamics and longevity in living MLV infected cells	87
3.3.11	The ANCHOR system enables detection and tracking of OR3 signal through division events and for up to three generations of infected daughter cells	89
3.3.12	The nuclear viral cDNA interacts with cGAS in the presence and/or absence of TREX1	91
3.3.13	Association of $\gamma$ H2AX with viral DNA in retroviral and lentiviral infected cells	92
<b>4</b>	<b>Discussion</b>	<b>95</b>
4.1	The spatio-temporal dynamics of MLV reverse transcription	96
4.2	Metabolic labeling of MLV genomes is hampered by nucleotide incorporation into host chromatin	98
4.3	Subviral particles with a full subset of CA molecules enter the nucleus during mitosis	100
4.4	MLV likely uncoats in the nucleus	101

4.5	IN.FP remains associated with a subset of uncoated MLV cDNA molecules	105
4.6	Visualization of integrated and non-integrated MLV cDNA in dividing cells	106
4.7	Protection of MLV nucleic acids by capsid is important in immunocompetent cells.	107
4.8	Nuclear environment and host cell factors interacting with MLV cDNA after the uncoating event	109
4.9	Outlook	111
4.10	Conclusion	112
5	Summary	114
6	Zusammenfassung	116
7	Reference List	118
8	Personal contribution to data acquisition / Assessment and Personal Publications	137
9	Appendix	139
10	Acknowledgments	141
11	Eidesstattliche Versicherung (Affidavit)	143

# I List of Abbreviation

AFP	Autofluorescent protein
Alexa647-aha	dUTP attached to Alexa647 Fluor by 5-aminohexylacrylamid
dUTP	linker
ANCHOR	System for dsDNA visualization based on ParB-parS
APC	Aphidicolin
APOBEC3	Apolipoprotein B editing complex
AZT	Azidothymidine
BET	Bromo- and extraterminal domain
BIV	Bovine immunodeficiency virus
BLA	Blasticidine
CA	Capsid protein
Capsid	The assembled spiral core consisting of CA
CARE	Content-aware image restoration software
CBS	Chromatin-binding sequence
CCD	Catalytic core domain of integrase
CCR5	C-C chemokine receptor type 5
cDNA	Copy DNA
cGAMP	Cyclic guanosine monophosphate–adenosine monophosphate
cGAS	Cyclic GMP-AMP synthase
ChIP	Chromatin ImmunoPrecipitation assay
CLEM	Correlative light electron microscopy
CLEM-ET	CLEM and electron tomography
CPSF6	Cleavage and polyadenylation specificity factor 6
cryo-ET	Cryoelectron tomography
CTD	C-terminal domain
CuAAc	Copper-catalyzed azide-alkyne cycloadditions
CXCR4	C-X-C Motif Chemokine Receptor 4
CypA	Cyclophilin A
CytoC	Cytochrome C
ddPCR	Droplet digital PCR
DDR	DNA damage response
DDX41	DEAD-box helicase 41
DHS	DNaseI-hypersensitive sites
dNTP	Deoxynucleoside triphosphates
dsDNA	Double stranded DNA
EdU	5-ethynyl-2'-deoxyuridine
EdUTP	5-Ethynyl-dUTP
Env	Envelope protein
ERT	Endogenous reverse transcription
ESCRT	Endosomal sorting complexes required for transport
ET	Extraterminal domain of Brd4

FCS	Fetal calf serum
FISH	Fluorescent in situ hybridization
FOV	Field of view
FP	Fluorescent protein
FRET	Förster resonance energy transfer
FV	Foamy viruses
FVM	Flow Virometry
GCE	Genetic code expansion
HCMV	Human Cytomegalovirus
gRNAs	Guide RNAs
h p.i.	Hour post infection
h p.t.	Hours post transfection
HEK293T	Human embryonic kidney 293 cells
HHCC motif	Conserved His and Cys motif in the NTD of integrase
HIV-1	Human immunodeficiency virus subtype 1
HR	Homologous recombination
HTLV-1	Human T cell leukemia virus-1
HUSH	Human silencing complex
IC	Intermediate chain of dynein
IF	Immunofluorescence
IFN	Interferon
IN	Integrase protein
IN.FP	Integrase tagged with a fluorescent protein
ISG	IFN-stimulated gene production
LCs	Light chains of dynein
LEDGF	Lens epithelium-derived growth factor
LMNA/C	Lamin A/C
LTRs	Long terminal repeats
MA	Matrix protein
mAb3	Mouse apolipoprotein B mRNA editing enzyme 3
mCAT-1	Murine cationic amino acid transporter-1
MEF	Murine embryonic fibroblast cells
MeOH	Methanol
MFI	Mean fluorescence intensities
MIP	Maximum intensity projection
mLMNB1	Murine Lamin B1
MLV	Murine leukemia virus
MMTV	Mouse mammary tumor virus
MOI	Multiplicity of infection
MPMV	Mason-Pfizer monkey virus
MTOC	Microtubule organizing center
MuLV	Moloney Murine Leukemia virus
NC	Nucleocapsid protein

NE	Nuclear envelope
NHEJ	Non-homologous end-joining
NNHIV	HIV-1 strain NL4-3 IND64N/D116N tat $\Delta$ 33-64bp
NPC	Nuclear pore complex
NTD	N-terminal domain
Nup153	Nucleoporin 153
OR3	ParB-derived fluorescently tagged protein for dsDNA visualization
PAMPs	Pathogen-associated molecular patterns
pbs	Primer binding site
PBS	Phosphate-buffered saline
PDB	receptor binding domains on the N terminus of SU
PFV	Prototype foamy virus
PIC	Pre-integration complex
PIT-2	sodium-phosphate symporter 2
PM	Plasma membrane
PPT	polypurine tract
PR	Protease protein
Prmt5	Protein arginine methyltransferases 5
puro	Puromycin
PV	Papillomaviruses
Ral	Raltegravir
rpp30	ribonuclease P protein subunit p30
RSV	Respiratory syncytial virus
RT	Reverse transcriptase protein
RTC	Reverse transcription complex
SC-1	Murine fibroblast cells
SCID	Severe combined immunodeficiency
SDCM	Spinning disk confocal microscopy
SERINC3	Serine incorporator 3
SERINC5	Serine incorporator 5
SG-PERT	SYBR green I-based real-time enhanced reverse transcriptase
SIN vector	Self-inactivation vector
SMC5/6	Structural maintenance of chromosome 5/6
ssDNA	Single strand DNA
ssRNA	Single strand RNA
TM	p15E transmembrane protein
TREX1	Three prime repair exonuclease 1
TRIM	Tripartite motif proteins are family of ubiquitin E3 ligases
TRIM5 $\alpha$	Tripartite Motif Containing 5
TRIM11	Tripartite Motif Containing 11
TRIM30	Tripartite Motif Containing 30
vDNA	viral DNA
Vpr-FP	direct fusion of Vpr with fluorescent proteins (FP)

VSV-G  
WASH  
yH2AX

Vesicular stomatitis virus G protein  
Wiskott-Aldrich syndrome protein and SCAR homolog protein  
H2A histone family member X phosphorylated at serine 139

## II List of Figures

Figure 1. MLV genome and particle structure	4
Figure 2. The MLV and HIV-1 mature capsid structure	6
Figure 3. MLV replication cycle	9
Figure 4. Reverse transcription of viral genomes and RT structure between MLV and HIV-1	13
Figure 5. Model of nuclear entry of MLV PIC mediated by p12 chromatin attachment and nuclear retention mechanism	17
Figure 6. Integration of viral cDNA mediated by the interaction of MLV IN and BET domain family	21
Figure 7. Establishment of experimental systems to quantify MLV particle yield and infectivity	50
Figure 8. Production in human HEK293T cells yields higher yield of wild-type and minus-glycoGag MLV particles	52
Figure 9. GlycoGag plays a role in early infection steps in a cell dependent manner	55
Figure 10. MLV viral DNA can be identified and imaged using FISH	57
Figure 11. EdUTP is readily incorporated by MLV and HIV-1 RT	59
Figure 12. Metabolic labeling of viral genomes with EdU click-chemistry is not efficient in MLV infected cells	61
Figure 13. Labeling of accessible MLV dsDNA using the ANCHOR system	62
Figure 14. Pseudotyped ANCH3 containing viral particles are infectious	63
Figure 15. OR3 fusion proteins bind and accumulate on ANCH sequence engineered into NNHIV in infected murine cells	64

Figure 16. The ANCHOR system enables visualization of MLV cDNA in infected murine cells	65
Figure 17. Cytoplasmic OR3 accumulations can be observed during MLV infection as well	67
Figure 18. MLV OR3 signals in contrast to lentiviral vectors can be visualized in the nucleus and cytoplasm	68
Figure 19. Cell division and MLV infection are inhibited upon lower concentration of aphidicolin treatment	69
Figure 20. Nuclear entry of viral cDNA is inhibited in aphidicolin treated cells	70
Figure 21. Aphidicolin treatment of MEFs increases eGFP.OR3 artifacts in the cytoplasm	71
Figure 22. Co-immunostaining of CA and p12 in infected cells requires methanol extraction	74
Figure 23. Nuclear viral cDNA is largely devoid of detectable p12 and CA by immunofluorescence	76
Figure 24. IN.SNAP is associated with a subset of MLV cDNA in the nucleus of infected cells	78
Figure 25. Visualization of MLV dsDNA in living cells using the ANCHOR system	80
Figure 26. Timelapse live-cell imaging of non-infected eGFP.OR3 and eBF2.LMNB1 expressing cells	81
Figure 27. Imaging and tracking of cell division events with eBFP2.mLMNB1 marker in living infected cells	83
Figure 28. Appearance of OR3 signal in the nucleus of daughter cells requires cellular division of the infected parent cell	85
Figure 29. Characterization of nuclear eGFP.OR3 signal dynamics post division in three generations of daughter cells	86

Figure 30. Real-time characterization of nuclear OR3 signal dynamics and lifetimes	88
Figure 31. An OR3 signal was tracked through several generations of infected daughter cells	90
Figure 32. Number of eGFP.OR3 foci and association with cGAS is not dependent on TREX1	92
Figure 33. Association of viral DNA with $\gamma$ H2AX	94
Figure 34. Model of MLV capsid core uncoating	104
Figure 35. IF staining of MLV CA under FISH hybridization conditions	139
Figure 36. Aphidicolin treatment prevents MLV, but not HIV-1 infection in SC-1 cells	139
Figure 37. Visualization of MLV cDNA in infected murine cells expressing mScarlet.OR3	140
Figure 38. Infection with MLV ANCH minus-glycoGag induces formation of nuclear OR3 signals	140

### III List of Tables

Table 1 List of Chemicals and Kits	30
Table 2 List of Antibodies and Staining Dyes	31
Table 3 List of plasmids	32
Table 4 List of Cell lines	34
Table 5 List of Software and Code	35
Table 6 List of primers	36

# 1 Introduction

---

## 1.1 MLV biology

Viruses are infectious agents that exploit cellular resources and machinery for replication intending to transmit their genetic information. All viruses have an RNA or DNA genome packaged within a protein coat and/or a lipid envelope derived from the host cell membrane. Following on from the discovery in 1892 of the first virus, the tobacco mosaic virus (Zerbini and Kitajima, 2022), there is now an estimated number of approximately  $10^{31}$  viruses existing on our planet infecting plants, animals, humans and microorganisms (Zobell and Rittenberg, 2011). The wide assortment of discovered viruses is classified according to their nucleic acid and replication strategy with the Baltimore scheme (Baltimore, 1971). Generally accepted is that most RNA viruses replicate with the help of their RNA-dependent RNA polymerase in the cytoplasm of the target cell, whereas DNA viruses require the nucleus to replicate. Especially interesting in terms of storing genetic information is class IV of the Baltimore scheme, the family of *Retroviridae*. Retroviruses have the unique ability to convert their two copies of single-stranded RNA (ssRNA) into double stranded DNA (dsDNA), which is subsequently integrated into the host genome. With the independent discovery of reverse transcriptase (RT) in 1970 by the laboratories of Harold Temin and David Baltimore, the enzyme responsible for this process was discovered (Coffin and Fan, 2016). Therefore, the central dogma of genetic flow proposed by Francis Crick was revised, showing that the flow is not limited from DNA to RNA only, but can be reversed (Coffin and Fan, 2016). Murine leukemia virus (MLV), belonging to the gammaretrovirus genus, was one of the first discovered viruses causing leukemia in mammals (Gross, 1957; Moloney, 1966). MLV infection of targeted cells like T cells, B cells, granulocytes, and their immature lineages can lead to tumor development such as leukemia or lymphoma. The transmission of this virus in mice occurs vertically from mother to offspring through breastfeeding and horizontally between male mice fighting or venereal between infected male and female mice (Buffett et al., 1969; Portis et al., 1987).

The discovery and investigation of MLV have had significant impact on the treatment of human immunodeficiency linked diseases. With the application of MLV-based vectors, great strides were made in human gene therapy trials and CAR-T cell therapies (Kohn, 2017; Milone and Bhoj, 2018). In the initial gene therapy trials, MLV-based vectors were used for the treatment of X-linked severe combined immunodeficiency (X linked SCID), which led to T cell leukemia in two patients (Kohn et al., 2003). However, the success in the rest of the patients spurred the generation of modified MLV based self-inactivation vectors (SIN) (Hacein-Bey-Abina et al., 2014). Furthermore, MLV has extensively been used as a “model” to study retroviral replication, specifically reverse transcription. It is often used as a representative of “simple” retroviruses with characteristically non-complex genome organization and is compared to the more “complex” lentivirus, the human immunodeficiency virus subtype 1 (HIV-1) that encodes six additional accessory viral proteins (Rein, 2011). Despite being studied since the 1950s, full understanding of the MLV replication cycle is still not fully achieved but will be important for a better understanding of retroviruses in general and for the development of improved gene therapy vectors.

## 1.2 The genome and production process of MLV particles

The genome of MLV is ~8.3 kb and consists of the three essential genes *gag*, *pol* and *env* flanked at the ends with two long terminal repeats (LTRs) (Figure 1A). The *gag* gene encodes for the structural polyprotein Gag, which is proteolytically cleaved by the viral protease (PR) into the matrix (MA), p12, capsid (CA), and nucleocapsid (NC) proteins (Rein, 2011). Interestingly, an alternative glycosylated form of Gag, known as glycoGag, with additional 88 amino acids at the N-terminus is synthesized as a minor species (Figure 1A). Due to the recognition of an alternative CUG start codon upstream and in frame of *gag* (Figure 1A), glycoGag is synthesized with a leader sequence that targets the protein to the endoplasmic reticulum for post-translational modification by N-glycosylation (Edwards and Fan, 1979; Prats et al., 1989; Renner et al., 2018). The glycoGag protein is then cleaved into two subunits, with the amino-terminal cleavage subunit inserted into the viral envelope of budding new viruses in N<sub>exo</sub>C<sub>cyto</sub> orientation as a type I integral membrane protein (Renner et al., 2018). The glycoGag protein appears to have various functions. It was reported to be important for: spreading in

mice but not in cell culture (Corbin et al., 1994; Low et al., 2007; Portis et al., 1994), particle release via lipids rafts (Low et al., 2007; Nitta et al., 2010), stabilization of the capsid core (Stavrou et al., 2013), counteracting the activity of serine incorporator 3 and 5 (SERINC3 and 5) (Li et al., 2019) and mouse apolipoprotein B mRNA editing enzyme 3 (mAb3) (Kolokithas et al., 2010; Renner et al., 2018; Rosales Gerpe et al., 2015; Stavrou et al., 2013).

Since *gag* and *pol* are encoded in the same reading frame, the Pol proteins are synthesized together with Gag as a large Gag-Pol polyprotein by suppression of the *gag* stop codon. For successful replication, MLV virions require a 20:1 ratio between the Gag and the Gag-Pol proteins (Rein, 2011). The ratio is mediated by a cis-acting signal, which induces the insertion of glutamine (CAG) instead of the UAG termination codon at the end of the *gag* coding region, resulting in 5 % of translation products giving rise to Gag-Pol (Hatfield et al., 1992). The Pol products are then cleaved into: RT needed for reverse transcription of the viral ssRNA genome into dsDNA, PR for cleavage catalysis needed for virus maturation, and integrase (IN) for integration into the host genome (Rein, 2011). Lastly, the *env* gene encodes for the envelope protein (Env), which is cleaved in the Golgi apparatus by furin protease into two subunits, the N-terminal surface glycoprotein (gp70<sup>SU</sup>) and the C-terminal p15E transmembrane (TM) protein. During maturation the envelope is cleaved again to remove a C-terminal residue (R peptide) from the TM protein (Rein, 2011). Both SU and TM are vital for viral particle attachment and membrane fusion.

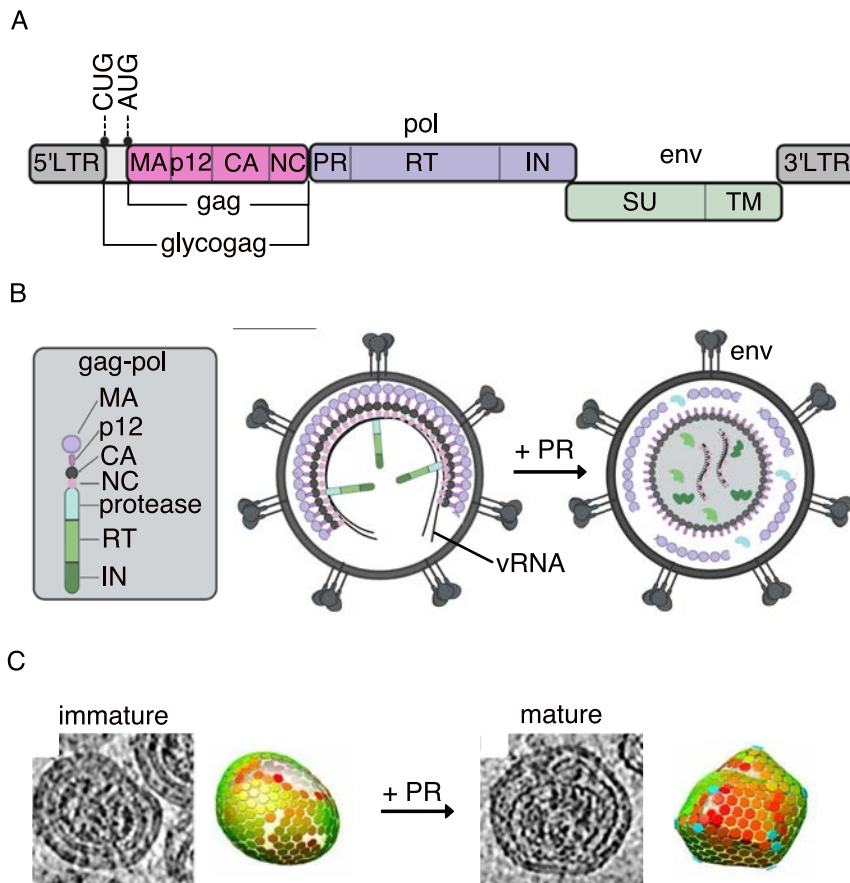


**Figure 1. MLV genome and particle structure.** A. The MLV genome organization. B. Scheme of an immature (left) and mature (right) MLV particle. Maturation process is initiated by the viral PR and the cleavage of viral proteins results in structural reorganization. Scheme created with BioRender. C. Maturation of Gag and the resulting hexameric lattice. Slices of tomogram reconstructions of immature (left) and mature (right) MLV particles and the reconstructed hexameric lattice maps. The color of the hexamers is according to the cross-correlation from low (red) to high (green). The panels are adapted from "[Structure and architecture of immature and mature murine leukemia virus capsids](#)" by Qu et. al. (2018), to use under [CC BY 4.0](#).

MLV Gag is the main driver of assembly and budding of virus particles at the plasma membrane (PM). The transport and anchoring of the Gag- and Gag-Pol polyproteins to the plasma membrane is mediated by myristylation of the N-terminal MA domain, whereas the Gag C-terminus with NC domain is facing inwards in progeny particle (Rein, 2011). Furthermore, the CA domain of Gag mediates protein interactions between the Gag polyproteins, representing the center of immature particle assembly (Sundquist and Kräusslich, 2012). Two molecules of viral RNAs (vRNAs) are recruited into the budding virion by the high-affinity nucleic acid binding site of the NC domain of Gag (Figure 1B) (Miyazaki et al., 2010). The MA domain of Gag recruits the Env proteins to

the viral budding site with the gp70<sup>SU</sup> glycoprotein spanning the exterior of the particle (Rein, 2011; Sundquist and Kräusslich, 2012). The immature particles are then released via the host endosomal sorting complexes required for transport (ESCRT) machinery and subsequently undergo proteolytic maturation (Sundquist and Kräusslich, 2012). The main dictator of the maturation process from immature to infectious viral particles is the viral PR. The proteolytic cleavage of Gag and the release of the cleavage products results in dramatic reassembly of the interior of the particle (Figure 1B, C). The now mature core encloses the viral RNA genome within a closed capsid core alongside the rest of the viral components essential for MLV replication (Figure 1B-C) (Sundquist and Kräusslich, 2012).

### 1.3 The architecture of MLV and HIV-1 capsids

Immature and mature MLV particles were initially studied at low resolution or in two dimensions by cryoelectron tomography (cryo-ET) (Hadravová et al., 2012; Yeager et al., 1998), reporting pleomorphic particles of 110-120 nm size in diameter. However, these studies did not provide enough information to reconstruct the 3D capsid core architecture. Qu et. al., (2018) with the combined use of x-ray crystallography and higher resolution Cryo-ET were able to resolve the structures of both immature and mature MLV capsids. This study reported the size of immature and mature virions to be in diameter of  $114 \pm 5$  nm, similar to earlier measurements (Qu et al., 2018; Yeager et al., 1998). Moreover, the structure of the immature capsid was shown to consist of hexameric Gag proteins and irregular defects to accommodate for the curvature. This architecture is similar to other immature retroviral particles and lacks pentameric defects (Figure 1C).

The general 3D architecture of the mature MLV particle is quite different from HIV-1 (Figure 2A-B), however the MLV mature capsid core is also made of CA hexamers assembling the curved lattice and pentamers incorporated in high curvature positions as reported for HIV-1. Furthermore, the mature HIV-1 cores have a cone-shaped architecture and consists of completely closed fullerene structures, with 12 CA pentamers in the lattice, five at the narrow and seven at the wide end (Figure 2B) (Mattei et al., 2016). In contrast, mature MLV capsids form multilayered or spiral structures that

do not appear to become completely closed and apparently incorporate most of the CA molecules inside the virion (Figure 2A). Accordingly, more than 12 pentamers are inserted per capsid (Figure 2A). Another distinct feature of MLV was observed between the immature and mature number of CA molecules. From HIV-1 studies, it was determined that ~2400 Gag molecules comprise the immature core and after the maturation process only ~50% of the CA molecules remain associated with the cone shaped cores (Briggs et al., 2004; Carlson et al., 2008). In contrast, the number of CA hexamers in the mature lattice of MLV capsids was the same as in the immature lattice, indicating that almost all CA molecules are involved in the mature assembly of the spiral multilayered cores of MLV (Qu et al., 2018).

Despite the difference in architecture, the mature cores of both MLV and HIV-1 appear to carry out similar functions in early replication including reverse transcription and shielding from the innate immune response. Understanding similarities and differences between different virus groups will improve our general view on retroviral host interaction.

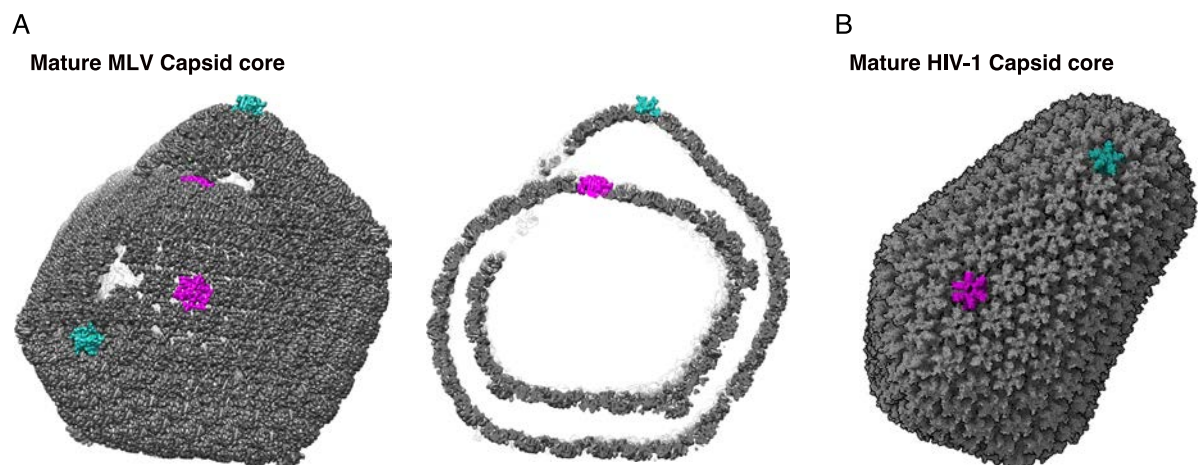


**Figure 2. The MLV and HIV-1 mature capsid structure.** A. Representative mature MLV spiral capsid core made of hexamers and pentamers is shown. On the right, a slice through the capsid core is shown to demonstrate the multilayer sheets arranged in spirals. Representative hexamers (magenta) and pentamers (blue) are shown. The structure was rendered in Chimera with a custom made plug-in [Place object v2.1.0](#) written by Dr. Kun Qu and available under [GPL v.3](#). The structures were kindly made and provided by Dr. Kun Qu. B. Representative closed fullerene capsid core of HIV-1 made of hexamers and pentamers is shown. One representative hexamer (magenta) and pentamer (blue). The structure [pdb:3j3q](#) was rendered using ChimeraX software.

## 1.4 MLV replication cycle

MLV infection is instigated by the binding of the cell receptor by the SU glycoprotein of a mature viral particle. After fusion of the viral and plasma membrane, the subviral particles are released into the cytoplasm. Next, to reach the nucleus the viral particles are transported using the microtubule network and host factors (Rein, 2011). During the transport in the cytoplasm, reverse transcription of the viral RNA genome into dsDNA is initiated (Telesnitsky and Goff, 1997). Retroviruses have very diverse means of nuclear entry with HIV-1 squeezing through the nuclear pore and MLV requiring nuclear envelope breakdown during cellular division (Suzuki and Craigie, 2007). Once inside the nucleus, IN can facilitate the viral DNA integration into the host genome; this integrated structure has been termed provirus. The proviral DNA is transcribed and translated by the host machinery (Rein, 2011). Subsequently, the viral proteins assemble on the plasma membrane, followed by budding of the immature particles. Lastly, the protease cleaves the viral proteins resulting in a fully mature particle as described above (Rein, 2011).

To successfully infect a target cell and release infectious units, retroviruses such as MLV must overcome numerous bottlenecks along their path. Specifically, the timing and mechanism of infection steps, innate immune response and host factors are responsible for drastically reducing the chances of productive infection. A study relating intact particle counts by Flow Virometry (FVM) to the transducing unit (TU) values has shown that approximately 200-400 MLV particles are required for a single productive infection event (Renner et al., 2020). This number is roughly similar to the ratio of viral particles per infectious units (P/IU) reported for other retroviruses, such as HIV-1 (Klasse, 2015). Furthermore, it was estimated that only ~50 out of the 400 MLV particles required for a single infection event, contain an RNA genome (Renner et al., 2020). Therefore, already during viral production the producer cells release large number of genome-deficient virions that cannot replicate (Renner et al., 2020). The relatively short half-life of MLV compared to HIV-1 was measured to be 4.5 h at 37°C (Higashikawa and Chang, 2001), meaning that viral particles also have limited time to attach and fuse before they are degraded. As the retroviral particle movement in cell culture is restricted by Brownian motion, large number of particles would not meet their target cells (Chuck

et al., 1996). Furthermore, it was reported that bound MLV particles in cell culture were detected after 1 min of incubation at 37°C and the maximum was reached at 30 min incubation with no increase detected after this point (Pizzato et al., 1999). Collectively, the data indicates that MLV viral particles have limited time to collide and attach to the target cell before they are degraded. Therefore, cell entry is already an effective first bottleneck preventing viral particles to successfully infect target cells. The population of remaining subviral particles that have entered the cells undergo other challenges which decreases these numbers even more.

This thesis focuses on early entry events of the MLV replication cycle; therefore, in the following sections only the pertaining steps were examined: cell attachment and fusion, cytoplasmic transport, nuclear entry, reverse transcription, capsid uncoating and integration. Taken into account are the bottlenecks posed by the replication itself as well as by cellular restrictions. This includes host proteins and their interactions with the viral structures on their path towards a productive infection.

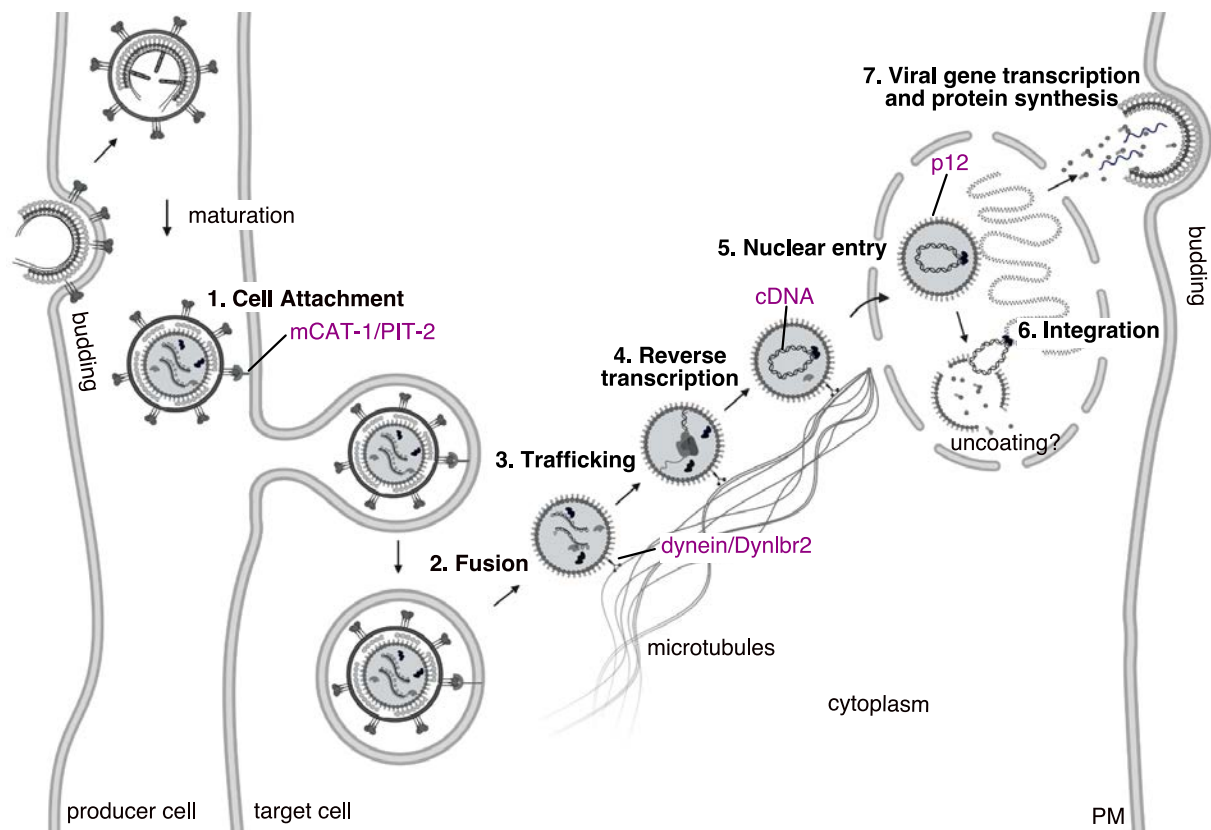


**Figure 3. MLV replication cycle.** Cell infected with MLV produces immature particles, which assemble at the PM and bud out. During maturation the viral proteins Gag and Gag-Pol are cleaved by PR resulting in infectious particles. After Env mediated attachment, the viral particles are endocytosed. The core is delivered into the cytoplasm by cell and viral membrane fusion. Once in the cytoplasm, the capsid core is transported to the nucleus on microtubules. During the transport, reverse transcription is initiated due to the presence of deoxynucleotide triphosphates (dNTPs). The capsid core then waits in the cytoplasm for nuclear envelope (NE) to break down so it can enter the nucleus. The nuclear retention upon mitosis is mediated by the viral protein p12 that anchors the RTC/PIC to chromatin during mitosis and retains the viral genome in the nucleus once the nuclear envelope reforms. The location and manner of uncoating is still not very well understood, but the capsid obviously needs to release the viral cDNA to integrate. Once the viral cDNA is integrated, now termed as provirus, transcription and translation occurs. The viral proteins travel to the plasma membrane where the cycle starts again. The figure was created with BioRender.com.

#### 1.4.1 Cell entry and transport

Enveloped viruses initiate infection by cell receptor binding and plasma membrane fusion using a variety of different mechanisms. MLVs can be divided into 6 subgroups (ecotropic, amphotropic, polytropic, xenotropic, MDEV, 10A1) depending on their envelope genes which bind to different cell receptors (Bachrach et al., 2000; Coffin et

al., 1997; Han et al., 1998). Different MLVs contain receptor binding domains (PDB) in the N-terminus of the SU that are highly sequence variable between isolates, which allows for such flexible interactions (Bachrach et al., 2000; Coffin et al., 1997). The ecotropic MLV infects cells by binding to murine cationic amino acid transporter-1 (mCAT-1), whereas the amphotropic MLV binds to a different cell receptor named sodium-phosphate symporter 2 (PIT-2) (Bachrach et al., 2000; Han et al., 1998; Overbaugh et al., 2001). For most retroviruses including MLV, only a single cell surface receptor is needed to initiate viral entry. In contrast, HIV-1 requires two cell surface molecules to perform attachment and fusion. The initial attachment of HIV-1 requires binding to the receptor CD4, whereas fusion is only initiated if a second co-receptor, CCR5 or CXCR4, is present on the cell surface (Coffin et al., 1997; Wilen et al., 2012). During the process, dramatic changes in the trimeric Env complexes are triggered, resulting in fusion of the viral with the cell membrane and the release of a subviral particle into the cytoplasm. While HIV-1 entry requires two consecutive receptors, gammaretroviruses such as MLV require both cell attachment and host cathepsin cleavage as triggers (Barnett and Cunningham, 2001; Kamiyama et al., 2011; Kumar et al., 2007; Wallin et al., 2005; Yoshii et al., 2009). After receptor binding, the ecotropic MLV particles are internalized into endosomes, followed by fusion and cytoplasmic release. Cathepsin B and L are found in the endosomal compartment, and cleave SU into precise fragments, which in turn enhances the membrane fusion activity of Env (Kumar et al., 2007). Cathepsins also play a role in triggering fusion during amphotropic, xenotropic and polytropic MLV infection.

After the viral core is delivered into the cytoplasm, it requires transport towards the nucleus. Since retroviral capsids exceed the size to diffuse through the highly viscous cytoplasm, they have resorted to other means for reaching the nucleus (Luby-Phelps, 1999). They rely on the microtubule network to transport and deliver their genome to the nuclear envelope. This is a complex network of tubes characterized by their structural polarity, where one end is considered plus end with the ability to expand and shrink and the other end is negative and anchored to the microtubule organizing center (MTOC) (Pietrantoni et al., 2020). The long-distance directional transport is achieved with the help of ATP-powered motor proteins called kinesins (transport in an anterograde manner, minus to plus end) and dyneins (transport in a retrograde manner,

plus to minus end) (Pietrantoni et al., 2020). It has been reported that retroviruses such as HIV-1, Mason-Pfizer monkey virus (MPMV), bovine immunodeficiency virus (BIV), and prototype foamy virus (PFV) use the dynein complex to travel towards the nucleus (Carnes et al., 2018; Dharan et al., 2017; Pietrantoni et al., 2021). Valle-Tenney et al. (2016) has demonstrated that dynein intermediate chain (IC) and regulators p50/dynamitin are associated with the MLV pre-integration complex (PIC) and its transport. Furthermore, the knockdown of the dynein regulators p50 and NudEL reduced infection significantly (Valle-Tenney et al., 2016). To determine the host protein that directly binds to MLV RTC/PICs, like Bicaudal D2 is binding to HIV-1, more components of the dynein complex were investigated (Carnes et al., 2018; Dharan et al., 2017). It was found that the knockdown of dynein light chains (LCs) specifically the knockdown of DYNLBR2 reduced the efficiency of MLV infection (Opazo et al., 2017; Pietrantoni et al., 2021). Moreover, using GFP tagged p12 particles the arrival of the MLV PIC in the nucleus of DYNLBR2 knockdown and overexpressed cells was evaluated. The knockdown resulted in loss of directional movement and nuclear entry, whereas a significant increase in the number of PIC was observed in the nucleus when DYNLBR2 was overexpressed signifying that DYNLBR2 is the likely transport partner to MLV (Pietrantoni et al., 2021).

#### 1.4.2 Reverse transcription

After cellular penetration and during cytoplasmic transport, reverse transcription of the viral RNA into DNA is initiated within the capsid core. The trigger of the process is the presence of nucleotide triphosphates in the cell. This has been confirmed using endogenous in vitro reactions with detergent-permeabilized mature virions, which required addition of nucleotide triphosphates to initiate reverse transcription indicating that the virion itself has all other required components to start the reaction (Telesnitsky and Goff, 1997). At this point of cytoplasmic replication, the viral complex is referred to as the reverse transcription complex (RTC). The MLV RT possesses DNA polymerase activity that is active on RNA and DNA templates, as well as RNase H activity able to digest RNA in RNA:DNA hybrid forms (Roth et al., 1985). Furthermore, MLV RT shares a similar 3D structure with other retroviruses despite low sequence homology (Figure 4A-B) (Coté and Roth, 2008; Oscorbin and Filipenko, 2021). The spatial architecture of

MLV RT is comprised of the hand-like domain containing fingers, palm, thumb as part of the N-terminus, whereas a connection domain and RNase H comprise the C-terminus of the enzyme (Figure 4A) (Das and Georgiadis, 2004; Georgiadis et al., 1995). Interestingly, MLV RT is active in its monomeric state, whereas other well-characterized RT such as that of HIV-1 are active as heterodimers only (Figure 4A-B) (Coté and Roth, 2008; Ooscorbin and Filipenko, 2021; Telesnitsky and Goff, 1997). Furthermore, reverse transcriptases when compared to replicative polymerases have shown to have low intrinsic fidelity, meaning the ability to copy a DNA or RNA template without inserting errors such as mismatches, deletion, insertions, and recombination. This lower fidelity is due to the lack of proof-reading exonuclease activity which will reduce errors (Ooscorbin and Filipenko, 2021; Telesnitsky and Goff, 1997). It was found that MLV RT is 15-fold more faithful than HIV-1 RT (Bakhanashvili and Hizi, 1992). Interestingly, the misincorporation rates of MLV and HIV-1 were comparable; however, the MLV RT was reported to have low affinity and slow extension rate of a mismatched template (Skasko et al., 2005).

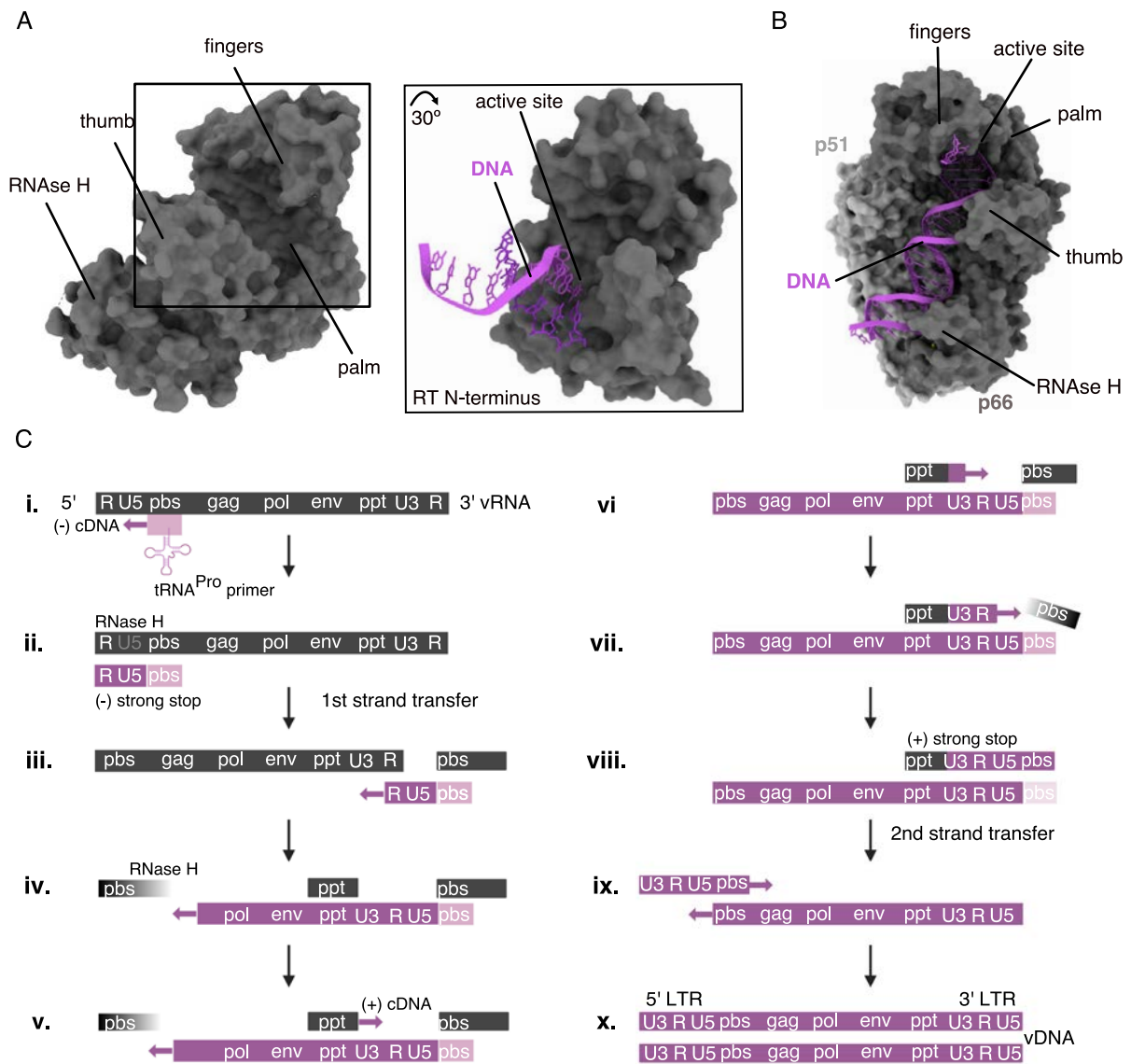


**Figure 4. Reverse transcription of viral genomes and RT structure for MLV and HIV-1.** A. Structure of the MLV monomeric RT (pdb: 4mh8) is presented on the left side. The RT N-terminus consisting of the palm, thumb, fingers, and hidden catalytic active site, which engages with nucleic acid for polymerization is shown on the right site (pdb: 1qaj). The RT N-terminus with the nucleic acids are rotated 30° for better visualization compared to the complete structure on the left. The RT components are in grey, and the nucleic acid is in magenta. The structures were generated with ChimeraX. B. Structure of HIV RT in complex with nucleic acid (pdb:1rtd). The rendering of the structure shows the p66 (dark grey) and p51 (light grey) subunits in complex with DNA (magenta). The active site of the polymerase is hidden behind the fingers and cannot be seen here. C. Schematic of the individual steps of reverse transcription involving 2 strand transfers to generate viral cDNA with full LTR sequence on each end. Color code: viral RNA in grey, DNA in purple and tRNA<sup>Pro</sup> in pink. R: repetitive region; U5: unique region of 5' LTR; pbs: primer binding site; ppt: polypurine tract; U3: unique region of 3'LTR. The scheme was created with BioRender.com.

The reverse transcription starts with binding of the RT to genomic viral RNA with a host derived tRNA serving as a primer. Diverse tRNA primers are used by retroviruses of different genera, for example proline and lysine tRNAs are used by MLV and HIV-1 respectively (Coté and Roth, 2008; Oscorbin and Filipenko, 2021; Telesnitsky and Goff, 1997). The tRNA primer binds in reverse orientation to the primer binding site (pbs) close to the 5' end of the viral genome (Figure 4C, part i.) and initiates the synthesis of the first intermediate named the minus-strand strong stop DNA (Figure 4C, part ii.) During the generation of the minus strong stop DNA, a DNA-RNA intermediate is formed, whose RNA strand is subsequently digested by the RNase H domain of RT (Figure 4C, part ii.) To resume cDNA synthesis, the R sequence in the newly made single strand DNA (ssDNA) detaches from the degrading RNA template and hybridizes to the identical R sequence in the 3'LTR on either of the two RNA templates signifying the first strand transfer (Figure 4C, part iii). With the binding of the R parts the synthesis of the remaining minus strand is initiated (Figure 4C, part iii). Thus, another RNA:DNA intermediate complex is formed, where subsequently the RNA is again degraded by RNase H (Figure 4C, part iv). The polypurine tract (PPT) in the RNA genome is resistant to digestion by RNase H (Figure 4C, part v), and serves as a primer for the synthesis of the plus strand (Figure 4C, part vi). With the synthesis of the 3'LTR region, there is now dsDNA that contains the tRNA primer pbs sequence (Figure 4C, parts vii and viii). At this point, the second strong stop is reached (Figure 4C, part viii), which results in a second strand transfer and the hybridization of the plus and minus strands by the binding of the respective pbs sequences (Figure 4C, part ix). Lastly, the dsDNA is completed via strand displacement synthesis (Figure 4C, part x). Moreover, the functional promoters are reinstalled, meaning the unique sequences U5 and U3 are copied to the 3'LTR and the 5'LTR, respectively. With reverse transcription completed, the subviral particles are now referred to as pre-integration complexes, PICs.

While much is known about the mechanism of reverse transcription, the location of this enzymatic process is not so clear. It is accepted that the process starts in the cytoplasm of the infected cell, however, the location of its completion seems to depend on the different retrovirus genus. For HIV-1, it was only recently revealed that reverse transcription is completed in the nucleus (Burdick et al., 2020; Dharan et al., 2020;

Francis et al., 2020b; Müller et al., 2021). To validate the location of reverse transcription completion, studies were utilizing RT inhibitor time of addition experiments (Burdick et al., 2020; Francis et al., 2020b), specific hybridization probes targeting either only minus strand DNA or both minus and plus strand DNA (Dharan et al., 2020), and the ANCHOR labeling system of viral DNA (Müller et al., 2021). On the other hand, for MLV the initiation as well completion of reverse transcription supposedly occurs in the cytoplasm of infected cells (Bowerman et al., 1989; Brown et al., 1987). Primarily, Brown et al. (1987) developed an *in vitro* integration assay and showed that linear MLV DNA isolated from the cytoplasm of infected cells is an active precursor of integration. This assay depended on the fact that the isolated cytoplasmic MLV DNA was able to integrate due to LTR presence. Since LTRs are completed in the last steps of reverse transcription, the authors proposed that the enzymatic process must have been completed in the cytoplasm. Another study using the same *in vitro* integration assay confirmed this finding and showed that the LTR containing linear vDNA co-precipitated with viral CA protein, indicating that the vDNA in the cytoplasm is part of an integration able subviral particle (Bowerman et al., 1989).

#### 1.4.3 Nuclear entry

Unlike lentiviruses such as HIV-1, MLV subviral particles upon arrival at the nuclear envelope depend on cellular division to gain access to the host chromatin and subsequently integrate (Roe et al., 1993). MLV particles gain access to the nucleus once nuclear envelope breaks down during mitosis by tethering to chromatin and are retained inside the newly formed nuclear membrane of the daughter cells (Elis et al., 2012; Lewis and Emerman, 1994; Roe et al., 1993; Wanaguru et al., 2018). Therefore, inhibitors blocking cellular division such as aphidicolin (APC) can be used to inhibit MLV infection (Lewis and Emerman, 1994; Roe et al., 1993). Interestingly, viruses such as gamma-herpesvirus and papillomavirus (PV) tether to chromatin during mitosis as well to retain their episomal genomes in the host cell (Aydin and Schelhaas, 2016).

Mutational studies of the Gag protein p12, outlined its importance in early events of viral replication as well as nuclear entry and retention (Elis et al., 2012; Schneider et al., 2013; Wight et al., 2014, 2012; Yuan et al., 2002, 1999; Yueh and Goff, 2003). The N-

terminal domain (NTD) of p12 has been shown to bind and stabilize the capsid (Wight et al., 2014), whereas the C-terminal domain (CTD) of p12 anchors PIC to chromatin (Elis et al., 2012; Wanaguru et al., 2018) (Figure 5). Furthermore, Wanaguru et al. (2018) showed that during mitosis there is increased phosphorylation of p12, which resulted in higher affinity of p12 to host chromatin (Figure 5). This contact between p12 and chromatin appears to be fast and transient, because once chromatin decondensation occurs the p12 is detached (Elis et al., 2012). In summary, the p12 protein appears to act similarly to a car towing service where on one side it anchors to the chromatin and on the other to CA containing PIC complex, thus “towing” the viral particle towards the chromatin and releasing it once the destination is reached (Figure 5). This manner of nuclear entry is mirrored by PFV which also belongs to the family of retroviruses (Bieniasz et al., 1995; Lesbats et al., 2017; Müllers et al., 2011; Tobaly-Tapiero et al., 2008). Müllers et al. (2011) utilized autofluorescent protein (AFP) tagged PFV Gag in live imaging and could show that Gag nuclear localization depends on mitosis *via* chromatin tethering. Moreover, Lesbats et al. (2017) identified a chromatin-binding sequence (CBS) located within the C-terminal region of PFV Gag that directly binds to mitotic chromatin similarly to the MLV Gag protein p12.

In the case of HIV-1, the CA protein and capsid lattice play a vital role in nuclear entry. At the nuclear envelope, the HIV-1 capsid interacts with and docks at a nuclear pore complex (NPC). The capsid interacts with several FG-repeat containing nucleoporins during transfer through the NPC channel and subsequently with cleavage and polyadenylation specificity factor 6 (CPSF6) on the nuclear side which binds to the same position and thus displaces nucleoporins from the entering capsid (Müller et al., 2022). Accordingly, the capsid is the main determinant for the successful infection of non-dividing cells by HIV-1 (Müller et al., 2022; Yamashita and Emerman, 2004). It was shown that a chimeric HIV-1, containing sequences for MA, p12 and CA from MLV instead of its own MA and CA, loses the ability to infect non-dividing cells thus highlighting the importance of CA in nuclear entry (Yamashita and Emerman, 2004). In summary, retroviruses have creative and diverse ways of nuclear entry with a common feature that Gag proteins play a significant role in this process.

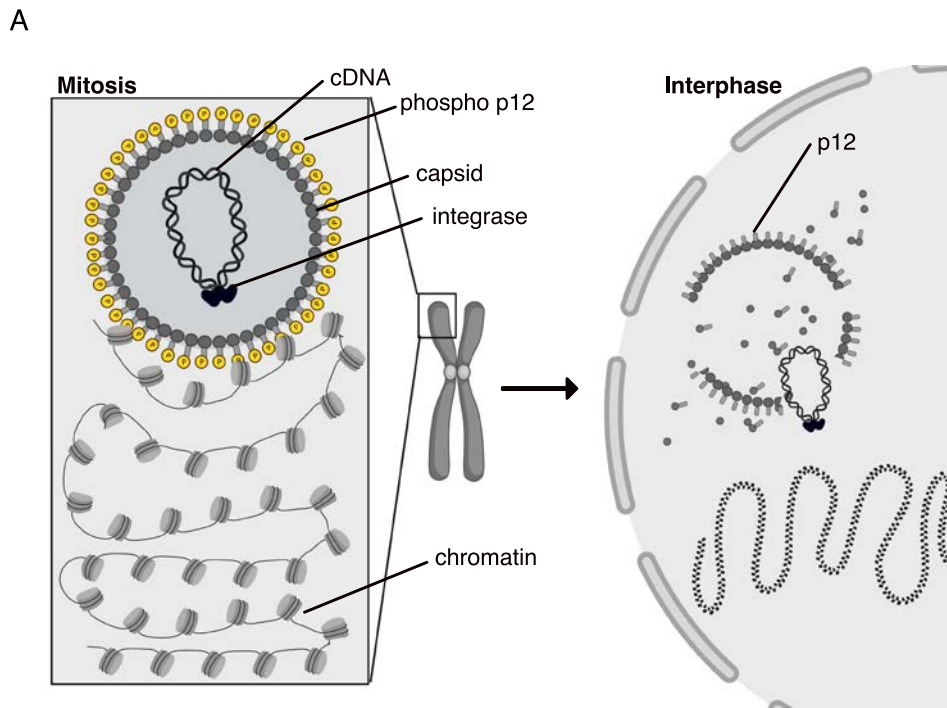


**Figure 5. Model of nuclear entry of MLV PIC mediated by p12 chromatin attachment and nuclear retention mechanism.** A. Scheme of p12 mediated nuclear entry of MLV RTC/PIC during mitosis. The phosphorylated p12 during mitosis attached to the chromatin by its NTD, whereas on the CTD side is attached to the CA containing RTC/PIC complex. Once mitosis ends, the p12 is dephosphorylated which could be the trigger for detachment and possible capsid uncoating. The scheme was made with BioRender.com.

#### 1.4.4 Uncoating

The viral DNA needs to be accessible for integration upon nuclear entry. Therefore, the capsid shell surrounding it needs to dissociate or be stripped in a process called uncoating. However, the location, kinetics, and mechanism of capsid uncoating in spatio-temporal context are heavily debated in the field of retroviruses.

The capsid in the cytoplasm is most often referred to as a biological container that allows access of dNTPs and provides enclosed space to allow for the reverse transcription components to interact efficiently and synthesize viral cDNA. Additionally, the capsid appears to be required to protect the viral genome from host nucleic acid sensors until the viral cDNA integrates (Goff, 2004; Moran and Ross, 2020; Stavrou et

al., 2015; Suzuki and Craigie, 2007). Lastly the capsid of HIV-1 plays a role in nuclear entry, while no such role has been described for MLV (Yamashita and Emerman, 2004).

Initially, the investigation of capsid uncoating utilized sedimentation analysis after lysis at different infection times together with detection of CA protein by immunoblots, and minus and plus strand DNA detection by PCR (Fassati and Goff, 1999). The study revealed large amounts of MLV CA to be associated with cytoplasmic RTC species that contained viral cDNA (Fassati and Goff, 1999). These findings confirmed previously published results from Bowerman et al. (1989), which showed that CA containing RTC is associated with integration able cDNA in the cytoplasm of infected cells (*cf.* 1.4.2). Furthermore, the size of the RTC/PICs changed over time, with a gradual shift in the sedimentation properties from 560S detected in the cytoplasm to 90S found in the nucleus (Fassati and Goff, 1999). Lastly, immunoblot analysis after the equilibrium density fractionation showed that CA is stripped from the RTC/PICs in the nucleus and that the CA/IN ratio is higher in the cytoplasmic than the nuclear fraction. Taking the findings together the authors claimed an organized gradual uncoating process starting in the cytoplasm and ending in the nucleus. Debating against this model is that complete MLV capsids are required for viral genome protection, which upon partial uncoating in the cytoplasm could give access to nucleic acid sensors. Along the same lines, negating this model are studies using glycoGag defective MLV mutants, which were shown to have destabilized capsids and subsequently activate the innate immune response in the cytoplasm (Moran and Ross, 2020). Therefore, the gradual loss of CA protein for MLV does not fully explain the uncoating process.

Hence, an alternative manner of uncoating was explored, mediated partly by the viral protein p12 and cellular division. Using Chromatin ImmunoPrecipitation (ChIP) based analysis of the association of viral cDNA and CA, it was revealed that higher levels of association were detected in aphidicolin arrested cells than in dividing cells (Wang et al., 2016). The data suggested that in absence of division a stabilization of viral DNA and CA complexes occurs. Moreover, p12 has been found to directly bind, stabilize the capsid core, and prevent premature loss of capsid until nuclear entry (Wight et al., 2014, 2012). This interaction of p12 and CA persists after entry into the nucleus, shown by high co-localization percentages (~70%) of nuclear subviral complexes in

immunofluorescence (IF) stained cells (Wanaguru et al., 2018). Lastly, Wang and Goff (2021) explored the importance of p12 on viral DNA chromatinization and CA uncoating. They used a p12 mutant (PM14) known to be defective in chromatin tethering; the viral cDNA synthesized by this mutant was excluded from the nucleus. Interestingly, the viral CA protein is more strongly associated with the viral DNA of the mutant than the wild-type, which in turn resulted in poor chromatinization of the mutant viral DNA (Wang and Goff, 2021). The results indirectly proved that successful chromatin attachment and nuclear retention mediated by p12 are necessary for CA uncoating. Based on the observations above, the following model of capsid uncoating was proposed. After Gag cleavage, the p12 binds via its N-terminus and stabilizes the capsid core. Followed by nuclear envelope breakdown the p12 attaches to chromatin *via* its C-terminus and pulls the CA core inside the nucleus of the daughter cell. Once the daughter cell exits mitosis, p12 detaches from chromatin. The viral cDNA is then released from the p12/CA complex and is chromatinized. It is still not completely clear how CA uncoating, chromatin tethering, and histone loading are connected and in which order, since all of these events have seemingly overlapping time frames. What can be concluded is that somewhere between nuclear entry and integration the viral cDNA is released by capsid uncoating.

Like MLV, the uncoating process, location and timing of HIV-1 are still under debate (Müller et al., 2022). Initial lines of evidence proposed rapid (Campbell and Hope, 2015) or gradual disassembly in the cytosol (Hulme et al., 2011; Mamede et al., 2017; Xu et al., 2013); however, direct interaction of HIV-1 CA with different host factors involved in late post entry events argued against it. More models, based on image-based analysis, were suggesting for CA uncoating at, in or through the nuclear pore (Burdick et al., 2020; Francis et al., 2020a, 2016; Francis and Melikyan, 2018; Müller et al., 2022). Lastly, recent studies by our lab detected HIV-1 viral cones in the nucleus by correlative light and electron microscopy (CLEM) (Zila et al., 2021) and observed separation of CA or IN from viral cDNA in the nucleus (Müller et al., 2021). In the same line of evidence, nuclear signals of directly labeled CA by genetic code expansion (GCE) and click labeling showed by CLEM to be cone-shaped HIV-1 capsid-like structures inside the nucleus (Schifferdecker et al., 2022).

In conclusion, the fate of retroviral capsids still needs to be investigated more closely, specifically the exact mechanism, timing, and location of uncoating. Moreover, comparing the capsid integrities of MLV and HIV-1 could provide a wealth of information on why these viruses are so different in their nuclear entry strategies and capsid structures.

#### 1.4.5 Integration

After nuclear entry and capsid uncoating, the viral DNA can be integrated into the host chromatin, which is mainly driven by the viral IN. The IN is structurally consisting of four conserved domains: N-terminal domain that coordinates a single zinc atom and multimerization of IN, the catalytic core domain (CCD) which contains the enzymatic active site, C-terminal domain implicated in host DNA binding and C terminal tail region (Figure 6A). The nuclear PICs contain linear viral DNA connected by the LTR ends by a multimer of IN in a complex called the intasome (Miller et al., 1997). Interestingly, the catalytically active form of IN is an oligomer. For example, a tetramer and dimer are proposed as active forms necessary for concentrated strand transfer of MLV (Jones et al., 1992; Jonsson et al., 1996; Villanueva et al., 2003; Yang et al., 1999; Yeager et al., 1998) and HIV-1 (Engelman et al., 1993; Faure et al., 2005; Guiot et al., 2006; Li et al., 2006) respectively.

Retroviral IN has two enzymatic activities, 3' end processing and strand transfer, which in concert enable the insertion of viral DNA into the host cell DNA. The 3' processing of the viral DNA is executed by cleaving a dinucleotide from each LTR end, in the case of MLV a TT is being cleaved. The viral DNA now has free Cytosine-Adenine 3'-hydroxyl groups on each end that serve as nucleophiles targeting the 5'-phosphate groups of the host DNA, which cut host DNA and initiate strand transfer (Engelman et al., 1991; Gupta et al., 2013). The repair of the integration intermediate yields a 4 bp duplication of chromosomal DNA flanking the integrated MLV provirus (Craigie et al., 1990; Roth et al., 1989).



disordered regions of both interacting protein partners from a structured intermolecular hybrid  $\beta$  sheet (Figure 6B). Similarly to BET, the host factor lens epithelium-derived growth factor (LEDGF) binds to HIV-1 IN and targets the PICs to actively transcribing genes. Interestingly, when artificial BET fusion protein was generated to contain the part of LEDGF/p75 (1-324 residues) instead of the BDs, MLV PIC was retargeted to actively transcribed regions (De Rijck et al., 2013). Along the same lines, in the absence of LEDGF HIV-1 is retargeted to regions known to be integration sites for other retroviruses such as MLV (Engelman and Cherepanov, 2008). From the large body of evidence, host cell factors such as BET family and LEDGF/p75 proteins are dictating the target site of integration. However, a study using HIV-1 chimeras containing MLV IN observed integration with specificity similar to MLV (Lewinski et al., 2006) indicating that integrase is the primary viral factor for choosing integration sites.

The difference between HIV-1 and MLV in integrase retention or separation from capsid proteins is seemingly based on the targeting of the viral cDNA to integration sites. HIV-1 PICs are targeted to actively transcribing gene domains mediated by the binding of the host factor LEDGF to IN (Cherepanov et al., 2003; Ciuffi et al., 2005; Singh et al., 2015). This process is quite similar to the mediated IN/BET targeting of MLV cDNA in the proximity of CpG islands and promoter regions where it preferentially integrates. Interestingly, depleting LEDGF did not inhibit integration of HIV-1, but the site of integration changed to regions usually targeted by other retroviruses, such as MLV (Engelman and Cherepanov, 2008). In the case of HIV-1, recent studies have also implicated the CA-CPSF6 interactions in PIC translocation to nuclear speckles and speckle associated domains (Francis et al., 2020b; Sowd et al., 2016). Of note, CPSF6 binds to the hexameric assembly of CA thus it is highly likely that complete or partial lattice of HIV-1 CA is involved in integration-site targeting, which contrasts with MLV where the capsid core is seemingly not required for this process.

In conclusion, CA protected HIV-1 cDNA is primarily targeted to integration sites mediated by IN/LEDGF and CA/CPSF6 interactions, followed by the uncoating process and release of the cDNA. In case of MLV, the viral cDNA is probably released by CA uncoating and then escorted to integration sites by IN/BET interactions.

Important to note that viral DNA is rapidly chromatinized upon nuclear entry where unintegrated species are silenced, thus resulting in poor expression (Goff, 2021). Integration of the viral cDNA in the host cell genome is prerequisite to drive high level expression of the viral genes (Goff, 2021). Using ChIP analysis of infected cells it was found that histones H3 and H2A are rapidly loaded on MLV DNA as soon as it is accessible and located in the nucleus (Wang et al., 2016). This study also showed that the H3 histones associated with unintegrated MLV DNA are marked by trimethylation of the tail on Lysine 9, which is a marker of silenced chromatin. On the unintegrated MLV DNA no histone modifications such as H3 and H4 acetylation were found, which are known to be transcription promoting. Furthermore, the lack of acetylation on histones was also observed with MLV IN defective virions (Goff, 2021). The silencing of the unintegrated MLV DNA is mediated by a DNA binding protein NP220 that recruits the human silencing complex (HUSH) and SETDB1, which is a histone methyl transferase that methylates the H3 histone (Goff, 2021). The main features of viral DNA silencing are conserved between MLV and HIV-1; however, for HIV-1 other host proteins such as structural maintenance of chromosome 5/6 (SMC5/6) ATPase were discovered to silence viral DNA instead of the HUSH complex (Goff, 2021).

## 1.5 Host cell protein interaction with viral DNA and capsid

The innate immune system is composed of host protein receptors and signaling pathways, which detect foreign components of pathogens termed pathogen-associated molecular patterns (PAMPs). Several lines of defense are part of the antiviral response to murine retroviruses, due to the generation of PAMPs at different stages of the replication cycle. The focus in this section will be on the host cell sensing and response to reverse transcribed DNA genomes and the shielding role of the MLV capsid core.

During infection with MLV, several forms of viral nucleic acids are generated through reverse transcription such as RNA/DNA hybrids, ssDNA, and dsDNA. These viral DNA forms are very important PAMPs, which are recognized by various nucleic acid sensors in the cytoplasm or nucleus (Moran and Ross, 2020). Sensing of cytoplasmic viral DNA by host sensors is readily observed in case of absence of a DNA exonuclease, the three

prime repair exonuclease 1 (TREX1), resulting in an increase of interferon production in MLV or HIV-1 infected cells (Stavrou et al., 2013; Yan et al., 2010). TREX1 binds and digests dsDNA as well as other reverse transcripts (ssDNA, and DNA in the RNA/DNA hybrid), thus reducing cytoplasmic viral DNA in early retroviral infection (Moran and Ross, 2020). Interestingly, depletion of TREX1 does not lead to an increase of proviral integrations in HIV-1 infected cells indicating that fully productive RTC/PIC are shielded from DNase (Kumar et al., 2018; Moran and Ross, 2020). It was therefore suggested that TREX1 modulates the immune response by degrading abortive or prematurely uncoated reverse transcripts, thus not alerting the nucleic acid sensors, and ensuring successful retroviral infection.

A common nucleic acid sensor for retroviral DNA is cyclic GMP-AMP synthase (cGAS), which upon binding to viral DNA will activate the STING signaling pathway, thus upregulating transcription of type I interferon (IFN). It was found that depletion of cGAS significantly reduces IFN production mediated by STING in infected MLV and HIV-1 cells (Cai et al., 2014; Gao et al., 2013; Luecke and Paludan, 2017; Stavrou et al., 2015, 2013). Moreover, it was discovered that cGAS is a predominantly nuclear protein in an inactive state, so it won't bind to host cell DNA. Upon cytoplasmic sequestration, cGAS becomes active and binds to non-self DNA (Volkman et al., 2019). Unexpectedly, a recent study has found that cGAS has a non-canonical sensing function in the nucleus (Cui et al., 2020). Upon infection, nuclear cGAS interacts with protein arginine methyltransferases 5 (Prmt5), which in turn catalyzes methylation of IFN promoters resulting in IFN production (Cui et al., 2020).

Several other host cell molecules have been found to induce an IFN response through the STING pathway. The cytosolic DEAD-box helicase 41 (DDX41) and the interferon inducible IFI203 have been identified as cytosolic sensors of abortive reverse transcripts found in TREX1 depleted macrophages and DCs. Additionally, DDX41 and IFI203 form a complex that binds to STING and acts independently from cGAS (Stavrou et al., 2015). The DDX41 has a different preference for DNA ligands than cGAS. While cGAS prefers binding to dsDNA, DDX41 binds to initial products of MLV reverse transcription, the RNA/DNA hybrids (Stavrou et al., 2018). Furthermore, the sequential binding of early and late RT products by DDX41 and cGAS causes a synergistic

induction of type I IFNs, and both of them are required for the sensing and control of MLV in vivo (Stavrou et al., 2018).

One of the most effective ways to inhibit nucleic acid sensing is by limiting accessibility to viral DNA. Despite ongoing debates, completion of reverse transcription and CA uncoating are probably coordinated events; therefore, maintaining capsid integrity is desirable at least until nuclear entry (Ambrose and Aiken, 2014). Gammaretroviruses, such as MLV, make glycoGag, that stabilizes the capsid and protects the viral genome from apolipoprotein B editing complex (APOBEC3) and nucleic acid sensors in the cytoplasm (Kolokithas et al., 2010; Renner et al., 2018; Stavrou et al., 2015, 2013). Comparably, the HIV-1 capsid core interacts with host proteins CPSF6 and Cyclophilin A (CypA) to shield from nucleic acid sensors such as cGAS (Lahaye et al., 2013; Manel et al., 2010).

Host cell proteins with antiretroviral function and counteracting viral proteins are in constant battle for dominance. The wide variety of host cell proteins and mechanisms dependent on cell type, indicates that there was a need for multiple means of protection and evolutionary pressure to develop them. On the other hand, the retroviruses experience the same pressure to counteract the immune response and replicate in the host cells. This closed circle could be explained by “The Red Queen” hypothesis in evolutionary biology proposed by Leigh Van Valen. The theory proposes a continuous pressure to adapt and evolve in order to persist when competing with opposing also ever-evolving species (Brockhurst et al., 2014; Joop and Vilcinskas, 2016; Van Valen, 1973). The analogy came from Lewis Carroll’s “Through the Looking-Glass”, where the Red Queen said to Alice that one needs to “run” or evolve to remain in the same place and survive.

## 1.6 Experimental systems for visualization of retroviral DNA

Our current knowledge of MLV early replication events comes from bulk analysis, which does not make a distinction between productive and non-productive events. With the development of more advanced imaging techniques, new possibilities arose in the field to allow identification of productive events and characterize infection based on a single

particle level. To do so, specific markers for productive infection were visualized either by IF staining or introduction of fluorescent labels in the protein of interest. Labeling of particles by IF staining posed challenges since not only does this method work under fixed conditions but it heavily depends on the accessibility of the epitope to which the antibody binds. On the other hand, introduction of fluorescently labeled proteins in the virion comes with the risk of losing viral infectivity due to the structural fragility of the viral components. To overcome the limitations posed, a Vpr-trans method was established to visualize HIV-1 viral particles (Desai et al., 2015; Mukherjee et al., 2021). Vpr through its interaction with p6 of Gag is incorporated in the viral particles, therefore fusing a fluorescent protein to the C-terminus of Vpr (Vpr-FP) results in shuttling of a label inside the particle as well (Desai et al., 2015; McDonald et al., 2002; Mukherjee et al., 2021; Muthumani et al., 2000). This method allowed for visualization of viral particles in living cells (McDonald et al., 2002; Mukherjee et al., 2021). Unfortunately, the Vpr-FP is lost from the capsid prior to nuclear entry (Caly et al., 2009; Desai et al., 2015). Instead, a fluorescently labeled IN protein (IN.FP) was developed and used to visualize MLV and HIV-1 particles (Albanese et al., 2008; Borrenberghs et al., 2019; Mukherjee et al., 2021; Quercioli et al., 2016). Moreover, for visualizing MLV particles an additional GFP labeled viral protein, p12-GFP, was developed and utilized for monitoring cellular transport (Pietrantoni et al., 2021). However, the p12-GFP particle production was complemented with MLV wild-type to maintain infectivity (Pietrantoni et al., 2021; Prizan-Ravid et al., 2010). Many of the particles that are imaged are actually trapped in endosomes, therefore labeling of the cellular membrane in addition to the fluorescently fused viral protein is needed for discrimination between successfully fused and trapped subviral particles (Campbell et al., 2007).

To identify actively reverse transcribing particles, imaging methods for labeling of viral cDNA were established. Fluorescent in situ hybridization (FISH) utilizes fluorescently labeled DNA probes which bind to its matching target viral sequence (Chin et al., 2015; Marini et al., 2015; Prizan-Ravid et al., 2010; Roe et al., 1993). This method requires harsh conditions for sample denaturation to enable probe hybridization, which in turn is deleterious to the viral and cellular protein environment resulting in IF staining impairment. To exclude some of these limitations, metabolic labeling of viral cDNA with modified nucleosides was developed. The method is based on incorporation of cell-

permeable nucleoside 5-ethynyl-2'-deoxyuridine (EdU) by reverse transcriptase in the viral genome, which is subsequently ligated to a fluorophore coupled azide using copper-catalyzed azide-alkyne cycloadditions (CuAAC). The copper catalyzed click reaction cannot be performed in living cells due to the strong extraction properties (Peng et al., 2014; Salic and Mitchison, 2008). Moreover, both FISH and metabolic labeling systems are limited to fixed conditions only, thus identification and tracking of cDNA positive viral particles is not possible in living cells.

An alternative method to label specific sequences in living cells utilizing DNA binding proteins from bacterial origin was developed. Well known examples are the Lac or Tet repressor operator systems, based on insertion of bacterial operator arrays in the target sequence that are then bound to fluorescently labeled repressor proteins (Belmont and Straight, 1998; Lucas et al., 2014; Robinett et al., 1996; Roukos et al., 2013). However, the size of these operator arrays is between 5-10 kb which makes them unsuitable for labeling small viral genomes like the ones from MLV (~8kb) or HIV-1 (~11kb). In addition, reverse transcriptase has the propensity to recombine at repetitive sequences which might result in removal of the bacterial operator arrays from the retroviral genome. Therefore, to surpass these limitations a labeling method based on the prokaryotic ParB-ParS chromosomal partitioning system was developed and named ANCHOR (Germier et al., 2017; Saad et al., 2014). This biphasic system consists of the ParB protein (named OR) that will specifically bind to parS seed sequences (named ANCH) introduced in the sequence of interest. The fluorescently labeled OR proteins will oligomerize on the seed sequences and spread to the neighboring sequences yielding a single focus during imaging. Moreover, the size of the ANCH sequences is much smaller than the bacterial operator arrays, ranging from 400-1000 bp which does not severely interfere with viral replication. This method has a binary result, meaning the OR signal is based on whether the sequence is present or not. On the other hand, the incorporation of modified nucleosides allows for the quantification of relative DNA content. Initially, this system was applied to visualization of single genes in mammalian cells (Germier et al., 2017; Saad et al., 2014). Ingeniously, the ANCHOR system was also applied to label and visualize viral DNA of adenoviruses (Komatsu et al., 2018), cytomegaloviruses (Mariamé et al., 2018), HIV-1 (Blanco-Rodriguez et al., 2020; Müller

et al., 2021), baculovirus (Hinsberger et al., 2020) and equine herpesvirus1 (EHV-1) (Quentin-Froignant et al., 2021) in infected living cells.

## 1.7 Aim of the thesis

In the absence of an experimental system to discriminate between productive and non-productive events of MLV, early post entry events are based on bulk analysis and indirect approaches. Therefore, the spatio-temporal and mechanistic understanding of viral DNA synthesis and its release by capsid uncoating are still not well understood. Despite it being possible to image labeled subviral particles utilizing viral fluorescent fusion proteins in living cells, the resulting data lacks information about the reverse transcription status of the MLV virion. On the other hand, experimental systems that are able to identify viral DNA in fixed cells have not been extensively applied to characterize and identify MLV productive particles. Therefore, visualizing the temporal progression of MLV cDNA in living infected cells is essential.

The project focused on three objectives. First objective was to establish and explore different imaging based experimental systems to visualize MLV cDNA and quantitatively assess the relative content in fixed and living conditions. For this purpose, I explored metabolic labeling with modified nucleosides, FISH, and DNA-binding proteins to specific sequences (ANCHOR system). Additionally, the compatibility of these DNA labeling systems was assessed with IF staining of vital viral proteins like CA. Quantitative assessment of relative MLV cDNA content using metabolic labeling proved difficult but understanding of the faults of this system as well as possible improvements was achieved. The ANCHOR labeling system bested the other experimental systems and was used to investigate MLV replication events.

The second major objective was to utilize the ANCHOR labeling system in early post entry infection events. Particularly, to investigate reverse transcription dynamics in relation to capsid uncoating, based on individual viral DNA molecules in living and fixed cells with confocal microscopy. The investigation of reverse transcription was supplemented by molecular virological methods. Moreover, focus was placed on the visualization of viral proteins CA and p12 in the nucleus as well as their association with

MLV dsDNA. The investigation of MLV capsid uncoating was complemented by infectivity experiments performed with a destabilized capsid variant lacking glycoGag. As a subgoal, the association of host cell and viral proteins with nuclear MLV cDNA were analyzed with special interest in the nucleic acid sensor cGAS and a component of the DNA damage response pathway  $\gamma$ H2AX.

The third objective was to visualize MLV cDNA in dividing cells. So far investigation of MLV DNA entry in the nucleus was with the use of cell division inhibitors such as APC. Utilizing the ANCHOR system and fluorescently labeled nuclear envelope expressing cells allowed investigation of the appearance of uncoated MLV cDNA in the nucleus related to the division status of the cell in real time. Moreover, the system provided a unique opportunity to follow daughter cells that retained the viral cDNA previously imaged in the parent cell, thus supporting extensive analysis in the behavior of integrated and non-integrated MLV cDNA.

## 2 Materials and Methods

Table 1 List of Chemicals and Kits

Reagents	Reference	Cat number
Aphidicolin from <i>Nigrospora sphaerica</i>	Sigma-Aldrich	A0781
Azidothymidine (AZT)	Sigma-Aldrich	A2169
Raltegravir (Ral)	AIDS Reagent Program, NIAID	ARP-11680
Click-iT EdU Alexa Fluor 647 Imaging Kit	Thermo Fisher Scientific	C10340
NEBuilder® HiFi DNA Assembly Master Mix	New England Biolabs	E2621L
SNAP-Cell® 647-SiR	New England Biolabs	S9102S
TURBO DNA-free™ Kit	Thermo Fischer Scientific	AM1907
5-Ethynyl-dUTP (5-EdUTP)	Jena Bioscience	Jena Bioscience
Alexa Fluor™ 647-aha-dUTP	Thermo Fischer Scientific	A32763
dATP	Thermo Fischer Scientific	R0141
dCTP	Thermo Fischer Scientific	R0152
dGTP	Thermo Fischer Scientific	R0161
dTTP	Thermo Fischer Scientific	R0171
Efavirenz (EFV)	Sigma-Aldrich	SML0536
Deoxyribonuclease I from bovine pancreas	Sigma-Aldrich	DN25
Nucleospin gel and PCR Cleanup Kit	Macherey Nagel, Germany	740609.50
NucleoBond PC 500, Maxi kit	Macherey Nagel, Germany	740574.50
Random primer set for qRT-PCR	Invitrogen	48190011
ddPCR GEX HEX Assay 1000R Rpp30, Mouse.	BioRad	10031259
MLV Reverse Transcriptase	200 000 U/ml; BioLabs New England;	M0253S
Recombinant MLV p30 protein	Icosagen	P-500-100

Table 2 List of Antibodies and Staining Dyes

Reagents	Reference	Comments
Rat monoclonal anti MLV CA	(Chesebro et al., 1983; Wanaguru et al., 2018); hybridoma cell line R187 ATCC®-CRL1912™	1:600
Rabbit polyclonal anti MLV CA	Icosagen, Cat# A1-910-100	1:600 for IF 1:1000 for WB
Rabbit polyclonal anti MLV p12	Cambridge Research Biochemicals; Cat# crb2005300 (Wanaguru et al., 2018)	1:1000
Rabbit monoclonal anti γH2AX (20E3)	Cell Signaling Technology; Cat# 9718S	1:600
Hoechst33258	Merck, Cat#: 94403	1:1000
Mouse monoclonal anti cytochrome C	BD Biosciences, Cat# 556432	1:1000
Goat anti Lamin A/C (N-18)	Santa Cruz Biotechnology, Cat#sc-6215	1:200
Rabbit monoclonal anti cGAS (D3080)	Cell Signaling technology, Cat#31659	1:200
Rabbit polyclonal anti-HIV-1 CA	In-house; Bejarano et al. (2019)	1:1000
Goat/donkey polyclonal Alexa Fluor (405, 488, 568, and 647) secondary antibodies	Thermo Fisher Scientific	1:1000

Table 3 List of plasmids

Reagent	Reference	Comments
pNCA	(Colicelli and Goff, 1988), Addgene#17363	Proviral molecular clone of MLV
pNCA-gg	(Colicelli and Goff, 1988; Pizzato, 2010), gift from Prof. Stefan Bauer (Institute for Immunology, Philipps-University Marburg)	Proviral molecular clone of MLV with nucleotide change on the CUG start codon to CA, thus introducing a frameshift.
pNCS	(Yueh and Goff, 2003), Addgene#17362	Proviral molecular clone of MLV with SV40 replication origin
pMLV-gag-pol-EGFP	(Quercioli et al., 2016)	Packaging plasmid for expression of eGFP-labeled IN
pMLV-gag-pol-IN.SNAP	(Quercioli et al., 2016), this thesis	Packaging plasmid for expression of SNAP-labeled IN
pNNHIV (pNLC4-3 IN <sub>D64N/D116N</sub> tat <sub>Δ33-64bp</sub> )	(Zila et al., 2021)	Integration and transcription deficient HIV-1 proviral plasmid; suitable for S2 work
pVprIND64N/D116N.SNAP	(Müller et al., 2021)	Expression of SNAP-labeled, catalytically dead HIV-1IN
pVpr-IN.SNAP	(Müller et al., 2021)	Expression of SNAP-labeled HIV-1IN
ANCHOR system	NeoVirTech (France)	dsDNA visualization system
pNCA ANCH	this thesis; unpublished	MLV proviral plasmid with ANCH3 within env
pNCS ANCH	this thesis; unpublished	MLV proviral plasmid (SV40 replication origin) with ANCH3 within env gene

pNNHIV ANCH	(Müller et al., 2021)	NNHIV with ANCH3 within <i>env</i> gene
pWPI eGFP.OR3 IRES puro	(Müller et al., 2021)	Lentiviral transfer plasmid with eGFP.OR3
pWPI mScarlet OR3 IRES puro	(Müller et al., 2021)	Lentiviral transfer plasmid with mScarlet
pWPI ANCH	(Müller et al., 2021)	Lentiviral based plasmid with ANCH3
pWPI eBFP2. mLMNB1 IRES BLA	(Müller et al., 2021), this thesis	Lentiviral transfer plasmid containing murine Laminb1 labeled with eBFP2
psPAX2	(Pfisterer et al., 2011), Addgene#35002	Lentiviral packaging vector
pAdvantage	Promega, Cat#E1711	Vector enhancing transient protein expression
pCMV-VSV-G	(Stewart et al., 2003), Addgene#8454	Expression of VSV-G
pcDNA3.1 <sup>(+)</sup>	ThermoFisher Scientific, Cat#V79020	Mammalian expression vector

---

Table 4 List of Cell lines

Reagents	Reference	Comments
Embryonic kidney 293 T cells (HEK293T)	(Pear et al., 1993)	Human cell line for viral particle production
MEF	this thesis; in collaboration	Immortalized murine embryonic stem cells
MEF KO TREX-1	this thesis; in collaboration	Immortalized murine embryonic stem cells with knockout TREX-1
SC-1	(Hartley and Rowe, 1975)	Murine fibroblast cells
SC-1 eGFP.OR3	this thesis	Polyclonal cell line expressing eGFP.OR3
SC-1 eGFP.OR3 eBFP2.mLMNB1	this thesis	Polyclonal cell line expressing eGFP.OR3 and eBFP2.mLMNB1
MEF eGFP.OR3	this thesis	Polyclonal cell line expressing eGFP.OR3
MEF eGFP.OR3 eBFP2.mLMNB1	this thesis	Polyclonal cell line expressing eGFP.OR3 and eBFP2.mLMNB1
MEF KO TREX1 eGFP.OR3 eBFP2.mLMNB1	this thesis	Polyclonal cell line expressing eGFP.OR3 and eBFP2.mLMNB1
MEF mScarlet.OR3	this thesis	Polyclonal cell line expressing mScarlet.OR3

Table 5 List of Software and Code

Reagents	Reference	Comments
Fiji 1.53c	(Schindelin et al., 2012)	Image analysis
Icy 2.0.3.0	(de Chaumont et al., 2012)	Image analysis, spot detection and intensity-based co-localization
Prism v9.4.1	GraphPad Software Inc	Data visualization and plotting
Imaris 9.7.2	Bitplane AG	Image analysis; spot detection, intensity-based co-localization
Volocity 6.3	Perkin Elmer	Image data acquisition
CSBdeep 0.4.1	(Weigert et al., 2018)	AI based signal restoration
NIS elements AR Analysis 5.21.0.	Nikon Instruments Inc.	Image analysis
AutoQuantX3.1	Media Cybernetics, Inc.	deconvolution
MathWorks	(Börner et al., 2010)	MatLab script for semi-automated quantification of infected cells
QuantaSoft™ v1.6	BioRad, Catalog#1863007	Real-time PCR data collection and analysis
UCSF ChimeraX	(Pettersen et al., 2021)	Visualization of protein structures
ChemDraw	Perkin Elmer, <a href="#">ChemDraw software</a>	Drawing of chemical structures
BioRender	<a href="#">Biorender.com</a>	Scientific schematics
Image Studio™ Lite 5.0	Li-COR Biosciences	Immunoblot acquisition and analysis

Table 6 List of primers

Primer	sequence	Comments
ddMLVgagfp	AAATGGTGGAGAAGCGACCC	forward primer, gag cDNA quantification by ddPCR
ddMLVgagr	TGAAGCTGTCCGTTTCCTCC	reverse primer, gag cDNA quantification by ddPCR
ddMLVgagprobe	AGGCACCGGACCCCTCCCCA ATGGCAT	5'FAM 3'BHQ1 probe, gag cDNA quantification by ddPCR
ga_m_lamin100fp	TAAACTACGGGCTGCAGGAA	linearize pWPI vector excluding human LaminB1
ga_m_lamin101rp	CTCGAGATCTGAGTCCGGAC	linearize pWPI vector excluding human LaminB1
ga084	CAAGTTGACCCTGTCCGAAG(Weigert et al., 2018)	Linearize pcDNA3.1 containing MLV env
ga085	TTAGACTTGATGAGGACTGG AGC	Linearize pcDNA3.1 containing MLV env
15TM153Snap2577f4	gagatccaccggtcgccaccATGG ACAAAGACTGCGAAATGAAGC	The SNAP-Tag gene was amplified with overlap in MLV-gag-pol-EGFP
16TM153Snap3119r3	ctagagtgcgcccgtttaCAGCC CAGGCTTGCC	The SNAP-Tag gene was amplified with overlap in MLV-gag-pol-EGFP
11M.INgfp6609rp	GGTGGCGACCGGTGGATC	Linearize MLV-gag-pol-EGFP excluding eGFP
12TM.INgfp7327fp	TAAAGCGGCCGCGACTCTAG	Linearize MLV-gag-pol-EGFP excluding eGFP

## 2.1 Generation of Plasmids

All plasmids were cloned using standard cloning techniques and were verified by Sanger sequencing (Eurofins Genomics, Germany or Microsynth Seqlab GmbH, Germany). Gibson assembly was applied in generating the plasmids with NEB HiFi Mastermix (New England Biolabs, USA) with ~20-35bp overlapping regions. The primers were ordered from Eurofins Genomics. The PCRs were performed with 1unit/50 $\mu$ L Q5 High-Fidelity DNA polymerase (New England Biolabs). The plasmids containing LTRs were amplified by Stbl2, and standard plasmids were amplified by *E. coli* DH5 $\alpha$ .

### 2.1.1 pNCA ANCH and derivatives

To construct a proviral MLV plasmid containing ANCH3, a more simplified cloning procedure was designed. A sequence fragment containing the *env* gene was subcloned from pNCA into pcDNA3.1<sup>(+)</sup> using SphI/PciI. The ANCH3, ~1000 bp, was amplified from pANCH3 (NeoVirTech, France) with sequences overlapping the *env* gene and a stop codon upstream of ANCH3. The ANCH3 fragment was then introduced in the *env* gene of a PCR linearized pcDNA3.1<sup>(+)</sup> using Gibson Assembly. With the introduction of ANCH3, 1000bp were deleted within the N-terminal region of *env*, thus the size of the plasmid remains the same. Lastly, the modified envelope fragment with ANCH3 sequence was then introduced in NCA and NCS backbones using SphI/PciI creating pNCA ANCH and pNCS ANCH.

### 2.1.2 pMLVgag-pol-IN.SNAP

To generate packaging plasmid for expression of fluorescently labeled IN that is compatible with the ANCHOR system, the GFP in the already published pMLV-gag-pol-EGFP plasmid (Quercioli et al., 2016) needed to be exchanged for SNAP-Tag. Using Gibson assembly, the eGFP gene was substituted for the coding sequence of SNAP-tag amplified from pVpr.IN.SNAP.

### 2.1.3 pWPI eBFP.mLMNB1

The aim was to generate a lentiviral transfer vector for transduction of cells to express eBFP2 tagged murine Laminb1. To construct the plasmid, the pWPI plasmid containing eBFP2.LMNB1 was linearized without the human *Laminb1* (LMNB1) gene. A synthesized murine LMNB1 sequence with 75 bp overhangs was ordered (Integrated DNA Technologies, Germany) and assembled into the pWPI eBFP.2 lentivector using Gibson Assembly to generate pWPI eBFP.2 murine LMNB1 (m. LMNB1) lentiviral vector.

## 2.2 Cell and tissue culture

Cells were cultured in humidified incubators at 37°C and 5% CO<sub>2</sub> in Dulbecco's Modified Eagle's Medium (DMEM; Thermo Fisher Scientific) containing 4.5 g l<sup>-1</sup> D-glucose and L-glutamine supplemented with 10% fetal calf serum (FCS; Sigma Aldrich, USA), 100 U/ml penicillin and 100 µg/ml streptomycin (PAN Biotech, Germany). The cells were regularly monitored for mycoplasma contamination using MycoAlert mycoplasma detection kit (Lonza Rockland, USA). The maintained cells are SC-1, MEF, MEF KO TREX1, HEK 293T and their respectively expressing stable cell lines.

### 2.2.1 Isolation of MEF cells and their immortalization

The isolation and immortalization of the MEF cell lines were done in collaboration with several members of University Hospital Heidelberg and German Cancer Research Center (DKFZ). First, fifteen embryos of wild-type and KO TREX1 C57BL/6 mother mice were isolated and cultured by Dr. Bettina Stolp and Dr. Julia Welsch (University Hospital Heidelberg, Fackler and Ruggieri research groups). The Embryos were genotyped and their wild-type and TREX1 knockout status was confirmed. The MEFs were then isolated from the embryos and immortalized with SV40 LT by Dr. Bruno Galy and Dr. Michael Bonadonna (German Cancer Research Center, Galy research group). The genotyping of the immortalized MEF wild-type and KO TREX1 was confirmed by an immunoblot with antibodies against TREX1 and control proteins β-Actin and Tubulin, done by Dr. Julia Welsch (University Hospital Heidelberg, Ruggieri research group).

## 2.2.2 Lentiviral vector transduction

HEK 293T cells were seeded in a 6 well plate with density of  $4 \times 10^5$  cells per well. The following day, the cells were co-transfected via polyethylenimine (PEI; 3  $\mu$ l of 1 mg/ml PEI per 1  $\mu$ g DNA) with packaging vector psPAX2, lentiviral transfer vector pWPI carrying either eGFP.OR3 or eBFP2.mLMNB1, pAdvantage and envelope expression plasmid pCMV-VSV-G in ratio of 1.5: 1: 0.2: 0.5  $\mu$ g. The pWPI vectors carried either blasticidin or puromycin resistance genes. The supernatant was harvested and filtered (MCE filter 0.45  $\mu$ m) 48 h post transfection. The supernatants were frozen in aliquots of 500  $\mu$ l.

SC-1 or MEFs were seeded in 12 well plates with density  $5 \times 10^4$  cells/well and transduced the next day with 500  $\mu$ l supernatant containing lentiviral particles with eGFP.OR3 and puro resistance. After 48 h post transduction the eGFP.OR3 expressing cells were FACs sorted (MEFs) or selected with 2 $\mu$ g/ml puromycin (SC-1). The cells were then transduced again with 500  $\mu$ l supernatant containing lentiviral particles with eBFP2.mLMNB1 and blasticidin resistance. Lastly, the cells were selected after 48h with 5 $\mu$ g/ml and 7.5  $\mu$ g/ml blasticidin in MEFs eGFP.OR3 and SC-1 eGFP.OR3 respectively. The resulting SC-1 and MEFs cell lines were stably expressing eGFP.OR3 and eBFP2.mLMNB1.

## 2.3 Virus particle production and quantification of titer

### 2.3.1 Viral production

Large-scale virus production was achieved in T175 flasks seeded with HEK293T cells with approx. 60-70 % confluency on the day of transfection. The cells were co-transfected via calcium phosphate with proviral DNA (pNCA/ pNCA-gg /pNCS ANCH/ pNNHIV/ pNNHIV ANCH/ pWPI ANCH) and if required with envelope expression plasmid pCMV-VSV-G in a ratio of 9:1  $\mu$ g (70  $\mu$ g per T175cm flask). To produce particles with fluorescently labeled IN, the cells were transfected with proviral DNA (pNCA ANCH or pNNHIV ANCH), packaging plasmid for expression of FP-labeled IN (pMLVgag-pol-IN.SNAP or pVpr-IND64N/D116N.SNAP), and envelope expression plasmid (pCMV-VSV-G) in ratio of 7.7: 1.3: 1  $\mu$ g (total of 70  $\mu$ g per T175cm flask). The cells were then

incubated with calcium phosphate and plasmid mix for 6-8h before removing and adding fresh media. The supernatant was harvested after 48h and filtered with MCE filter 0.45  $\mu\text{m}$ , which was subsequently then loaded on a sucrose (20% w/w) cushion and ultracentrifuged (2h at 4°C with speed of 107,000 x g). The pellet was resuspended in phosphate-buffered saline (PBS) containing 10% FCS and 10 mM HEPES (pH 7.5). The virus stocks were then stored at -80°C.

### 2.3.2 SG-PERT assay

The virus was quantified by SYBR Green based Product Enhanced Reverse Transcription Assay based on self-made standard using supernatant of pNCA transfected HEK293T cells and normalized to a commercially bought MLV Reverse Transcriptase (Biolabs New England, GER; 200 000 U/ml).

### 2.3.3 Infectivity assays

The assays to determine infectivity of viral particles preparation was performed in both SC-1 and MEF cell lines. The assays were based on gag expression by IF staining with antibodies raised against MLV CA in dilution 1:600 (hybridoma cell line R187 ATCC®-CRL1912™, rat anti p30 or commercially bought from Icosagen, rabbit anti p30). The cells were seeded in 15 well ibidi  $\mu$ -Slide angiogenesis with  $3.3 \times 10^3$  cells/well or in black 96-well plates (Costar, Cat#3606) with  $8.0 \times 10^3$  cells/well. The next day, the viral particle stock was titrated on cells followed by fixation at 48 h p.i. and IF staining for CA protein. The 15 well ibidi  $\mu$ -Slide angiogenesis dishes were imaged with the SDCM with 20x oil objective and the 96 well plates were imaged with a semi-automated high-throughput wide-field Olympus IX-81 inverted microscope with the 10x air immersion objective. In 5-9 random FOVs, the number of infected and non-infected cells were counted. Non-infected cells were imaged as well and used to set a threshold based on background CA intensities for the quantification of infection. The cells were counted with a Fiji plugin CellCounter in the images acquired with the SDCM or with a MatLab script (Börner et al., 2010) with the images acquired by the Olympus IX-81. Furthermore, the number of infectious units (IU/ml) was calculated by multiplying the percentage of

infected cells detected with the number of cells per well (double of the seeded cell number the day before infection) then divided by the volume of virus suspension used for infection. With the formula below the multiplicity of Infection (MOI) was calculated:

$$MOI = \frac{IF}{ml} \times \frac{\text{virus volume}}{\text{total cell number}}$$

#### 2.3.4 Immunoblotting

Concentrated wild-type and minus glycoGag particles were lysed for 10 min at 95°C in 3x SDS buffer (150 mM Tris-HCl, 30% glycerin, 0.06% bromophenol blue, 20% β-mercaptoethanol and 6% SDS). The samples were run on a 10 x 10 x 0.2 cm 15% SDS-PAGE gel in Laemmli buffer for 1 h at 100 V and 400 mA, followed by semi-dry blotting (0.8 mA/cm<sup>2</sup>) to a nitrocellulose membrane for 1h. The membrane was blocked with Odyssey blocking buffer (Li-COR Bioscience, 1:4 predilution) for 15 min at room temperature. The primary antibody against CA protein (rabbit polyclonal anti p30, 1:1000) was incubated with the membrane overnight at 4°C. The membrane was then washed with PBS and the secondary antibody anti rabbit 800CW (1:10 000; Li-COR Biosciences) was incubated for 1h at room temperature. After washing the blot was scanned and quantified by Li-COR Odyssey Clx infrared scanner with the Image Studio lite software 5.0 (Li-COR Biosciences). A capsid standard was tittered and blotted (Icosagen; 10, 20, 40 ng) to quantify the absolute CA amounts of the viral particles.

#### 2.4 Endogenous reverse transcription (ERT) reaction

MLV wild-type and NNHIV IN.SNAP particles were incubated in an ERT buffer added as 5x concentrate, which contained 10mM Tris-HCl (pH 7.6), 150mM NaCl, 1 mM MgCl<sub>2</sub>, 400μM dCTP, 400μM dGTP, 400μM dATP, 0.05% Triton X-100. The 5x concentrate was also supplemented with 100μM of modified dUTP. The particles and modified dUTP nucleoside containing 5xERT buffer were incubated overnight at 37°C (total sample volume of 10μl). Modified nucleosides used were EdUTP (Jena Biosciences) and Alexa Fluor™ 647-aha-dUTP (Thermo Fischer Scientific). In addition, the ERT reaction was

blocked by the addition of 100  $\mu$ M of AZT for MLV particles. The sample was diluted in 150  $\mu$ l of PBS containing 100  $\mu$ M EDTA and added to a PEI (1mg/ml) coated 8 well LabTek imaging dish. After 40-60 min of incubation at room temperature, the samples are fixed, permeabilized, click labeled and immunostained against MLV or HIV-1 CA protein. The CuAAC was performed with the EdUTP samples using the Click-iT EdU Alexa Fluor 647 Imaging Kit. The image analysis was done with the Icy spot detector to score co-localization of modified nucleoside signals with the CA signals.

## 2.5 Infection, treatment and staining of cells

### 2.5.1 Infection of MEFs and SC-1 with wild-type and minus glycoGag variant

SC-1, MEF wild-type and MEF KO TREX1 were seeded in 96-well plates with density of  $8.0 \times 10^3$  cells/well and infected with 219 RT  $\mu$ U/cell. The cells were infected with normalized input of wild-type or minus glycoGag variants according to RT Units measured prior to infection with SG-PERT assay.

### 2.5.2 Infection of eGFP.OR3 eBFP2.mLMNB1 expressing cells with ANCH viruses

MEFs or SC-1 cells expressing eGFP.OR3 eBFP2.mLMNB1 were seeded in 15-well  $\mu$ -slides angiogenesis dishes with a density of  $3.3 \times 10^3$  cells/well. The cells are infected the next day with MLV ANCH VSV-G particles, 822  $\mu$ U RT/cell in 50  $\mu$ l total volume, which corresponds to  $\sim 6.3$  MOI. Infection of MEF cells with MLV ANCH IN.SNAP VSV-G uses significantly lower particle concentration of 66  $\mu$ U RT/cell, attributed to transfection with the 3-plasmid system resulting in low particle yield. Prior to infection, the particle stocks were also incubated with 2  $\mu$ M of SNAP-Cell® 647-SiR for 30 min at 37°C. Whereas infection of SC-1 and MEFs with NNHIV ANCH VSV-G and pWPI ANCH VSV-G used 30  $\mu$ U and 42  $\mu$ U RT/cell respectively. Lastly, in the live imaging experiments the SC-1 cells were infected with higher particle concentration of 2000  $\mu$ U RT/cell corresponding to 19.5 MOI.

### 2.5.3 Cell division, RT, and integration inhibitors

In experiments using aphidicolin (Sigma-Aldrich) to block cellular division, the drug was added during cell seeding at concentration of 1 $\mu$ M and 2 $\mu$ M in MEF and SC-1 respectively. Aphidicolin was incubated overnight and kept throughout infection. AZT (Sigma-Aldrich) with concentration of 100 $\mu$ M was also added to MLV viral particles in the ERT experiment to block reverse transcription. Raltegravir (AIDS Research and Reference Reagent Program, Division AIDS, NIAID), an integration inhibitor of MLV and HIV-1, was added to cells together with the viral particles in concentration of 10 $\mu$ M.

### 2.5.4 Fixation, extraction and IF staining

Cells were washed with PBS and fixed with 4% PFA for 10 min followed by three washes with PBS. Next, the samples were permeabilized with 0.5% Triton X-100 for 10 min. In indicated experiments after permeabilization and three washes with PBS, the samples were extracted with ice-cold MeOH for 5 min. The samples are then washed three times with 3% BSA/PBS and incubated with rat anti CA (CRL-1912, ATCC; 1:600) and rabbit anti p12 (Cambridge Research Biochemicals; 1:1000) in 0.5% BSA/PBS for 1h at room temperature. After washing three times with 3% BSA/PBS, the secondary antibody was added in 0.5% BSA/PBS for 1 hr. at room temperature. Lastly, the samples were washed and stored in PBS at 4°C.

### 2.5.5 Labeling of viral cDNA with modified nucleosides in cells

SC-1 cells were incubated with 6  $\mu$ M of APC overnight. The following day 10 $\mu$ M EdU (component from Click-iT EdU Alexa Fluor 647 Imaging Kit; Thermo Fisher Scientific) was added at time of infection. The cells were fixed at 24 h p.i. as detailed in section 2.5.4., followed by click labeling using a copper-catalyzed azide-alkyne 1,3-dipolar cycloaddition provided in the Click-iT EdU-Alexa Fluor 647 Imaging Kit (Thermo Fisher Scientific). The click labeling was performed according to the manufacturer's instructions with incubation of the click mix for 30 min at room temperature prior to immunostaining. The cells were washed with PBS and immunostained with antibodies

raised against MLV CA and cytochrome C. The complete IF staining protocol was performed as detailed above (*cf.* 2.5.4).

#### 2.5.6 DNA FISH staining

The experiment was performed in collaboration with Dr. Mia Lusic (University Hospital Heidelberg). The probes targeting MLV DNA were generated with Nick translation kit (Roche) and purified with Illustra Microspin G-25 columns (GE Healthcare). The probes are based on the plasmid DNA from the proviral plasmid pNCA. The generated labeled probes are then precipitated by treatment of ethanol, human Cot-I DNA (Roche) and herring sperm DNA (Sigma Aldrich). The precipitated probes were resuspended in 10 $\mu$ l formamide at 37°C for ~20 min, followed by addition of 10 $\mu$ l of dextran/4x saline - sodium citrate (20%; SSC) buffer.

SC-1 cells were seeded in 24-well plate with density of  $1.0 \times 10^5$  cell/well and infected the next day with MLV wild-type 1000  $\mu$ U RT/cell. The cells were fixed with 4% PFA for 10 min at 6, 12 and 48 h p.i., followed by permeabilization with 0.5% Triton X-100/0.1% Tween in PBS for 10 min. The slides were then washed with 0.1% Tween/PBS and the primary antibodies against MLV CA and Lamin A/C in 1% BSA/PBS were incubated overnight at 4°C. The samples were once more washed with 0.1% Tween/PBS and followed by incubation of the secondary antibodies in 1%BSA/PBS for 1 h at room temperature. The cells were fixed using 0.5 mM ethylene glycolbis succinimidyl succinate (EGS) in PBS. After the fixation, the sample was washed with 0.1% Tween/PBS, and the cells were permeabilized with 0.5% Triton X-100 and 0.5% saponin for 10 min. The samples were then added in 20% glycerol/PBS for 1h, followed by 5-6 times freezing and thawing of the cells in glycerol/liquid N<sub>2</sub>. The sample was washed in PBS followed by denaturation in 0.1M HCl for 10 min, addition of 2x SSC for 20 min and addition of hybridization buffer consisting of 50% formamide in 2x SSC for 30 min. Next, the sample was washed and partially digested with 0.002% pepsin/0.01 M HCl for 3 min at 37°C. The digestion is stopped with the addition of 1M MgCl<sub>2</sub>/PBS. The samples are fixed once more using 4% PFA, washed with PBS, followed by RNA digestion for 30 min at 37°C with 100 $\mu$ g/ml Purelink RNaseA (Invitrogen) in 2xSSC buffer. The samples are washed with PBS and stored in hybridization buffer overnight. The probes are denatured

for ~10 min at 95°C and 5  $\mu$ L was added to the slides. The slides are sealed in a metal chamber and denatured for 5-7 min at 80°C. The metal chamber is then transferred to 37°C incubator for 48hr, where the probes are slowly annealing to the sample. Next, the sample is washed with 2x SSC at 37°C, and three times with 0.5x SSC at 56 °C. Lastly an anti-biotin antibody was incubated and detected using the secondary antibodies from TSA plus Kit (Perkin Elmer). Afterwards, the sample was stained with Hoechst and the coverslips were mounted and imaged with SDCM.

## 2.6 Imaging systems

### 2.6.1 Spinning disk confocal microscopy

All images from the fixed experiments were acquired using the Perkin Elmer Ultra VIEW VoX 3D spinning disk confocal microscope (Perkin Elmer, USA). 3D stacks of 10-30 random positions of infected cells or immobilized particles with a z-spacing of 0.2-0.5  $\mu$ m per sample were imaged using the oil immersion 60x objective. In infectivity gag-based assays the oil immersion 20x objective was used. The equipped lasers/filter sets utilized for recording are: blue 405/420-460 nm (Hoechst/DAPI, Alexa 405), green 488/510-540 nm (Alexa488, eGFP), red 568/589-625 nm (Alexa568, mScarlet) and far-red 647/665-705 nm (Alexa 647, SiR).

### 2.6.2 Live imaging

Prior to imaging the cells, they are cultured in FluoroBrite DMEM Imaging medium (Thermo Fischer Scientific) supplemented with 10% FCS, 100 U/ml penicillin, 100 $\mu$ g/ml streptomycin, 4mM GlutaMAX (Gibco Life Technologies), 20 mM Hepes pH=7.4 and 2mM sodium pyruvate (Gibco Life Technologies). The inverted microscope Nikon ECLIPSE T12 (Nikon, JPN) contains a spinning disk unit from Yokogawa (CSU-W1, Nikon), emission light detector with two EMCD cameras (Andor, Oxford Instruments; iXon DU-888) and humid incubation chamber which maintains 37°C and 5% CO<sub>2</sub>. The cells were placed in the incubation chamber kept at conditions and imaged with the 100x oil-immersion objective (Nikon CFI Apochromat TIRF, NA 1.49). 3D stacks of 10

positions with z-spacing of 0.5  $\mu\text{m}$  were recorded every 30 min for a time frame of 48 h with the automated stage controlled by Nikon Imaging Software Elements v5.02. The acquisition laser power and exposure were set to minimum to protect the samples from cytotoxicity.

## 2.7 Image analysis and visualization

### 2.7.1 Noise filter, deconvolution, and signal restoration software application in image processing

Infected cells with ANCHOR viruses induced formation of eGFP.OR3 signals with moderate signal to noise ratio. After subtracting of the camera background, the noise observed in the raw images was reduced with a mean filter of 1-2 pixel kernel size using Fiji (Schindelin et al., 2012). Furthermore, the Content-aware image restoration (CARE) software (Weigert et al., 2018) was used to denoise and reconstruct the eBFP2.mLMNB1 signals of acquired images from live microscopy experiments (Müller et al., 2021). The software was trained on a set of images recorded with high laser power and exposure compared to recorded images with low laser power and exposure, which produced an example how the noisy images should be reconstructed using the python toolbox CBSdeep (Weigert et al., 2018). The model was then used to reconstruct and enhance the eBFP2.mLMNB1 in images taken during live imaging with low laser power/short camera exposure using the CBSdeep CARE plugin. Furthermore, the raw images of the eGFP channel from the live imaging experiments were deconvolved using AutoQuantX3 (Meyer Instruments Inc).

### 2.7.2 Manual analysis of eGFP.OR3 signals with Fiji

Detection of eGFP.OR3 foci was performed manually and scored only if the intensity was  $\geq 20\%$  and  $\geq 180\%$  above the background diffuse expression level of the respective cell measured with the line profile in Fiji, in fixed and live imaging experiments respectively. Furthermore, the co-localization of eGFP.OR3 foci with viral and host proteins were scored with the profile tool in Fiji. The signals are considered to co-

localize only when the pixel area of the signals overlap. The co-localization of IF detected cGAS,  $\gamma$ -H2AX, p12 and/or CA with eGFP.OR3 was scored in this manner.

### 2.7.3 Labeling efficiency of viral DNA with EdUTP on immobilized particles with Icy

The total number of particles were detected by the Icy software with the spot detector based on CA signals. The background mean signal intensity of EdUTP was measured on 3 randomly drawn rectangles per biological replicate where no particles were detected. The measured mean background was subtracted from the EdUTP channel, and a manual threshold was set according to visual inspection ( $t=2000$  a.u.) In the same positions of the identified CA objects, the mean EdUTP signal intensities were measured. The EdUTP signals above the threshold were scored to be particles containing labeled viral DNA.

### 2.7.4 Semi-automated 3D quantification with Imaris

The co-localization of viral proteins in infected cells and immobilized particles were scored with the help of Imaris 9.2 software (Bitplane AG, SUI). The infected cell volume as well as the particle signals were 3D reconstructed using the z-slices and the spot detector module from Imaris, respectively. The 3D objects, with 300 nm diameter in x-y and 600 nm in z dimension, were based on the detected p12 IF or the IN.SNAP signal. The threshold for detection of p12 or IN.SNAP remained the same per biological replicate. The background of CA IF was measured in non-infected cells with 3 randomly drawn rectangles in 3 images per biological replicate, and subsequently subtracted from infected cells prior to analysis. The mean signal intensity in the CA channel was detected within all the p12 or IN.SNAP generated objects. A threshold was set to identify real CA signal for each biological replicate, marginally adjusted per cell. To determine the particle localization within the cell, the eBFP2.LaminB1 mean signal intensities were used to classify NE-associated objects with a threshold range of  $t= 100-300$  a.u. All other particles are classified to be in the cytoplasm with the help of the diffuse expression level of the eGFP.OR3 to outline the cell.

### 2.7.5 Data visualization and statistical analysis

Data was solely visualized using Prism v9.1.0 (GraphPad Software Inc, USA) except for the graphical representation of cell division of daughter cells (Figure 27B) and their eGFP.OR3 foci appearance (Figure 30F) which used the online tool BioRender. Violin plots are overlaid with point plots. Information about datapoints, error bars, and mean or median values are found in the figure legends. Statistical analysis was done using a two-tailed Student's t-test with Prism.

### 2.8 Quantification of RT products using ddPCR

The virus preparation was done as described in section 2.3.1., except for the treatment with DNase I. The treatment was done either on the filtered supernatant with 20 units/ml of Dnase I from bovine pancreas (Sigma Aldrich) for 2 h at 37°C before ultracentrifugation or 1h with the TURBO DNase Kit (1 U of Turbo Dnase per 10µl virus; TURBO DNase, Thermo Scientific) for the concentrated resuspended viral particles (Diehl et al., 2008; Wang et al., 2016). SC-1 cells expressing eGFP.OR3 eBFP2.mLMNB1 were seeded in 24 well plate with density of  $5 \times 10^4$  per well and infected the next day with MLV ANCH VSV-G using (55 µU RT/cell, 25 ±11% infected cells). Furthermore at 4, 8, 24 and 48 h p.i. the cells were washed, scraped, and lysed with 50µl of 10 mM Tris-HCl pH 9.0, 0.1% TX-100, 400 µg/mL proteinase K (Thermo Fisher Scientific) at 55°C overnight. The Proteinase K was inactivated at 95°C for 10 min and lysates were stored at -20°C. The diluted (1:12) lysates were directly used as input for ddPCR. The droplets were generated using the QX200 droplet generator/reader (BioRad, USA) and the analysis was done with QuantaSoft v1.7.4 (BioRad, USA) (Bejarano et al., 2018; Müller et al., 2021; Zila et al., 2019). *Gag* viral cDNA and *housekeeping ribonuclease P protein subunit p30 (rpp30)* cDNA was detected. The detected *gag* copies per cell were normalized with the detected housekeeper gene *rpp30*.

## 3 Results

---

### 3.1 Experimental system establishment for characterization of infection with MLV wild-type and destabilized capsid variants

#### 3.1.1 Assay establishment for virus production, characterization of viral titer and infectivity of MLV

To investigate MLV replication, experimental systems were established for viral particle production, particle yield assessment and infectivity characterization. Initially, large-scale lentiviral particle production was adapted, which uses calcium phosphate mediated transfection of immortalized human embryonic kidney (HEK293T) cells, for MLV particle production (Dudek et al., 2001; Graham and van der Eb, 1973; Kwon and Firestein, 2013). The reverse transcriptase activity of a viral preparation was used as a surrogate measure to determine the particle number in concentrated or in supernatant of virus producing cells (Pizzato et al., 2009). Therefore, to test the yield of the MLV virus particle preparation a SYBR green I-based real-time enhanced reverse transcriptase assay (SG-PERT) was established (Pizzato et al., 2009). MLV reverse transcriptase standard was prepared, by quantifying the RT units of filtered supernatant from MLV producing transfected HEK293T cells using fully functional purified MLV RT (200,000 units/ml, NEB, Germany). The SG-PERT assay was then used together with this MLV standard to determine the particle yield of all MLV viral particle stocks in this project. Furthermore, the analysis of SG-PERT measurements of 6 independent viral particles stocks showed a reproducible yield of  $1.20 \pm 1.41 \times 10^{11}$  pU RT/ $\mu$ l (Figure 7A).

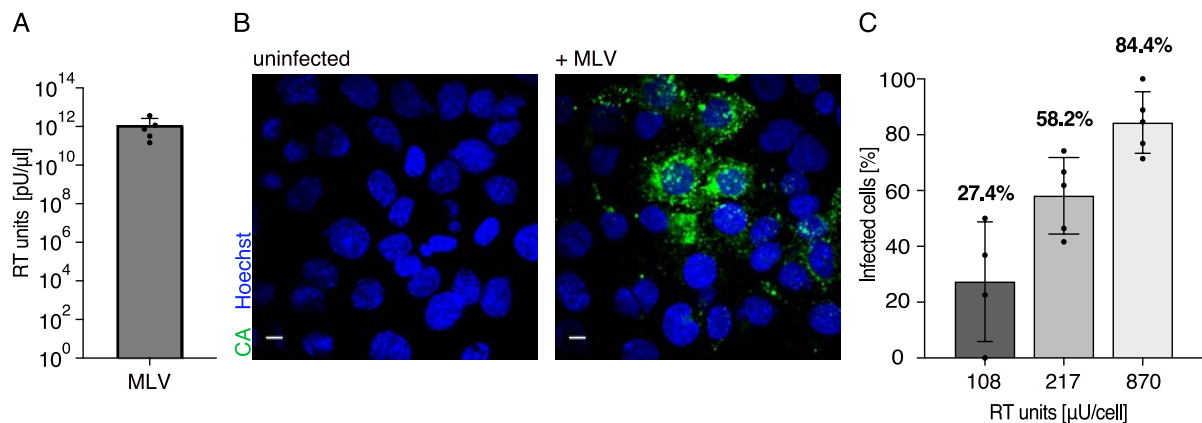


**Figure 7. Establishment of experimental systems to quantify MLV particle yield and infectivity.** A. The supernatant of MLV producing HEK293T cells transfected with pNCA was filtered and concentrated at 48 hours post transfection (h p.t.). The particle yield was compared to in-house MLV RT standard and subsequently quantified by the SG-PERT assay. The graph shows mean value and SD from 5 independent experiments. B. Representative images of uninfected and MLV wild-type (217  $\mu$ U RT/cell) infected murine embryonic fibroblast cells (MEF). The cells were fixed at 48 hours post infection (h p.i.), stained by IF with antibodies against MLV CA, and imaged by spinning disk confocal microscopy (SDCM). Scale bar = 10  $\mu$ m. C. Quantification of percentage of infected versus non-infected cells based on Gag expression from images shown in B. MEF cells were infected with three different concentrations of MLV wild-type RT units per cell as shown on the x-axis. The graph shows mean values and SD of one experiment performed with 5 field of views (FOVs) per sample quantified.

MLV particles after infection produce full-length Gag, which can be used as a marker of productive infection. Therefore, to determine the bulk infectivity of the particle stocks, a microscopy-based infectivity assay that relies on the expression of Gag was developed. The MLV particles were titrated on MEF cells, fixed at 48 h p.i., and immunostained against MLV CA (Figure 7B). The fraction of Gag expressing cells upon infection was quantified (Figure 7C) and used to determine the infectivity of the viral stock. The fraction of infected cells was dose-dependent on the used amount of RT units. At lower particle amounts the increase in infected cells (27.4 % and 58.2 %, respectively) was linearly correlated to the RT units (108 and 217 RT  $\mu$ U/cell, respectively), whereas a 4-fold increase of the virus dose from 217 to 870 RT  $\mu$ U/cell resulted in only a ~1.5-fold increase of infected cells (58.2% to 84.4%). This indicates saturation of the MEF cell system; likely not all cells in the culture are permissive to infection under these conditions (Figure 7C).

Due to diverse reported experimental systems used for MLV particle production, specifically the use of different producing cell lines from murine or human origin, the particle yield produced from transfected human HEK293T cells to murine fibroblast cells (SC-1) was compared (Fan et al., 1983; Landau and Littman, 1992; Pizzato, 2010; Sharma et al., 1997; Wang and Goff, 2015). Furthermore, the production yield of wild-type particles was compared to the yield of a destabilized capsid variant that lacks glycoGag. The absence of glycoGag was previously reported to decrease infectivity in vivo but not in vitro studies (Chun and Fan, 1994; Corbin et al., 1994; Fan et al., 1983; Low et al., 2007; Schwartzberg et al., 1983). Additionally, the infectivity phenotype of the minus-glycoGag variant was found to be partly determined by the producer cell lines (Pizzato, 2010). Therefore, it was also of interest to investigate whether the production of minus-glycoGag particles in murine versus human producer cell lines influences the infectivity phenotype in vitro.

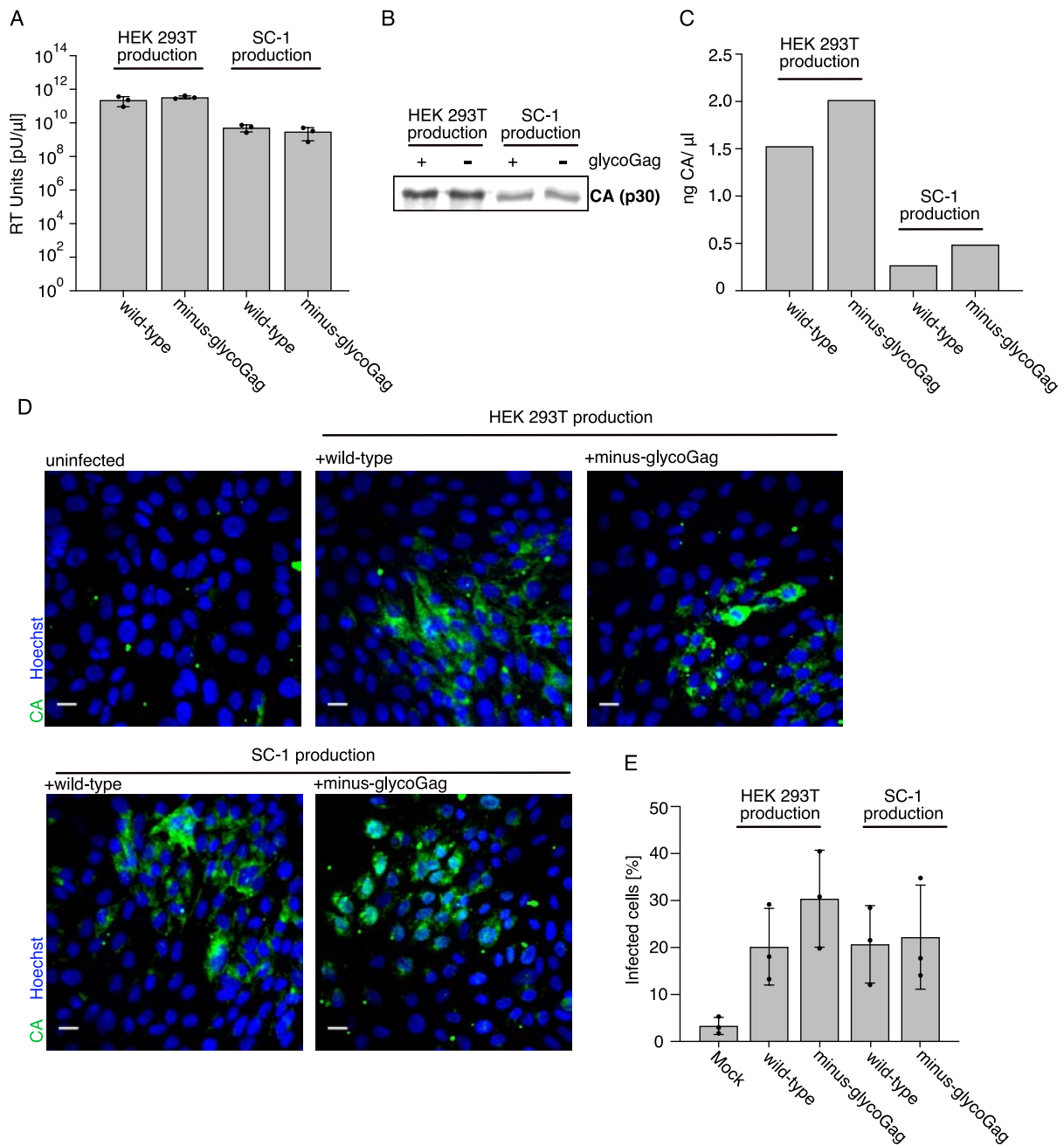


**Figure 8. Production in human HEK293T cells yields higher yield of wild-type and minus-glycoGag MLV particles.** A. Wild-type and minus-glycoGag MLV particles were produced by calcium phosphate mediated transfection in either human HEK293T or murine SC-1 (fibroblast) cells. The supernatant was filtered and concentrated before measuring the RT activity using SG-PERT assay. B. Immunoblot of wild-type and minus-glycoGag variant particle lysates produced from HEK293T cells and SC-1. The particles were separated with SDS-PAGE, blotted on a nitrocellulose membrane using the semi-dry blotting method, and stained using antibodies against MLV CA. Secondary antibodies were detected with the LiCOR CLx scanner. The representative immunoblot is shown from one experiment. C. The CA yield for wild-type and minus-glycoGag variant from both producing cell types was determined by semi-quantitative immunoblot analysis shown in B. D. SC-1 cells were infected with wild-type or minus-glycoGag variant stocks produced in either HEK293T or SC-1 cells. The infection of the viral stocks and

variants were normalized by RT activity (23 mU RT/well). The cells were fixed at 48 h p.i., stained by IF with antibodies against MLV CA. Representative single z-slices of imaged infected and non-infected cells by SDCM are shown from one experiment out of three preformed. Scale bars: 10  $\mu$ m. E. Infectivity of particles in SC-1 cells was quantified from images shown in D. The number of infected cells was quantified based on detected CA signal and total number of nuclei, based on the Hoechst stain, counted manually in Fiji. A., C., E. The graphs show mean values and SD from three independent experiments.

The particle yield showed one to two log lower RT activity of both wild-type and minus-glycoGag variant produced by the murine system compared to the human system (Figure 8A). No clear difference in particle yield was observed between the wild-type virus and minus-glycoGag variant in either the murine or the human system production (Figure 8A). The protein yields of the particle preparations were also checked by quantification of MLV CA by immunoblot (Figure 8B). The CA quantifications analyzed were in accordance with the SG-PERT values, showing lower protein production (~4 fold) in transfected murine cells compared to the human cells (Figure 8B-C). In addition, no clear difference in CA yield could be seen between the wild-type and minus glycoGag particle production (Figure 8C). Apart from examining protein expression and RT activity, the infectivity of the viral particles obtained from transfected murine or human cells was determined and compared in SC-1 (Figure 8D-E). The viral input was normalized by RT activity. Infectivity of the particles was independent of their production cell type and/or the presence of glycoGag. It was observed only a slight increase in infectivity for the minus-glycoGag variant made in human cells; however, the high variation between experiments renders this result uncertain (Figure 8E). Importantly, minus-glycoGag viral particles utilizing murine versus human producer cells did not decrease infectivity in cell culture experiments, thus reporting similar phenotype as previously published studies.

Since virus produced in human HEK293T cells gives higher yields with similar infectivity compared to SC-1 cells, all particle productions in this work were performed in HEK293T cells.

### 3.1.2 GlycoGag is an infectivity factor conditional on the target cell type

To investigate the function of glycoGag further, target cell-dependent infectivity requirements (Pizzato, 2010) as well as the effect of TREX1 on overall infectivity in immunocompetent cell lines needed to be considered. From previous studies, it was found that nucleic acid sensing and IFN response to reverse transcripts produced by the minus-glycoGag variant is dependent on TREX1 (Moran and Ross, 2020; Stavrou et al., 2015). Therefore, infection with wild-type and minus-glycoGag viral particles with ecotropic envelope were compared in SC-1, MEF and MEF TREX1 KO cells. No significant difference in infectivity was observed between wild-type and minus-glycoGag particles in SC-1 with  $40.8 \pm 10.9$  % and  $36.3 \pm 7.2$  % of infected cells, respectively (Figure 9A). In contrast, a 2-fold drop was measured in the immunocompetent cell line MEF, reporting  $45.5 \pm 6.3$  % and  $21.5 \pm 3.8$  % of infected cells for wild-type and minus-glycoGag particles, respectively (Figure 9A). The ~2-fold drop in infectivity of minus-glycoGag variants in MEFs was also found in the KO TREX1 cell line (Figure 9A). These data suggest that the effect of glycoGag is dependent on the target cell type, potentially reflecting different immune sensing capabilities. However, this effect appeared to be independent of TREX1 since the infectivity defect of the minus-glycoGag variant was not rescued in the KO TREX1 cell line.

Lastly, the effect of glycoGag on the amount of reverse transcribed cDNA in infected MEF cells was investigated. The total *gag* cDNA levels were measured at 12 h p.i. by droplet digital PCR (ddPCR) assay with wild-type and glycoGag minus variant scoring ~400 and ~130 copies/cell respectively (Figure 9B). The lower copies of cDNA generated by the minus-glycoGag variant at 12 h p.i. (3-fold reduction, Figure 3B) mirrored the ~2-fold drop observed in infectivity (Figure 9A). Moreover, the lower abundance of RT products in infection without glycoGag suggested that the activity of glycoGag on MLV infection occurs during early steps of infection. This was only observed in immune competent MEF cells, where either the efficiency of reverse transcription was reduced, or, more likely (since SC-1 cells showed no effect) the reverse transcription products were exposed to a TREX1-independent sensing or degradation pathway.

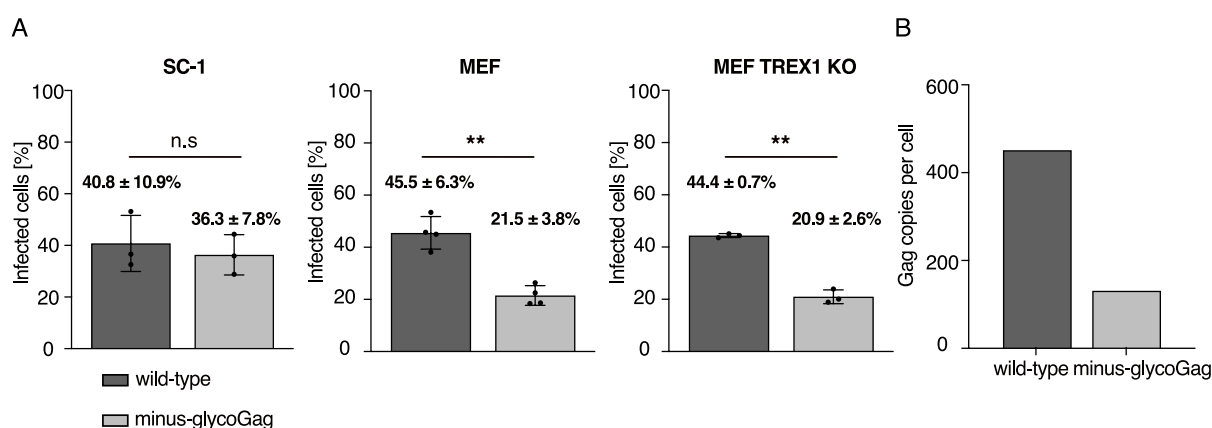


**Figure 9. GlycoGag plays a role in early infection steps in a cell dependent manner.** A. Infection of SC-1, MEF and MEF TREX1 KO with MLV wild-type and minus glycoGag variant normalized to 219 RT  $\mu$ U per cell. At 48 h p.i. the cells were fixed, permeabilized, and immuno-stained against MLV CA and Hoechst. Infected cells were quantified based on detected CA signal and total number of nuclei counted with Fiji. Bar graphs show mean values and SD of three independent experiments. Statistical significance was calculated by paired two-tailed Student's t-test. The difference in infectivity between wild-type and minus-glycoGag was only significant with p value <0.05 in MEF (p = 0.0011, \*\*) and MEF TREX1 KO (p = 0.0038, \*\*). B. cDNA amounts of RT product *gag* was quantified in MEF cells infected with wild-type and minus glycoGag variant (1480  $\mu$ U RT/cell) using ddPCR. Infected samples were isolated at 12 h p.i. One independent experiment was performed.

### 3.2 Establishment of experimental systems for visualization of MLV DNA

To successfully characterize early post entry MLV events, it is vital to develop experimental systems able to identify productive out of the majority of non-productive infectious events in cells. Since this cannot be achieved by bulk infectivity assays such as the assay based on Gag expression (Figure 7), alternative experimental systems using viral cDNA as a marker for identifying actively reverse transcribing complexes had to be established and used. So far, retroviral cDNA has been visualized by FISH, metabolic labeling of retroviral genomes by incorporation of modified nucleosides and the ANCHOR labeling system. Hence, in this project it was attempted to find the best suitable method to visualize MLV genomes under live and fixed conditions.

### 3.2.1 Visualization of MLV DNA using hybridizing fluorescently labeled probes

Infection of SC-1 cells with wild-type MLV was analysed by FISH staining that showed distinct vDNA foci in the cytoplasm as well as the nucleus (Figure 10B). The binding of the labeled probes was specific for MLV DNA, since no foci could be detected in non-infected cells (Figure 10A). Furthermore, an increase in vDNA foci over time was observed (Figure 10B). However, this method required fixation and harsh conditions for the hybridization of the labeled probe by denaturation of the samples, which limited the experiments to fixed conditions and impaired the IF staining of MLV CA (Appendix, Figure 35). Due to the difficulties in IF staining of viral proteins in the intracellular subviral complexes, particularly the IF staining of the CA protein which is vital for this project, it was decided not to use FISH exclusively to identify viral DNA containing particles.

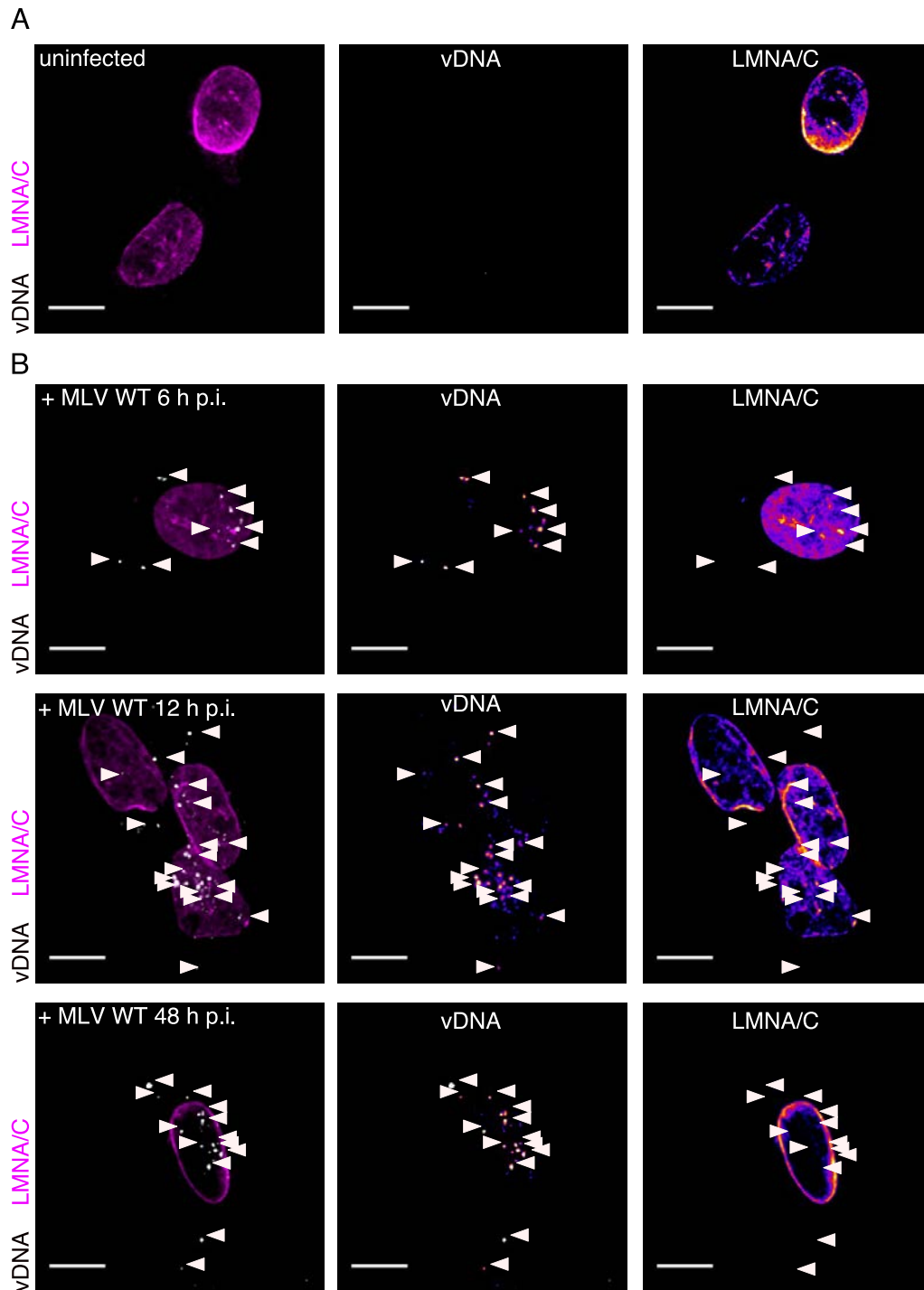
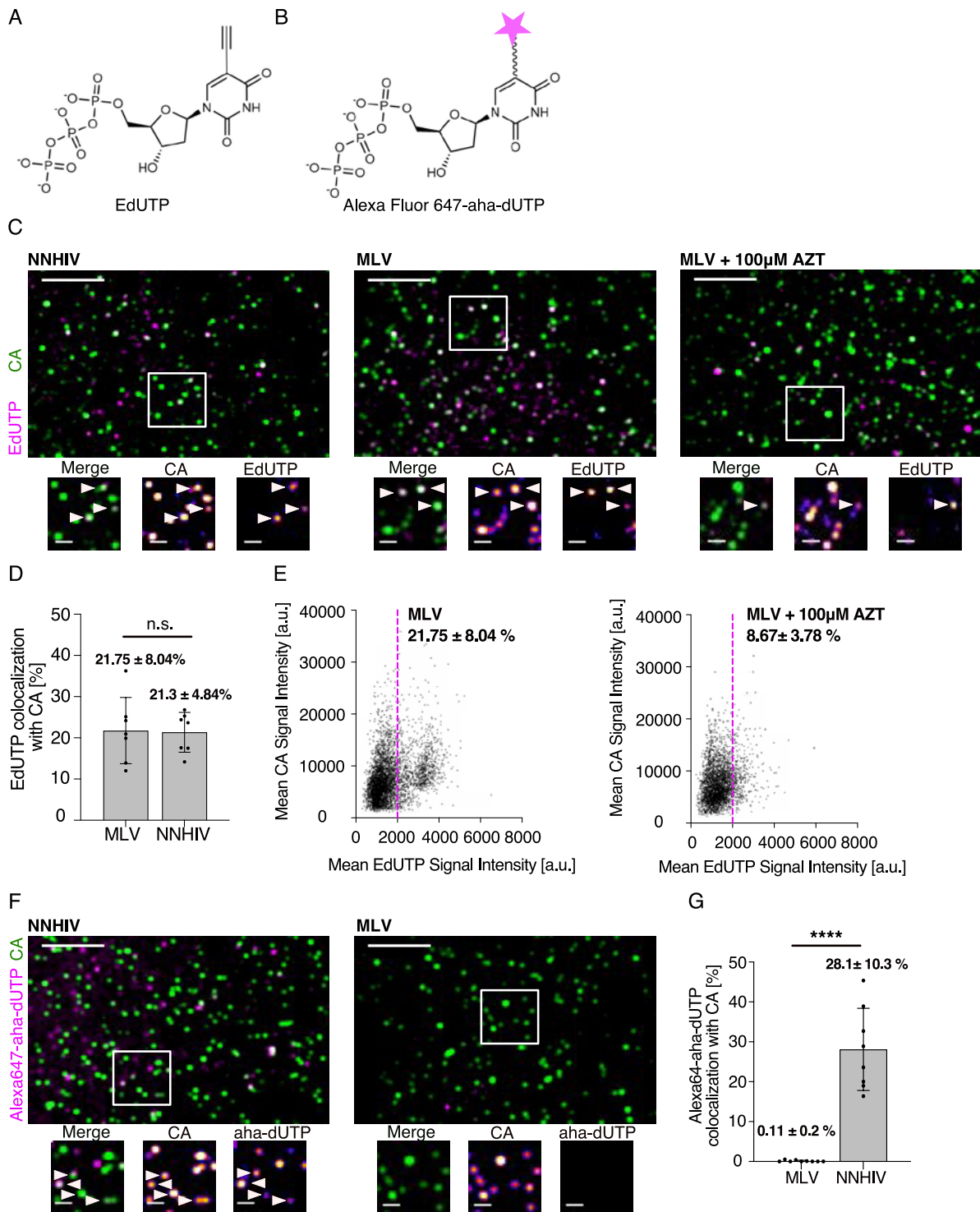


Figure 10. MLV viral DNA can be identified and imaged using FISH. A-B. SC-1 cells were either not infected (A) or infected with MLV wild-type (1000  $\mu$ J RT/cell) for 6, 12, and 48 h (B) before fixation and FISH staining. The cells were also IF stained with antibodies raised against lamin A/C (LMNA/C) and CA (see Appendix Figure 28). The hybridization probe generation and FISH staining were done by Mia Stanic (University Hospital Heidelberg). Scale bar: 10 $\mu$ m. Representative images from one experiment are shown.

### 3.2.2 Visualization of MLV DNA using metabolic labeling with cell-permeable modified nucleosides

In order to overcome the IF staining limitations in FISH, metabolic labeling of retroviral genomes by incorporation of modified nucleosides during reverse transcription was attempted to identify viral cDNA positive subviral complexes by click chemistry (Bejarano et al., 2019; Peng et al., 2014; Salic and Mitchison, 2008). First, it was important to confirm that the modified nucleosides were readily incorporated by MLV RT. Therefore, 5-Ethynyl-dUTP (EdUTP) was added to purified MLV particles in an endogenous reverse transcription (ERT) reaction (Figure 11A-C). As a control, the incorporation of EdUTP was compared to HIV-1 RT (Figure 11C), since EdU click-labeling was already used to identify HIV-1 viral cDNA in cells under fixed conditions (Bejarano et al., 2019; Müller et al., 2021; Peng et al., 2014). For this purpose, I used an integration and transcription deficient derivative of HIV-1<sub>NL4-3</sub> (NNHIV) that can be used in the BSL-2 facilities (Zila et al., 2021). The addition of EdUTP to MLV and NNHIV resulted in a comparable percentage of co-localization of CA protein with click-labeled viral DNA (Figure 11D). The incorporated EdUTP signal by MLV RT was reduced from 21.75±8.04 % to 8.67±3.78 % by adding azidothymidine (AZT), an RT inhibitor, in the endogenous reverse transcription (ERT) reaction (Figure 11E).

Lastly, the promiscuity of MLV was probed by incorporation of bulky dUTP variant directly attached to Alexa647 Fluor by 5-aminohexylacrylamid linker (Alexa647-aha-dUTP) and compared to HIV-1 (Figure 11B, F). The incorporation of Alexa647-modified dUTP by NNHIV resulted in comparable level to the incorporation of EdUTP with 21.3±4.84 % and 28.1±10.3% co-localization, respectively (Figure 11D, F-G). In contrast, no Alexa647 signal with CA was detected in the MLV sample (Figure 11 F-G) indicating that nucleosides with such large modification are not readily accepted by MLV RT or cannot efficiently penetrate into the MLV capsid.



**Figure 11.** EdUTP is readily incorporated by MLV and HIV-1 RT. **A.** Structure of 5-Ethynyl-dUTP (EdUTP). **B.** Structure of Alexa647 labeled 5-aminohexylacrylamid dUTP (Alexa647-aha-dUTP) **C.** Purified particles of MLV and HIV-1<sub>NL4-3</sub> IN<sub>D64N/D116Ntat<sub>Δ33-64bp</sub></sub> (NNHIV) were incubated in ERT buffer that contains dNTPs and EdUTP overnight. Separately purified MLV particles were incubated in ERT buffer that contains dNTPs, EdUTP and 100µM AZT overnight. The ERT solution was then added to PEI coated dishes, fixed, click-labeled and IF stained with antibodies raised against MLV CA or HIV-1 CA. **D.** Quantification of co-

localization percentage of EdUTP labeled viral DNA and CA in MLV and NNHIV containing samples of experiments shown in C. The automated analysis was performed with software Icy. Mean and SD of three independent experiments is shown. The difference in EdUTP incorporation between HIV-1 and MLV RT was not significant ( $p > 0.05$ , ns) by unpaired two-tailed Student's t-test. E. Fluorescence intensity of CA and EdU was measured from ERT buffer containing dNTPs, EdUTP, MLV particles with and without AZT. The measurements were performed with Icy software. The threshold was set to  $t = 2000$  a.u. indicated with magenta line. F. Purified particles of MLV and NNHIV were incubated in ERT buffer that contains dNTPs and Alexa647-aha-dUTP overnight. The ERT solution was then added to PEI coated dishes, fixed, click-labeled and IF stained with antibodies raised against MLV CA or HIV-1 CA. C., F. Scale bar:  $10\mu\text{m}$  (overview) and  $2\mu\text{m}$  (enlargements). White arrows point towards co-localization event between CA and viral DNA. G. Quantification of co-localization percentage of Alexa647-aha-dUTP labeled viral DNA and CA in MLV and NNHIV containing samples of experiments shown in F. The automated analysis was performed with software Icy. Mean and SD of three independent experiments is shown. The difference in Alexa647-aha-dUTP incorporation between HIV-1 and MLV RT was significant ( $p < 0.0001$ , \*\*\*\*) by unpaired two-tailed Student's t-test.

After showing that EdUTP can be efficiently incorporated into purified MLV particles in vitro, the respective nucleoside EdU was added to cells during infection with MLV (Figure 12A). The cells were also treated with aphidicolin, a DNA polymerase  $\alpha/\delta$  inhibitor, which prevents cellular DNA synthesis and incorporation of EdU into host chromosomal DNA (Figure 12B). Since mitochondrial DNA synthesis is not inhibited with APC, *bona fide* subviral complexes containing vDNA, can be characterized as CA and EdU positive objects, which are negative for the mitochondrial marker cytochrome C (CytoC). However, APC did not completely block cellular DNA synthesis and the remaining signal obscured identification of viral particles containing viral DNA in the nucleus and surrounding area in most cells (Figure 12B). More importantly, APC treatment blocks mitosis (see Appendix Figure 36) and the copper-catalyzed click chemistry is toxic to the cells, thus limiting analysis to non-dividing and fixed cells.

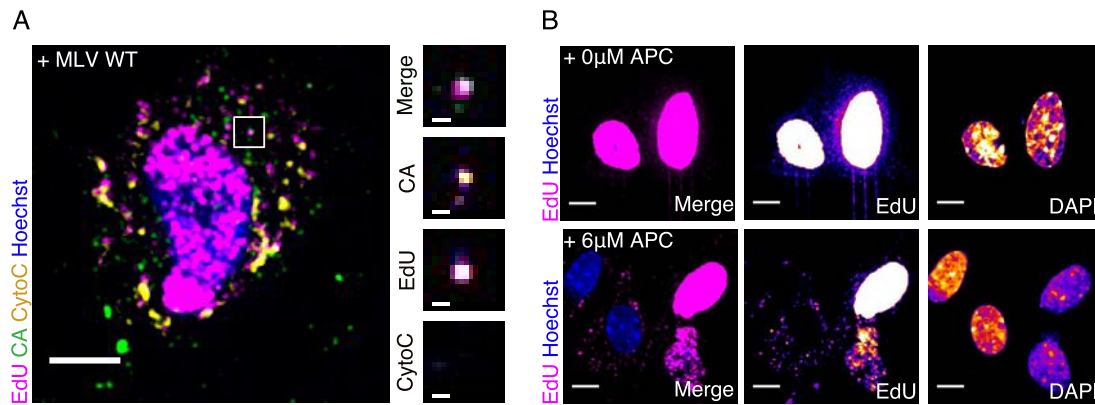


**Figure 12. Metabolic labeling of viral genomes with EdU click-chemistry is not efficient in MLV infected cells.** A. SC-1 cells were infected with MLV wild-type virus (1000  $\mu$ J RT/cell) in presence of APC (6  $\mu$ M) and EdU (1  $\mu$ M) for 12 h before fixation, click-labeling and IF staining using antibodies against MLV CA and cytochrome C. Hoechst dye was used to stain the nucleus. A representative image was chosen of the rare CA and EdU positive but CytoC negative subviral complex. Single z-slice was presented for the overview and enlargements. Scale bar: 10  $\mu$ m (overview) and 2  $\mu$ m (enlargements). B. SC-1 cells incubated with EdU (1  $\mu$ M) in absence or presence of aphidicolin treatment (6  $\mu$ M) for 12 h prior to fixation, click-labeling and nuclear staining with Hoechst. Scale bar: 10 $\mu$ m

### 3.2.3 Adapting a genetically encoded DNA-binding protein labeling system for visualization of MLV DNA

To overcome the limitations presented by metabolic and FISH labeling of MLV genomes, a live cell imaging technique that allows for single-molecule gene labeling called the ANCHOR system was adapted. First, an ANCH containing MLV derivative was generated by introduction of  $\sim$ 1000bp of ANCH3 sequence into the MLV proviral plasmid pNCS (MLV ANCH) in the 5'-terminal part of the *env* gene (Figure 13A). The ANCH3 sequence replaced 1000bp of MLV sequence and introduced a stop codon at the beginning of *env* resulting in no change of the overall size of the viral MLV DNA (Figure 13A). The particles were pseudotyped with vesicular stomatitis virus G protein (VSV-G) to make infectious virus. Second, to visualize the ANCH sequence as a part of reverse transcribed viral DNA during infection, polyclonal SC-1 and MEF cell lines expressing OR3 protein coupled to eGFP or mScarlet were generated (Figure 13B, see Appendix Figure 37) (Müller et al., 2021). To ensure easy discrimination of the spatial location of events, the cells were transduced for a second time to express fluorescently tagged murine Lamin B1 (mLMNB1). Therefore, infection with VSV-G pseudotyped

ANCH MLV virus of murine cells is expected to induce the binding and oligomerization of the fluorescently labeled OR3 protein to accessible and reverse transcribed viral DNA forming distinct foci (Figure 13C).

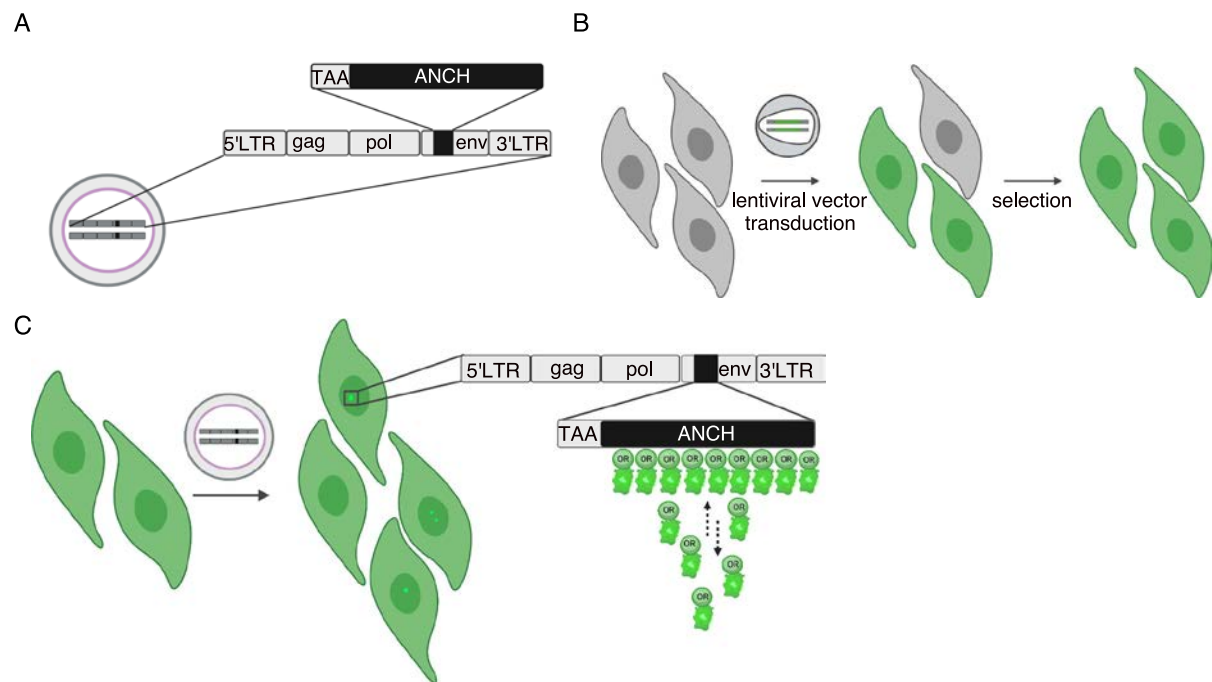


**Figure 13. Labeling of accessible MLV dsDNA using the ANCHOR system.** A. Scheme of the insertion of ANCH3 (~1000kb) in the env region of proviral MLV NCA or NCS plasmid. A stop codon was introduced directly upstream of ANCH3; therefore, to produce infectious particles pseudotyping with VSV-G was used. B. The OR3 expressing cell lines were generated by transduction with pWPI lentiviral vector particles carrying eGFP.OR3 or mScarlet.OR3. The cells were then selected with puromycin (puro) or sorted with flow cytometry. A second transduction with pWPI carrying eBFP2.mLMNB1 followed selection with blasticidin (BLA), thus generating MEF or SC-1 eGFP.OR3 eBFP2.mLMNB1 expressing cell lines. C. Scheme of viral dsDNA visualization of MLV with the ANCHOR system. The OR3 fusion protein (eGFP or mScarlet) will bind and oligomerize on the ANCH3 sequence in the viral genome.

### 3.2.4 Validation of the ANCHOR system as a suitable tool for MLV DNA visualization in murine infected cells

To confirm that the ANCHOR system is suitable to visualize MLV genomes, it was vital for this system to generate infectious ANCH3 containing virus and ensure specific binding and accumulation of OR3 fusion proteins to the ANCH sequence in the viral genome. Therefore, I made VSV-G pseudotyped MLV ANCH virus and tested its infectivity on eGFP.OR3 expressing MEF cells. The infection was scored based on Gag expression, which clearly revealed that ANCH containing MLV virus is infectious and

can successfully integrate its cDNA (Figure 14A). Furthermore, infection was blocked using the integration inhibitor Raltegravir (Ral) with an 8-fold decrease compared to non treated cells (Figure 14B). The cells were also infected with a minus envelope ANCH containing virus (MLV ANCH (-) env) that resulted in no Gag-expressing cells, thus proving that the ANCH3 insertions produced non enveloped viral particles (Figure 14 A-B).

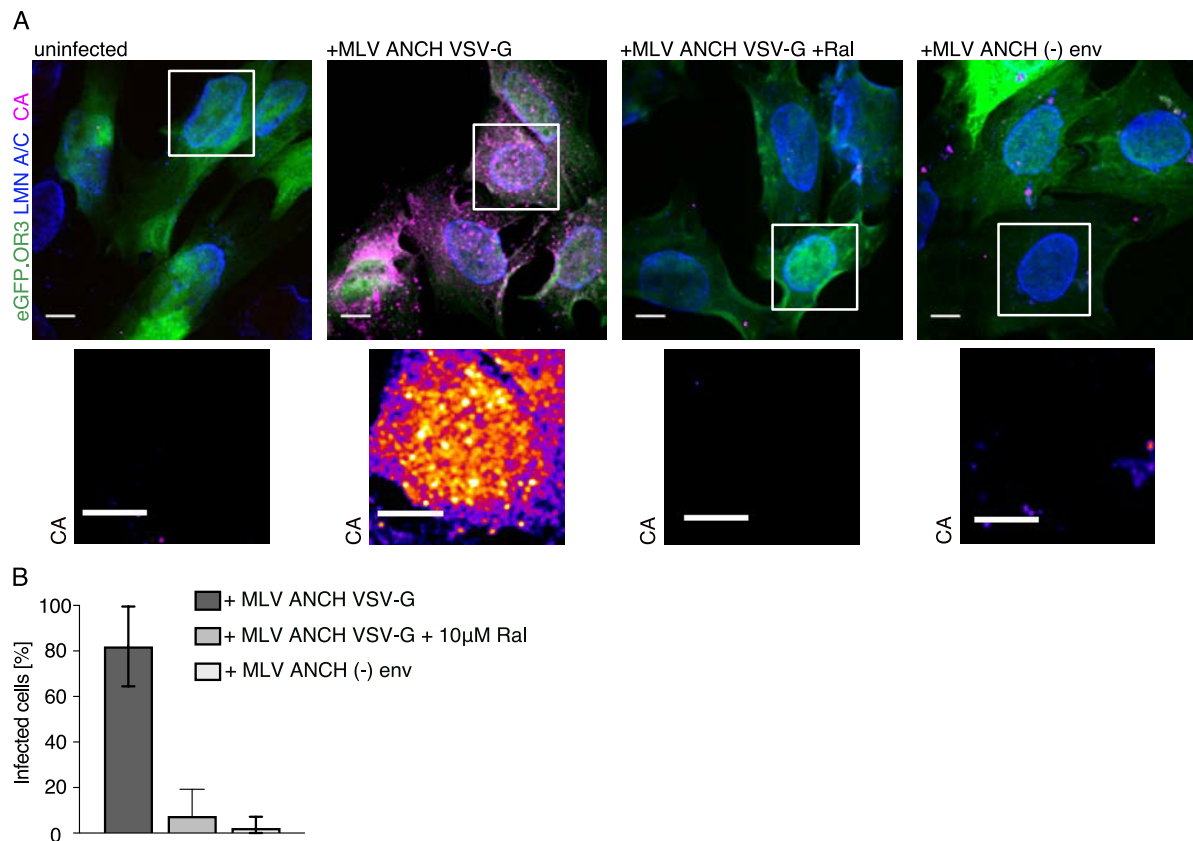


**Figure 14. Pseudotyped ANCH3 containing viral particles are infectious.** A. MEF expressing eGFP.OR3 were infected with MLV ANCH VSV-G (1266  $\mu$ J RT/cell) treated with 10  $\mu$ M Raltegravir or DMSO during infection. As a control, the cells were also infected with MLV ANCH (-) env. The cells were fixed, immunostained against MLV CA and Lamin A/C at 72 h p.i. Representative images were shown as a single z-slice. Scale bars: 10  $\mu$ m (overview and enlargements). B. Quantification of infected cells of experiment shown in A. The number of infected cells was quantified based on detected CA signal and total number of nuclei, based on IF stained LMN A/C, counted manually in Fiji. One independent experiment was performed with 5-6 FOV analyzed per sample, error bars represent SD of the mean.

The eGFP.OR3 expressing murine MEF and SC-1 cell lines were assessed for the ability to produce reverse transcribed ANCH specific foci upon infection. For this purpose, I used VSV-G pseudotyped NNHIV that can be used in the BSL-2 facilities to infect eGFP.OR3 expressing MEF and SC-1 cell lines (Müller et al., 2021). Müller et al., have shown that NNHIV ANCH infection is able to induce nuclear foci formation in human

Hela-based TZM-bl eGFP.OR3 expressing cells. Distinct nuclear foci formation was also observed in murine cells, which were absent in uninfected control cells (Figure 15). Thus, the generated stable murine OR3 expressing cell lines are competent for detection of ANCH DNA sequences inside the nucleus.

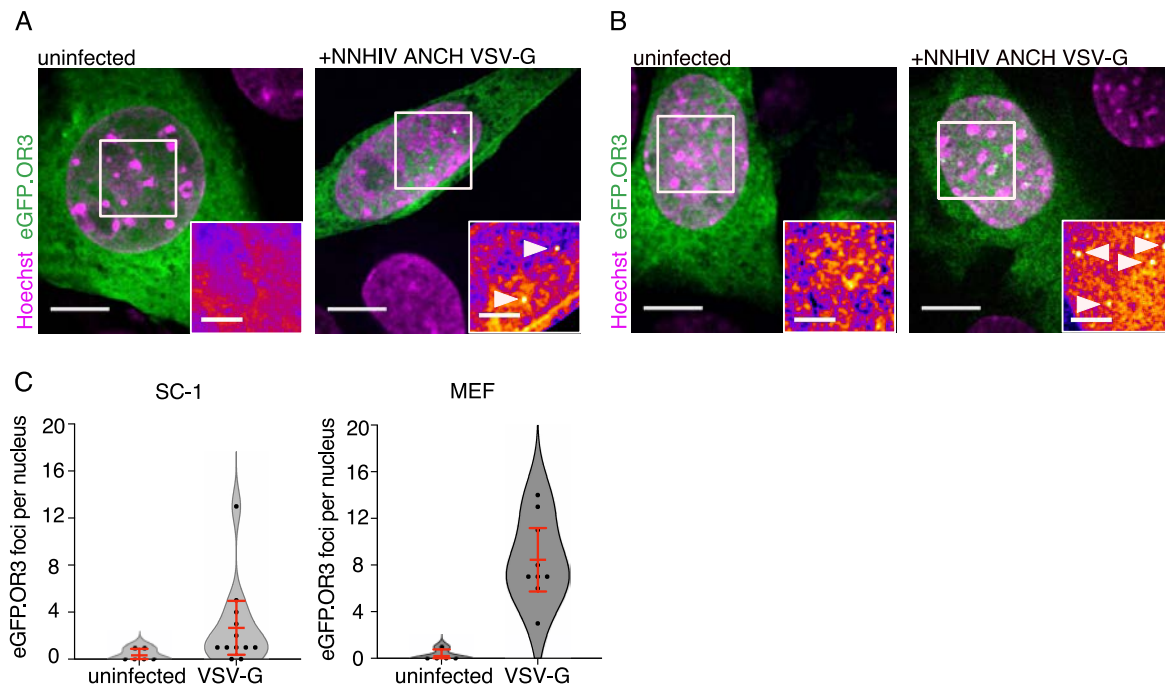


**Figure 15. OR3 fusion proteins bind and accumulate on ANCH sequence engineered into NNHIV in infected murine cells.** A. SC-1 eGFP.OR3 expressing cells were infected with NNHIV ANCH VSV-G (30 $\mu$ U RT/cell) for 24 h before fixation and imaging with SDCM. Active site mutations D64N and D116N in the in gene as well as a deletion within the tat gene ( $\Delta$ 33-64bp) causing truncation and frameshift deems this virus suitable for S2 use. The cells were stained with Hoechst to visualize the nucleus. B. The experiment was performed in parallel in eGFP.OR3 expressing MEF cells under the same conditions as in A. A-B. Scale bars: 10  $\mu$ m (overview) and 5  $\mu$ m (enlargements). Representative single z-slices of imaged cells are shown from one biological replicate. White arrows point to a detected eGFP.OR3 foci. C. Quantification of eGFP.OR3 foci per cell from images shown in A and B. Data presented from one independent experiment with mean and error bars representing 95 % CI (n=10-15 cells per sample).

### 3.3 Visualization of MLV cDNA and interactions with viral and host cell proteins in fixed and living conditions

#### 3.3.1 Visualization of MLV cDNA using the ANCHOR system in murine cells

Next, the validated OR3 cell lines were used to visualize reverse transcribed MLV genomes in murine cells (Figure 16A-B). Distinct infection-induced signals were observed in the nucleus of both SC-1 and MEFs cells at 24 h p.i (Figure 16A-B), with a similar number of eGFP.OR3 signals in MEFs and SC-1 (3.7 and 3.4 per nucleus, respectively) in line with the infectivity data in those cell lines (Figure 9A). No such distinct nuclear signals were observed in the uninfected or infected cells with MLV ANCH (-) env (Figure 16A-B). The background signal of these controls was quantified to be  $\sim 0.2$  foci/cell (Figure 16C).

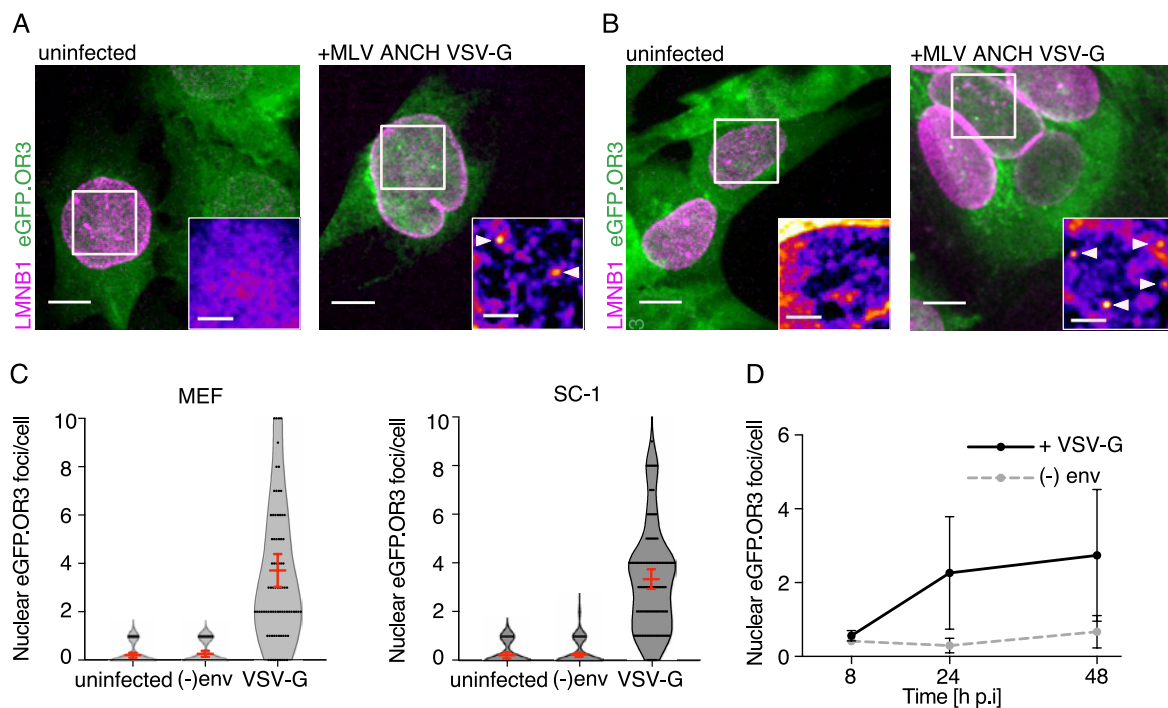


**Figure 16.** The ANCHOR system enables visualization of MLV cDNA in infected murine cells. A. MEF expressing eGFP.OR3 eBFP2.mLMNB1 were infected with MLV ANCH VSV-G (822  $\mu$ U RT/cell, MOI 6.3) or left uninfected. The cells were fixed and imaged by SDCM after 24 h p.i. B. The same experiment was performed in parallel in eGFP.OR3 eBFP2.mLMNB1 expressing SC-1 cells under the same conditions as in A. A-B. Scale bars: 10  $\mu$ m (overview) and 5  $\mu$ m (enlargements). Representative maximum intensity projections (MIPs) are shown from one out of the three performed biological replicates. The enlargements of the nuclei are shown as single z-slices. White arrows point to detected eGFP.OR3 foci. C. Quantification of eGFP.OR3 foci in SC-1 and MEFs infected with MLV ANCH VSV-G, MLV ANCH (-) env

(822  $\mu$ U RT/cell) and non-infected cells. Quantification of experiments shown in (A-B). Three independent experiments were performed, pooled together, and depicted in violin plots. N = 50-80 cells per condition, with mean and error bars representing 95 % CI. D. MEF cells were infected with MLV ANCH VSV-G (822  $\mu$ U RT/cell, MOI 6.3) or MLV ANCH (-) env (822  $\mu$ U RT/cell). The samples were fixed and imaged at 8, 24, 48 h p.i. Number of nuclear eGFP.OR3 foci per cell were quantified for each timepoint. N = 57-79 cells per condition, error bars represent SD of the mean. Three independent experiments were performed and analyzed.

To determine when these events occur, the number of signals in cells fixed at different time points after infection was scored. The nuclear number of foci per cell saturated at 24 h p.i. with a mild increase at 48 h p.i. (Figure 16D). These initial results indicate that the ANCHOR system can visualize accessible synthesized viral dsDNA after nuclear entry, and it is a suitable system to investigate the outcome and composition of MLV subviral complexes in a spatio-temporal context during infection.

### 3.3.2 Visualization of cytoplasmic OR3 signals in infected MLV cells

Previous studies using the ANCHOR system reported that completion of reverse-transcription as well as capsid uncoating occurs in the nucleus, therefore HIV-1 cDNA can be only visualized in the nucleus (Müller et al., 2021). Furthermore, occasional cytoplasmic events were described as perinuclear accumulations of the OR3 fusion protein in non-infected cells, and shown to be trapped in multivesicular bodies by CLEM analysis (Müller et al., 2021). In the murine non-infected cells similar accumulations were observed in the cytoplasm (Figure 17A). Interestingly, a mild increase of these cytoplasmic events was observed in samples infected with MLV (Figure 17B).

The discovery of potential MLV dsDNA in the cytoplasm, could indicate the location of completion of reverse-transcription and/or the spatio-temporal capsid uncoating to be quite different than HIV-1. To distinguish if these cytoplasmic events are artifacts or perhaps a specific phenotype attributed to MLV infection, it was decided to characterize these events in further experiments.

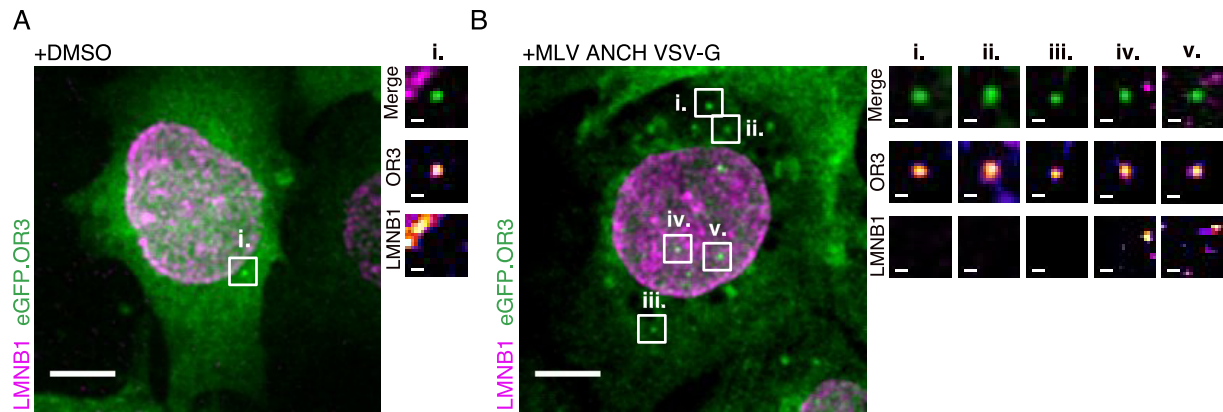


**Figure 17. Cytoplasmic OR3 accumulations can be observed during MLV infection as well.** A. Representative image of non-infected eGFP.OR3 eBFP2.mLMNB1 SC-1 cells. B. SC-1 expressing eGFP.OR3 and eBFP2.mLMNB1 were infected with MLV ANCH VSV-G (822  $\mu$ J RT/cell, MOI 6.3). A-B. The cells were fixed and imaged by SDCM after 24 h p.i. Representative single z-slice images are shown from one out of the three performed independent experiments. Enlargements are presented of nuclear foci with background contrast adjustment for better visualization. Scale bars: 10  $\mu$ m (overview) and 2  $\mu$ m (enlargements).

### 3.3.3 Comparison of lentiviral and retroviral location of OR3 signals in infected murine cells

To explore the possibility of cytoplasmic infection induced OR3 signals attributed solely to MLV, a comparative experiment with HIV-1 was performed. Already in Figure 15, the findings of Müller et al. (2021) were confirmed that upon infection with NNHIV ANCH VSV-G no cytoplasmic events were detected. However, to have a larger data set, three biological replicates and more comprehensive results, MEF cells were infected in parallel with HIV-1 based lentiviral vector containing ANCH (pWPI ANCH VSV-G) (Figure 18B) and MLV ANCH VSV-G (Figure 18C). As expected, infection with MLV and pWPI resulted in nuclear signal formation (Figure 18B-D). Furthermore, quantitative analysis of cytoplasmic events showed that there is no difference between the mock sample and pWPI infection averaging  $\sim 1$  cytoplasmic focus detected per cell (Figure 18D). A slight increase of the cytoplasmic foci to  $\sim 2$  per cell was detected in the sample infected with MLV (Figure 18D). Lentiviral infection does not increase the levels of cytoplasmic events above the detected background levels, whereas MLV infection caused a mild increase. This result suggested that the cytoplasmic phenotype may be MLV infection induced.

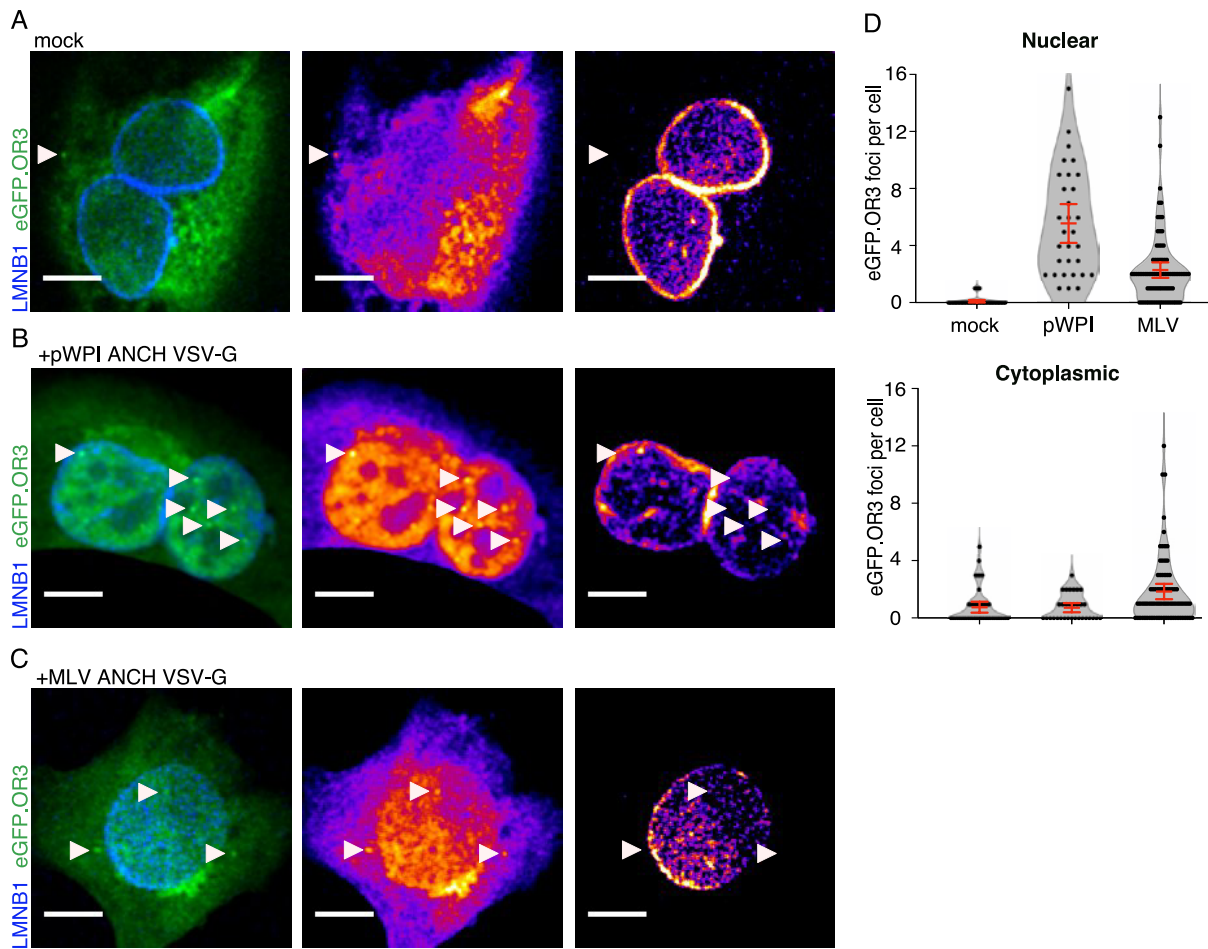


**Figure 18.** MLV OR3 signals in contrast to lentiviral vectors can be visualized in the nucleus and cytoplasm. A-C. MEF cells expressing eGFP.OR3 eBFP2.mLMNB1 uninfected (A) or infected with pWPI ANCH VSV-G with 42  $\mu$ U RT/cell (B) or infected with MLV ANCH VSV-G with 822  $\mu$ U RT/cell (C). The cells were fixed at 24 h p.i. and subsequently imaged by SDCM. Representative images from one out of three independent experiments are shown as single z-slice. Scale bars: 10  $\mu$ m. White arrows indicate a detected eGFP.OR3 focus. D. Quantification of eGFP.OR3 foci per cell from images shown in (A-C). The foci are plotted according to their location in the cell, nuclear or cytoplasmic. Data presented from three independent experiments (mean and error bars representing 95 % CI, n = 44-79 cells).

### 3.3.4 Nuclear entry of MLV cDNA is blocked upon aphidicolin treatment

To explore the validity of cytoplasmic event detection with the ANCHOR system, a strategy to prevent cellular division and by that potentially increase cytoplasmic events was designed. Cell-cycle inhibitors like aphidicolin (Ligasová and Koberna, 2021; Roe et al., 1993) and/or serum starvation are frequently used to prevent translocation of MLV subviral complexes to the nucleus (Elis et al., 2012; Hagino-Yamagishi et al., 1981; Lewis and Emerman, 1994), which consequently inhibit MLV infection.

Originally, in this project high concentrations of aphidicolin (6  $\mu\text{M}$ ) were used as a part of the EdU click-labeling system to prevent cellular incorporation of EdU (see Appendix Figure 36). Hence, the effect of aphidicolin at different concentrations on cell division and infectivity were tested on OR3 expressing cell lines. The aim was to determine the lowest optimal concentration of aphidicolin where the desired effect on infectivity and cell division is maintained and cell death is avoided when the cells are treated for longer periods of time.

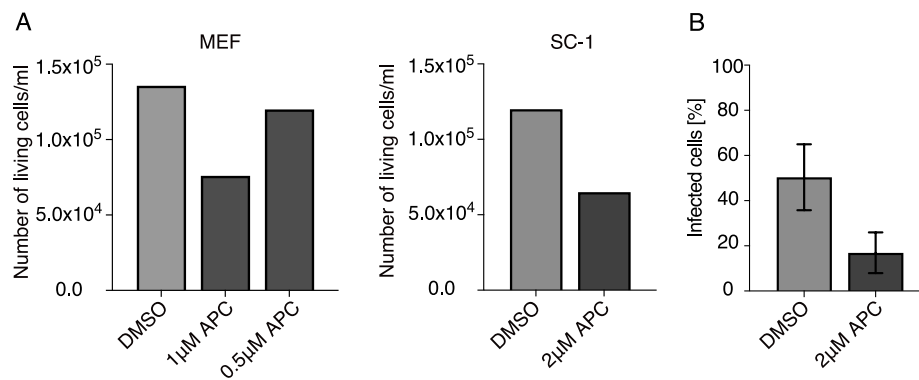


**Figure 19. Cell division and MLV infection are inhibited upon lower concentration of aphidicolin treatment.** A. MEF and SC-1 eGFP.OR3 expressing cells were seeded with  $5.0 \times 10^4$  per well and treated with DMSO or aphidicolin with concentration of  $1 \mu\text{M}$  or  $0.5 \mu\text{M}$ . The number of living cells were counted at seeding and after 24h treatment with aphidicolin or DMSO in a single experiment. The cells were counted with TC20 Automated Cell Counter (BioRad) B. SC-1 cells eGFP.OR3 eBFP2.mLMNB1 cells were treated with DMSO or aphidicolin ( $2 \mu\text{M}$ ) at seeding. After 12 h treatment the cells were infected with MLV ANCH VSV-G ( $1300 \mu\text{M}$  RT/ cell) in the presence of aphidicolin or DMSO. The cells were fixed at 24 h p.i. and stained by IF using antibodies raised against MLV CA. The number of infected cells was quantified based on detected CA signal and total number of nuclei, based on the Hoechst stain, counted manually in Fiji. The graph shows mean values and SD from 5 FOV per sample performed in one independent experiment.

It was quantified that aphidicolin treatment for 24 h of MEF cells with  $1 \mu\text{M}$  was needed to prevent cell division and doubling of the initially seeded cell population (Figure 19A). For SC-1, aphidicolin treatment with  $2 \mu\text{M}$  was needed to prevent cell division (Figure 19A, see Appendix 35). Furthermore, aphidicolin treated cells showed a 3-fold decrease in infectivity when compared to DMSO treated cells (Figure 19B).

To resolve whether the interesting cytoplasmic phenotype observed in Figure 17 was infection induced and genuine MLV cDNA, the effect of aphidicolin was investigated using the ANCHOR system. Adding aphidicolin prior and during infection of eGFP.OR3 expressing cells with MLV ANCH largely prevented the formation of nuclear signals (Figure 20 A-B). As shown in Figure 20C, non-treated samples scored  $\sim 3$  foci per nucleus and upon APC treatment only 0.6 foci per nucleus were scored. Moreover, a mild increase of cytoplasmic events during APC treatment was observed (Figure 20B). This was also evident in the doubling of the number of cytoplasmic foci counted in the aphidicolin treated sample ( $\sim 2$  foci/cell) compared to non-treated sample ( $\sim 1$  foci/cell) (Figure 20C). However, to exclude for the possible effect APC has on OR3 accumulations without infection, the number of foci was also quantified in non-infected samples (Figure 21A) and infected with MLV ANCH (-) env (Figure 21B).

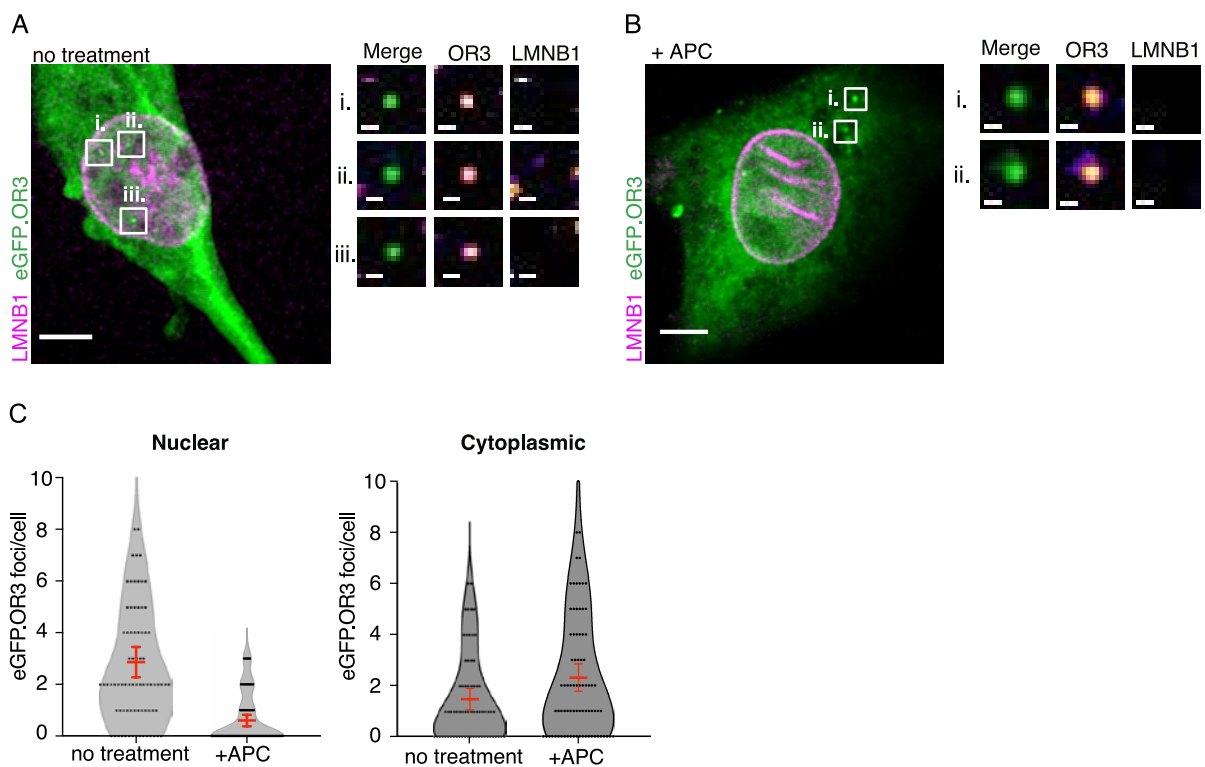


**Figure 20. Nuclear entry of viral cDNA is inhibited in aphidicolin treated cells.** A. eGFP.OR3 eBFP2.LAMNB1 expressing MEF cells were treated 12 h prior infection and during infection with DMSO or B. 1  $\mu$ M APC. A-B. The cells were infected with MLV ANCH VSV-G (822  $\mu$ U RT/cell, 6.3 MOI) and fixed at 24 h p.i. Representative single z-slices of imaged cells are shown. Enlargements are presented of nuclear foci with background contrast adjustment for better visualization. Scale bars: 10  $\mu$ m (overview) and 2  $\mu$ m (enlargements). C. Quantification of eGFP.OR3 foci formation in cells shown in A-B. n = 73-80 cells per condition, with mean and error bars representing 95 % CI. Three independent experiments were performed.

Treatment with APC increased the number of cytoplasmic eGFP.OR3 foci in both controls as well. In the non-infected cells treated with and without APC, 2.4 and 0.7 foci per cell were scored, respectively (Figure 21C). Similarly, the same increase under APC treatment in the minus env infected sample was observed with 2.4 compared to 1 focus per cell without the APC treatment (Figure 21C).

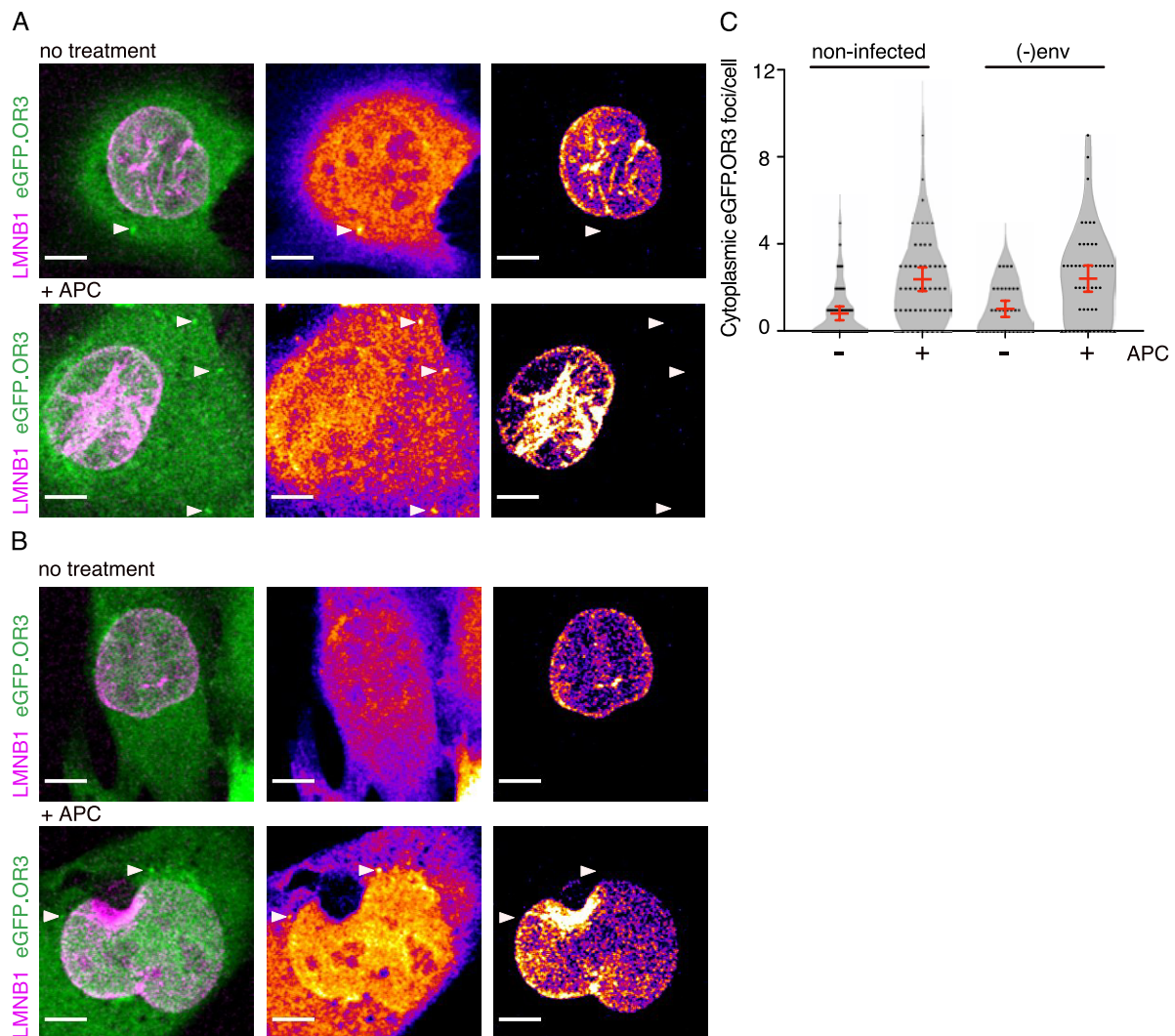


**Figure 21.** Aphidicolin treatment of MEFs increases eGFP.OR3 artifacts in the cytoplasm. A-B MEF eGFP.OR3 eBFP2.mLMNB1 cells were treated with 1  $\mu$ M APC or DMSO for 12 h prior infection and during infection. The cells were fixed at 24 h p.i. A-B. Representative images of non-infected cells (A) or MLV ANCH (-) env (822  $\mu$ J RT/cell) infected cells (B) treated with APC or DMSO. MIPs of 1.5  $\mu$ m are shown. Scale bar: 10  $\mu$ m. White arrows indicate detected eGFP.OR3 foci. C. Quantification of cytoplasmic eGFP.OR3 foci per cell from images shown in A-B. n = 34-61 cells per condition, with mean and error bars representing 95 % CI. Three independent experiments were performed.

Considering the data from Figure 20 and 21, it can be confirmed that aphidicolin is effective in inhibition of nuclear eGFP.OR3 foci formation by inhibiting cellular division. Aphidicolin treatment, independently of infection, also induced an increase in the number of background eGFP.OR3 foci accumulations, perhaps due to increased cellular stress. Therefore, the use of aphidicolin, except for nuclear entry block of MLV cDNA, is not a suitable tool to validate the possible cytoplasmic MLV dsDNA detections. Due to this difficulty, I refrained from stating any conclusions about cytoplasmic MLV dsDNA detections in this study and instead focused on nuclear detections, which can unambiguously be identified.

### 3.3.5 MLV cDNA accessible for protein-binding does not associate with CA and/or p12 proteins in the nucleus

After establishment and validation of the ANCHOR system for reliable detection of MLV complexes containing cDNA in the nucleus, the system was applied on investigating the outcome and protein composition of MLV subviral complexes in spatio-temporal context during infection. Candidates of interest were CA and p12, who are vital components of the RTC/PIC complex alongside IN and NC. The viral capsid is offering protection of the reverse-transcribed genome and ensuring its safe transport to the nucleus (Fassati and Goff, 1999; Goff, 2004; Moran and Ross, 2020; Stavrou et al., 2015; Telesnitsky and Goff, 1997); whereas, p12 is vital in tethering the PIC to chromatin during mitosis thus mediating nuclear entry (Elis et al., 2012; Wanaguru et al., 2018). Past studies have reported inconclusive results concerning the percentage of co-localization between CA and p12 (Elis et al., 2012; Wanaguru et al., 2018). Similar issues were observed when staining the HIV-1 capsid in the nucleus where the staining efficacy is heavily dependent upon sample fixation and extraction (Chin et al., 2015; Müller et al., 2021; Schifferdecker et al., 2022; Zila et al., 2019).

Therefore, infected cells or isolated particles immobilized on imaging slides were co-immunostained using antibodies against CA and p12 under different extraction conditions. Isolated particles showed  $80.0 \pm 10.3$  % co-localization between CA and p12 (Figure 22A-B). In MLV infected cells that were fixed with PFA alone (Figure 22C) only  $35.0 \pm 14.2$  % of p12 and CA co-localization was scored (Figure 22E). However, cells that

were extracted with ice-cold methanol (MeOH) for 5 minutes after fixation (Figure 22D) showed an increase of co-localization percentage to  $74.6 \pm 11.5\%$  (Figure 22E). Therefore, in infected cells MeOH extraction proved to be necessary to reach a similar degree of co-localization as for isolated particles (Figure 22B), indicating some degree of epitope masking for antibody staining within cells. To check if there is staining efficacy problem of MLV CA in the nucleus similarly to HIV-1 CA, the percentages of co-localization per cellular compartment were analyzed in the samples (Figure 22F). No difference in percentages was observed between the cytoplasm ( $25.2 \pm 14.7\%$ ) and nucleus ( $36.95 \pm 14.62\%$ ) in the non-extracted sample (Figure 22F). Likewise, no difference in percentages of co-localization was detected between the nuclear compartment with  $62.0 \pm 15.6$  versus the cytoplasmic compartment with  $80.2 \pm 12.6$  in the methanol extracted sample (Figure 22F). Thus, it can be concluded that the problem in efficacy of CA and p12 co-staining is not organelle specific but is likely caused by a factor that associates with the capsid in the cytoplasm and is retained in the nucleus (Figure 22F). Lastly, the CA staining intensities were quantified of subviral complexes which showed similar intensities in the nucleus and cytoplasm with mean fluorescence intensities (MFI) of 4133 and 5253 a.u. respectively, indicating that likely the full complement of CA proteins is retained inside the nucleus (Figure 22G).

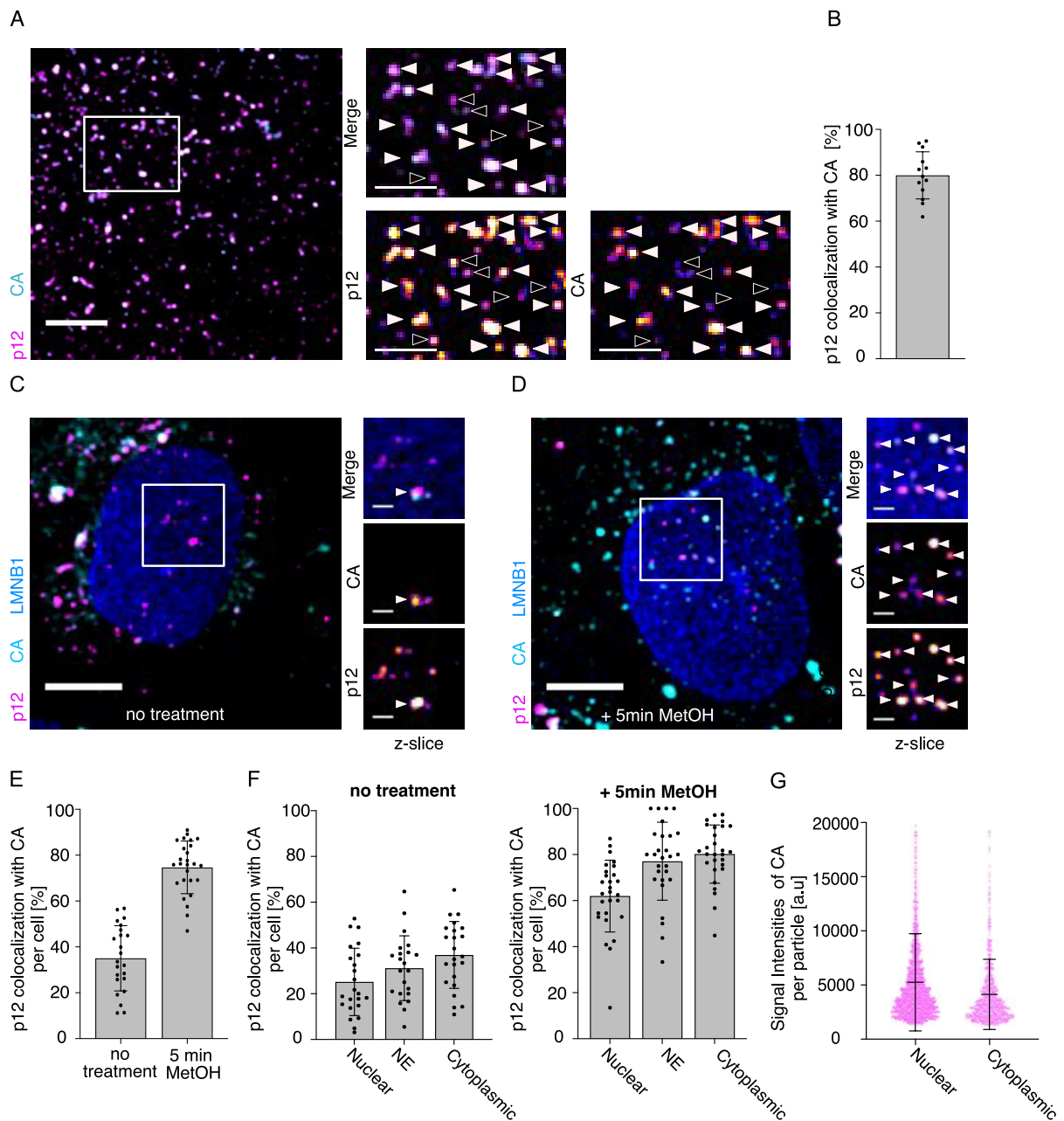


**Figure 22. Co-immunostaining of CA and p12 in infected cells requires methanol extraction.** A. MLV ANCH VSV-G particles were immobilized on PEI coated 15-well ibidi chamber slides. Samples were fixed, permeabilized and treated with ice-cold MeOH for 5 min. Followed by IF staining with antibodies raised against p12 (anti-p12 1:1000, magenta) and CA (anti-CA 1:600, cyan). Scale bars: 10  $\mu$ m (overview) and 2  $\mu$ m (enlargement). Overview image is presented as MIP of 1  $\mu$ m and enlargements are shown as single z-slice. B. Quantification of co-localization percentages of p12 and CA per cell from images shown in A. 15 FOVs of one independent experiment were analyzed using Imaris. C-D. eGFP.OR3 eBFP2.mLMNB1 expressing MEF cells were infected with MLV ANCH VSV-G (822  $\mu$ U RT/cell, MOI 6.3). The cells were fixed at 24 h p.i. with 4 % PFA for 10 min and permeabilized with 0.25% Triton X-100 for 10 min without (C) or with additional 5 min extraction using of ice-cold MeOH (D). The samples are then IF stained with antibodies raised against p12 (anti-p12 1:1000, magenta) and CA (anti-CA 1:600, cyan). All images are presented as single z-slice. Scale bars: 10  $\mu$ m (overview) and 2  $\mu$ m (enlargements). E. Analysis of CA and

p12 co-localization percentages per cell was done with Imaris in a semi-automated way from images shown in (C, D). Three independent experiments were performed with total of 23-26 cells analyzed per sample. Error bars represent SD of mean. F. Quantification of CA and p12 co-localization percentages per cell in nuclear, NE and cytoplasmic compartments of the non-extracted and MeOH extracted samples. N = 23-26 cells analyzed from three independent experiments; error bars represent SD. G. CA signal intensities of p12 positive particles were quantified with the help of Imaris. The signal intensities were then plotted according to the subviral complex location in the cell, either the cytoplasm or nucleus. Data collected from three independent experiments and error bars represent SD from the mean.

Next, with the improved co-immunostaining protocol, in infected cells the viral cDNA identified by OR3 proteins was analyzed for co-localization with p12 and/or CA at 8 h p.i. (Figure 23A) and 24 h p.i. (Figure 23B). The results showed that a low number of foci were detected in the nucleus at 8 h p.i. with  $\sim 1$  per nucleus, whereas at 24 h p.i. the number increased to  $\sim 3$  foci per nucleus (Figure 23C). Out of 249 eGFP.OR3 nuclear foci detected at 24 h p.i. only 3.3 % were CA positive, 5.4 % were p12 positive and only 1.6 % were positive for both, CA and p12 (Figure 23D). At 8 h p.i. out of a smaller number of foci (44 foci analyzed in 51 cells), similar low co-localization percentages for CA (11.3%) and/or p12 (11.3%) were detected (Figure 23D).

In conclusion, these data indicate that subviral complexes comprised of largely complete set of CA and p12 proteins enter the nucleus (Figure 22), whereas accessible viral double-stranded cDNA is largely devoid of detectable CA and p12 proteins inside the nucleus (Figure 23). This may imply that after nuclear entry the viral DNA is being released and separates from the CA and p12 subviral complex. Since the OR3 protein will only bind to accessible dsDNA, complete or partial uncoating is necessary to generate the signal. Alternatively, the MLV capsids in the nucleus are permeable for OR3, but the dsDNA is not completed. At present the data does not allow to exclude one or the other and warrant further investigation in future studies.

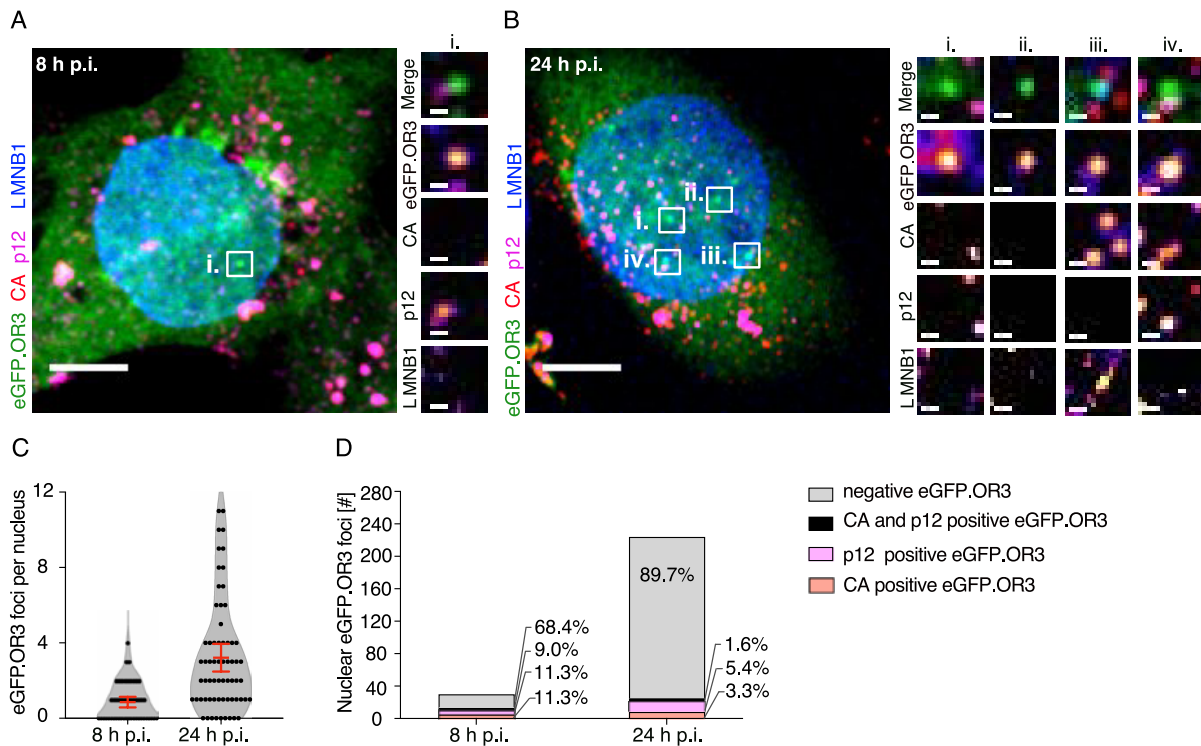


**Figure 23. Nuclear viral cDNA is largely devoid of detectable p12 and CA by immunofluorescence.** A-B. Expressing eGFP.OR3 eBFP2.mLMNB1 MEF were infected with MLV ANCH VSV-G (822  $\mu$ U RT/cell, MOI 6.3). The cells were then fixed at 8 (A) or 24 h p.i. (B) and IF stained using antibodies against p12 and CA. Representative images shown as MIP overview and single z-slices enlargements from one out of three independent experiments. Enlargements are presented of nuclear foci with background contrast adjustment for better visualization. Scale bars: 10  $\mu$ m (overview) and 2  $\mu$ m (enlargements). C. Quantification of nuclear eGFP.OR3 foci per cell from images shown in A-B. Data analyzed from two independent experiments for the 8 h timepoint (n = 51 cells analyzed) and from three independent experiments for the 24 h timepoint (n = 68 cells analyzed). The error bars are SD of the mean. D. Co-localization of nuclear eGFP.OR3 foci with CA and/or p12. Total number of foci analyzed were 44 foci from 51 cells at the 8 h p.i. timepoint and 249 foci in 68 cells analyzed at 24 h p.i. Percentage of colocalization of eGFP.OR3 foci with CA and/or p12 was calculated and shown. Data presented from three independent experiments for the 24 h p.i. and two independent experiments for 8 h p.i.

### 3.3.6 IN. FP is associated with a subset of MLV cDNA foci in the nucleus

Next, the viral IN enzyme, a necessary component of the RTC/PIC complex for integration and infection (Suzuki and Craigie, 2007), was analyzed for co-localization with OR3 signals. For this purpose, VSV-G pseudotyped ANCH3 and IN. FP containing particles were produced with a 3-plasmid transfection system (MLV ANCH IN. FP VSV-G). The isolated particles were assessed for IN.SNAP incorporation efficiency through

immobilization on glass slides, fixation, and immunostaining with antibody against CA (Figure 24A). Almost all CA identified signals were found to co-localize with IN.SNAP (~96 %; Figure 24B). Analysis of intracellular co-localization with OR3 signals was done at different time points in infected eGFP.OR3 eBFP2.mLMNB1 MEF cells (Figure 24C-D). The number of eGFP.OR3 foci at 8 h of infection was quite low, yielding only ~ 0.3 nuclear foci per cell (Figure 24C), which is barely above the number of background foci detections (Figure 16C) and thus should be interpreted with caution. At 24 h after infection this number increased to ~0.6 nuclear foci per cell (Figure 24E). The relatively low number of foci reflected the low particle yield attributed to the 3-plasmid transfection system. At 8 h post infection, only 24 foci were identified in 78 analyzed cells, of which ~28 % were positive for IN.SNAP (Figure 24F). At 24 h of infection, a similar fraction of ~34 % of eGFP.OR3 signals (44 identified foci in 64 cells) were positive for IN.SNAP (Figure 24F).

These data indicated that ~ 30 % of nuclear MLV cDNA objects were associated with a fluorescently tagged IN protein. It is possible that the IN marker is present at unintegrated cDNA and lost upon integration, but this requires further analysis in future work.

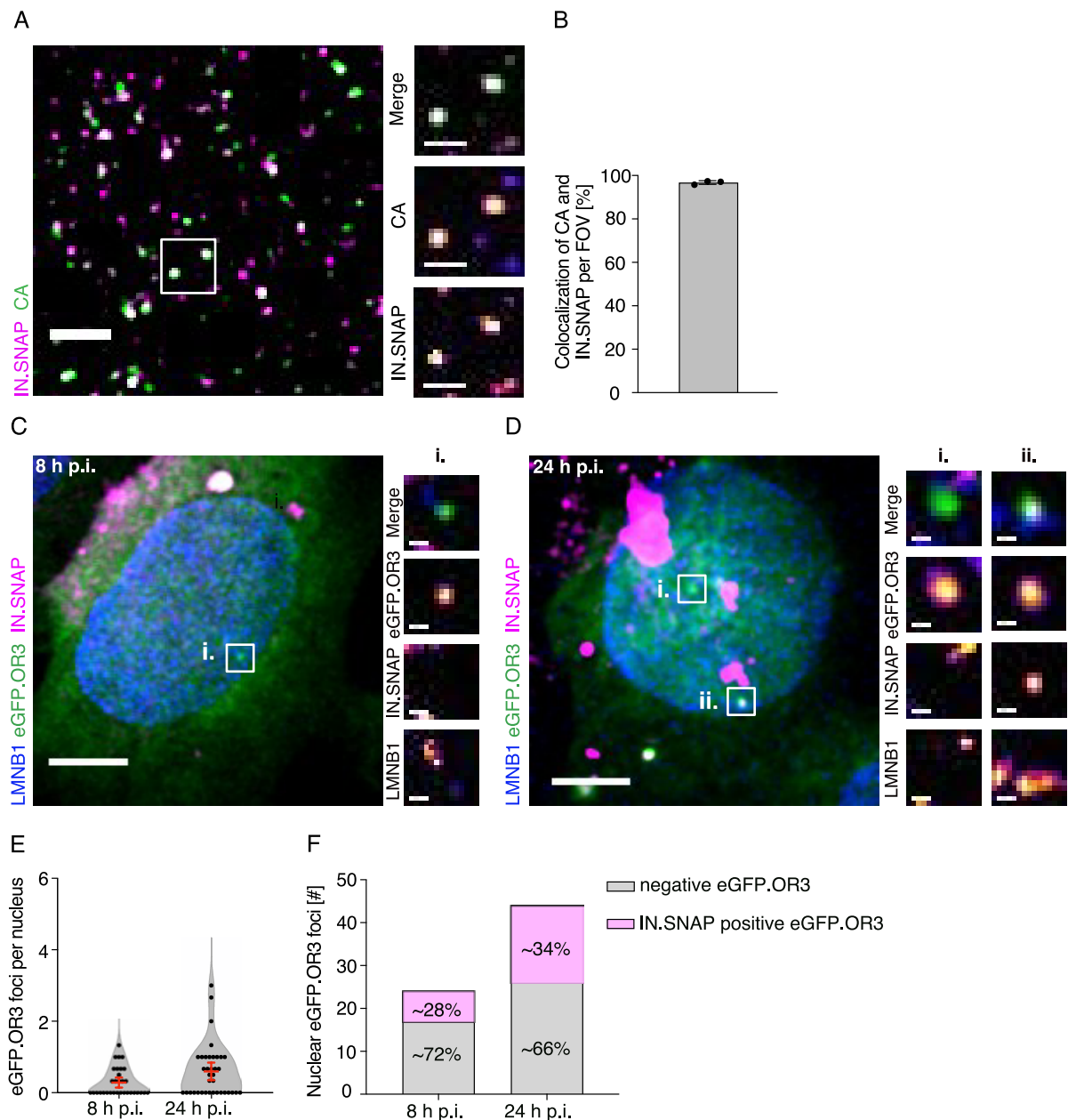


**Figure 24.** IN.SNAP is associated with a subset of MLV cDNA in the nucleus of infected cells. **A.** Incorporation efficacy of IN.SNAP in MLV ANCH particles was quantified by co-localization study with CA proteins. The MLV ANCH IN.SNAP VSV-G particles were produced in a 3-plasmid transfection system. They were then isolated, immobilized on PEI coated glass slides, and IF stained with antibodies raised against MLV CA. Scale bar: 1  $\mu$ m. **B.** The co-localization of IN.SNAP with CA identified signals was detected with Imaris from images presented in **A**. The percentage of co-localization from 15 FOV was plotted from one performed independent experiment. Errors bar are SD of mean. **C-D.** Expressing eGFP.OR3 eBFP2.mLAMNB1 MEF cells were infected with MLV ANCH IN.SNAP VSV-G (66  $\mu$ U RT/cell). The cells were then fixed at 8 (**C**) or 24 h p.i. (**D**). Representative images shown as MIP overview and single z-slice enlargements from one out of two independent experiments. Enlargements are presented of nuclear foci with background contrast adjustment for better visualization. Scale bars: 10  $\mu$ m (overview) and 2  $\mu$ m (enlargements). **E.** Quantification of nuclear eGFP.OR3 foci per cell from images

shown in C-D. Data analyzed from three independent experiments (mean and error bars representing 95 % CI, n= 64-78 cells per time point analyzed). F. Co-localization of nuclear eGFP.OR3 foci with IN.SNAP. Total number of foci analyzed were 24 foci from 64 cells at the 8 h p.i. timepoint and 44 foci in 78 cells analyzed at 24 h p.i. Percentage of co-localization of eGFP.OR3 foci with IN.SNAP was calculated and shown. Data presented from three independent experiments with SD.

### 3.3.7 Real-time visualization of MLV DNA in infected living cells

The advantage of the ANCHOR system is its applicability for live microscopy that was not possible with EdU click-labeling and FISH. This has already been shown in studies with ANCHOR labeled cDNA of HIV-1 (Müller et al., 2021), Adenovirus (Komatsu et al., 2018) and Human Cytomegalovirus (HCMV) (Mariamé et al., 2018). Therefore, the dynamics and appearances of OR3 signal upon MLV infection were analyzed by the application of the ANCHOR system in live-cell microscopy. SC-1 cells were infected with VSV-G pseudotyped MLV ANCH and 3D stacks were acquired every 30 min for 48 h (Figure 25A). The onset of OR3 signals in the nucleus was detected at 7-8 h p.i., whereas the maximum was reached at 24 h p.i. (Figure 25B). The kinetics of OR3 appearance and signal number were compared to the kinetics of viral DNA copies measured by ddPCR. The total *gag* cDNA levels were measured to be 60% of the maximum signal already at 4 h p.i., a timepoint where no eGFP.OR3 signal was detected (Figure 25C). The peak of *gag* cDNA levels was reached at 8 h p.i. with a steady decline until 48 h p.i. (Figure 25C). Thus, cDNA synthesis appears to be largely completed well before detection of nuclear OR3 signals. Importantly, however, the number of *gag* copies per cell was ~2 orders of magnitude higher than the number of detected OR3 signals: 15 *gag* copies were detected in cells infected with 55  $\mu$ U RT/cell compared to ~2 nuclear OR3 signals per cell infected with 2000  $\mu$ U RT/cell. A possible viral replication bottleneck in completion and uncoating of viral cDNA or largely aberrant and incomplete cDNA synthesis could explain the ~270 higher number of *gag* cDNA copies by ddPCR compared to OR3 signals. However, the large surplus of *gag* cDNA makes it difficult to interpret the kinetics of cDNA synthesis by ddPCR and OR3 spot detection.

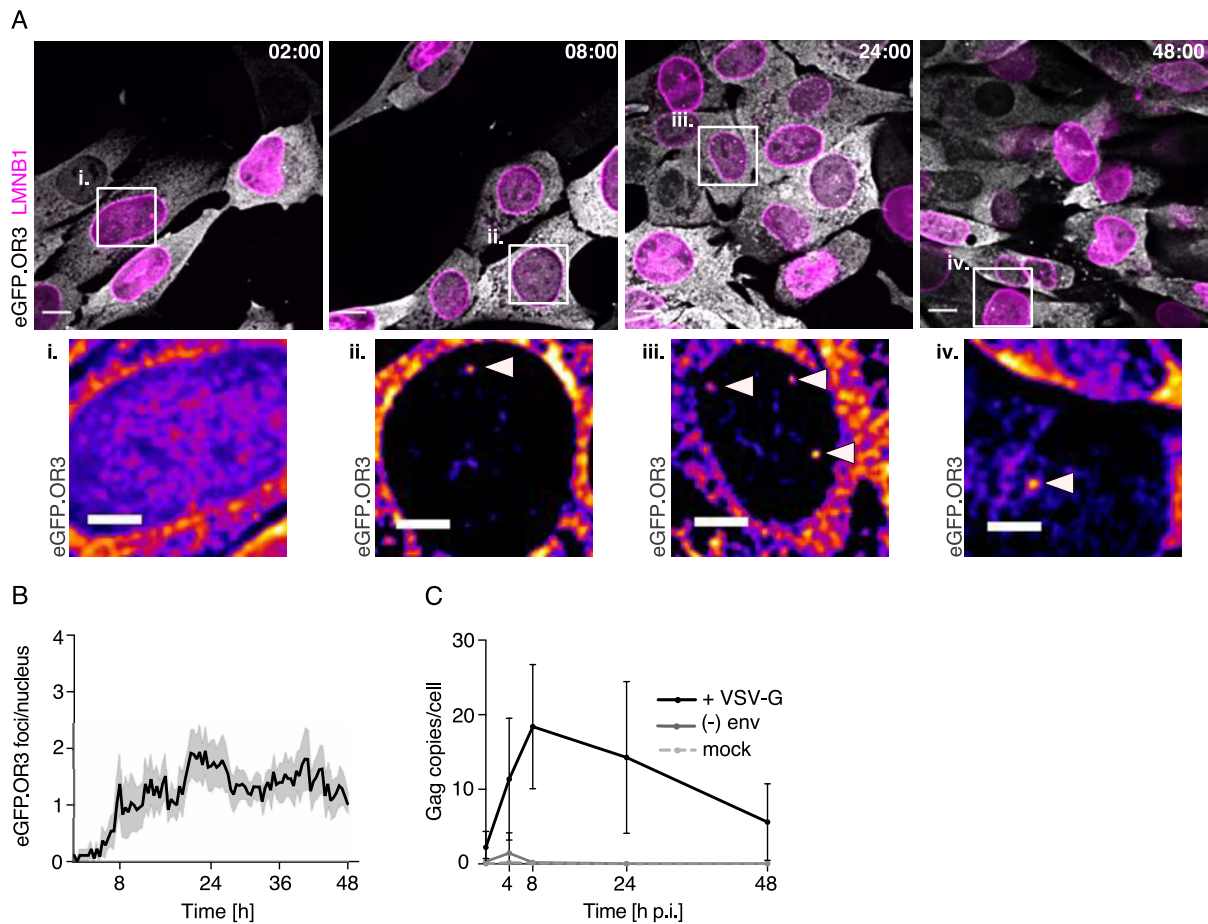


**Figure 25. Visualization of MLV dsDNA in living cells using the ANCHOR system.** A. Timelapse live-cell imaging of SC-1 eGFP.ORG3 eBFP2.mLMNB1 infected with MLV ANCH VSV-G (2000  $\mu$ U RT/cell, 19.5 MOI). Image acquisition by SDCM was initiated 30-45 min after infection, followed by 3D stack acquisition every 30 min for 48 h. Representative images from one out of the three independent experiments are shown as MIP. Enlargements are presented of nuclear foci with background contrast adjustment for better visualization. White arrows point to an eGFP.ORG3 signal. Scale bars: 10  $\mu$ m (overview) and 5 $\mu$ m (enlargements). B. Quantification of nuclear eGFP.ORG3 foci per cell over time from images show in A. Nuclear eGFP.ORG3 foci per cell are plotted over time of imaging lasting for 48 h. On the x-axis 0 h time point indicates the start of live imaging which is 30-45 min after infection. Three independent experiments were performed and a total of 107 cells were analyzed. C. RT kinetics was investigated in SC-1 cells expressing eGFP.ORG3 eBFP2.mLMNB1 SC-1 infected with MLV ANCH VSV-G (55  $\mu$ U RT/cell, corresponding to 25% $\pm$ 11 infected cells) using ddPCR. Infected samples with VSV-G pseudotyped virus (+ VSV-G), without envelope fusion protein ((-) env) and uninfected samples (mock) were isolated at indicated timepoints. Copies of late RT product *gag* per cell were quantified over time. Three independent experiments were performed. The error bars represent SD of the mean.

To verify whether the nuclear OR3 signals detected in Figure 25 are formed due to infection and are not cellular background accumulations, the appearance of possible OR3 signals in the nuclei of uninfected cells was also analyzed. Using the same live conditions as in Figure 25, with greatly reduced laser intensities to prevent photobleaching and phototoxicity, the nuclear background OR3 accumulations in uninfected cells (180 % a.u. above measured cell background) were rare (Figure 26).

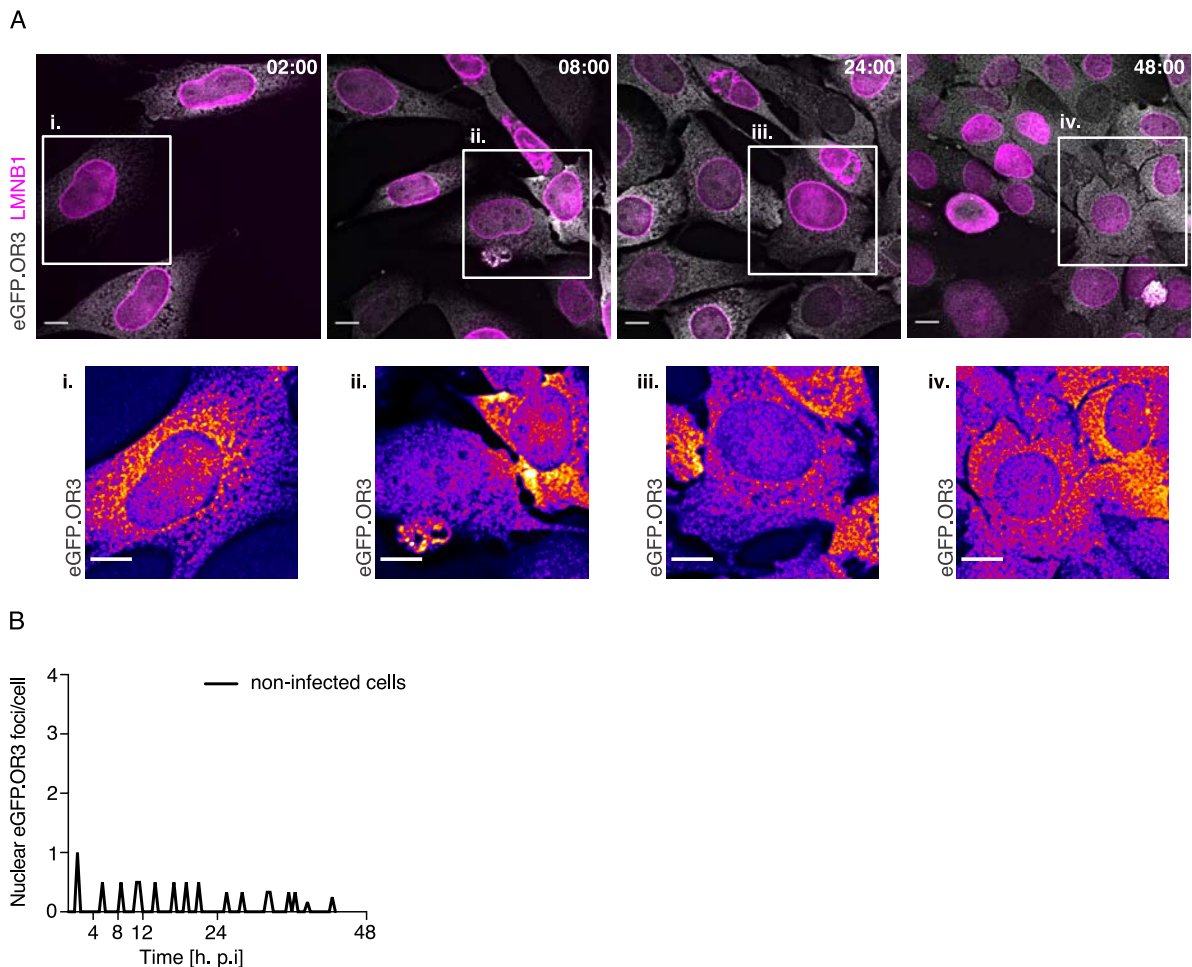


**Figure 26.** Timelapse live-cell imaging of non-infected eGFP.OR3 and eBF2.LMNB1 expressing cells. A. Imaging of SC-1 eGFP.OR3 eBFP2.mLMNB1 treated with DMSO. Image acquisition by SDCM was initiated 30-45 min after addition of DMSO, followed by 3D stack acquisition every 30 min for 48hr. Representative images from one independent experiment preformed are shown as MIP. Scale bars: 10  $\mu$ m. B. Quantification of nuclear eGFP.OR3 foci per cell over time from images show in A. Nuclear eGFP.OR3 foci per cell are plotted over time of imaging lasting for 48hr. On the x-axis 0 h time point indicates the start of live imaging which is 30-45 min after infection. One independent experiment was preformed, and 13 cells were analyzed.

### 3.3.8 Tracking up to three generations of infected living daughter cells with eBFP2.mLMNB1 as a division marker

Cellular division plays a vital role in nuclear entry of MLV and subsequently of successful viral replication (Roe et al., 1993; Suzuki and Craigie, 2007); therefore, the ability to visualize cellular division in living MLV infected cells is of importance. For this purpose, cells had been transduced to express murine LaminB1 protein tagged with eBFP2 fluorophore, to enable visualization of the nuclear envelope under fixed and live imaging conditions (Figure 27A). A division event was characterized by the morphological changes of the nuclear envelope visualized by eBFP2.mLMNB1; starting with the blurring of the envelope and loss of circular shape and ending with the reformation in two separate circular shapes of nuclear envelopes (Figure 27A). Next, the time of division for each parent cell was noted and all upcoming division events of the daughter cells originating from this ancestral parent cell (Figure 27B). With this data, I could trace and generate family trees of up to three generations of daughter cells originating from one ancestral parent cell (Figure 27A). The data showed that on average, infected parent cells divide within ~7 h post infection (Figure 27B, C), which coincided with the onset of eGFP.OR3 foci appearance (Figure 25B). Furthermore, the event of division from the loss of characteristic nuclear shape up to the reformation of two nuclear shapes lasted on average for 0.6 h (Figure 27C). These data showed that entry and detection of the viral cDNA is correlated to cellular division.

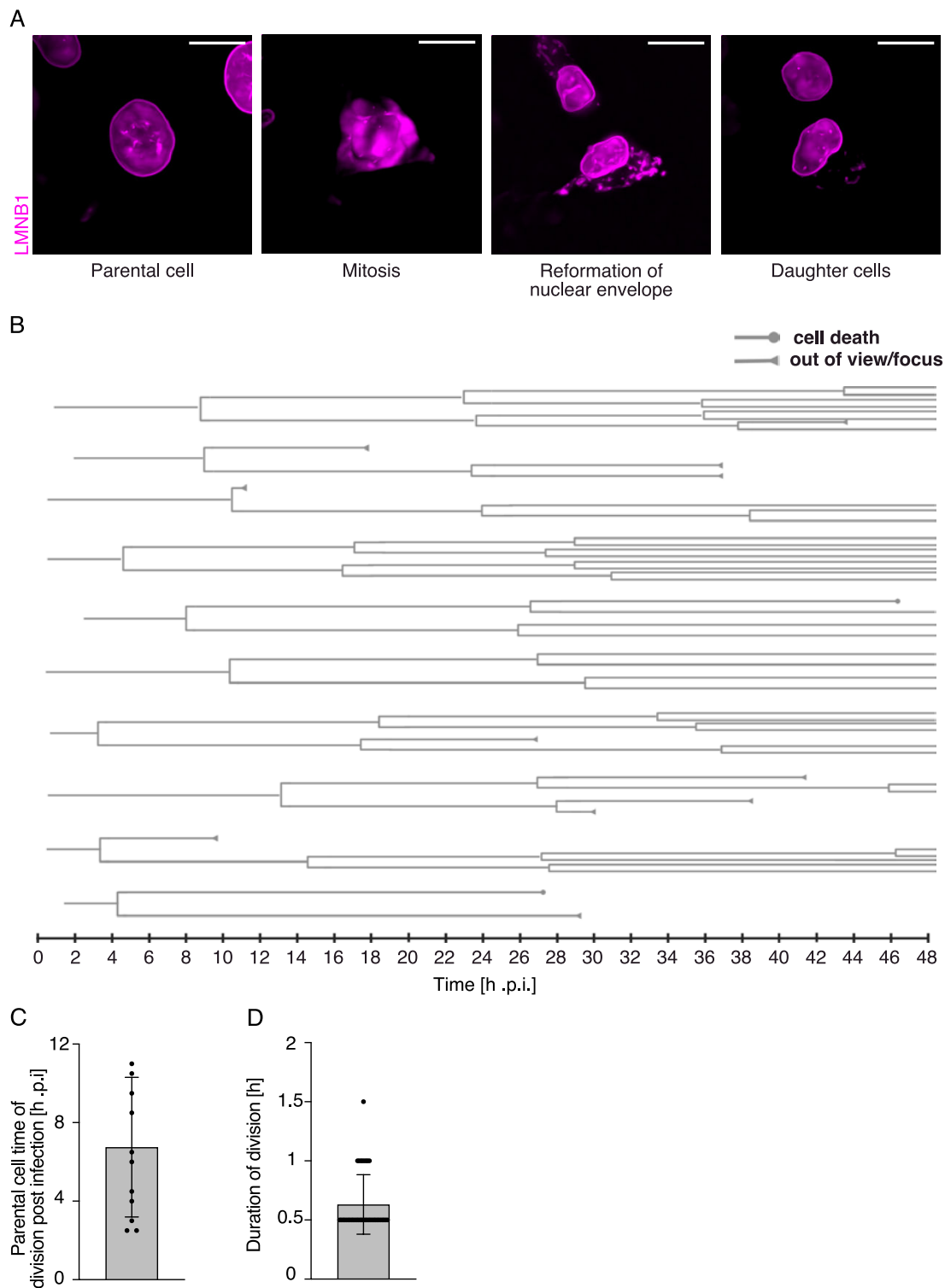


**Figure 27. Imaging and tracking of cell division events with eBFP2.mLMNB1 marker in living infected cells.** A. SC-1 eGFP.OR3 eBFP2.mLMNB1 SC-1 cells infected with MLV ANCH VSV-G (2000  $\mu$ U RT/cell, 19.5 MOI) were imaged live by SDCM. A 3D stack acquisition was initiated in 30 min intervals for 48 h. Representative images from one out of three independent experiments are shown as MIP. Scale bars: 10  $\mu$ m. B. Graphical representation of 10 lineages of cells, starting with identification of a parent cell from the beginning of imaging or cell entry in FOV and all the following daughter cells originating from it. End of line with a ball indicates cell death and end of line with triangle indicates the cell is out of view or focus.

Number of cells analyzed is 107. Three independent experiments were performed. C. For all identified parent cells with traced lineages, the time of first division event was measured. The time from the start of the imaging session or parent cell entry in field of view until the division event of the identified parent was measured. Three independent experiments were performed, and 12 infected parent cells were analyzed. The error bars represent SD of the mean. D. The duration of division was measured for 12 lineages. The start of measurements is the blebbing phenotype of the cells to the reformation of the nuclear envelope of the daughter cells. Three independent experiments were performed, and 38 cells were analyzed. The error bars represent SD of the mean.

### 3.3.9 Cellular division is necessary for visualization of viral cDNA in the nucleus of MLV ANCHOR infected cells

Next, the role of cellular division in nuclear entry of viral cDNA as a bottleneck was examined in MLV infected live cells in detail. The first division event as well as cDNA appearance of the identified and tracked parent cell was characterized in 5 stages: identification of parent cell (P1), mitosis of the parent cell (P2), daughter cell formation (P3) and nuclear foci appearance in the daughter cells (P4-5) (Figure 28A). Furthermore, the time of division (Figure 27C) as well as the foci appearance of each daughter cell arising from the first generation was measured (Figure 28B). As expected, the appearance of viral cDNA, identified by the OR3 marker, occurred only after cellular division. Distinct nuclear foci were not identified in the infected parent cells prior to the first cell division (Figure 28B) with only occasional single-frame nuclear aggregations as characterized in Figure 26B. This system enabled for the first time to visualize the spatial position of MLV cDNA inside the nuclei of specific living cell-lineages and confirmed the requirement of cellular division for nuclear entry of MLV cDNA.

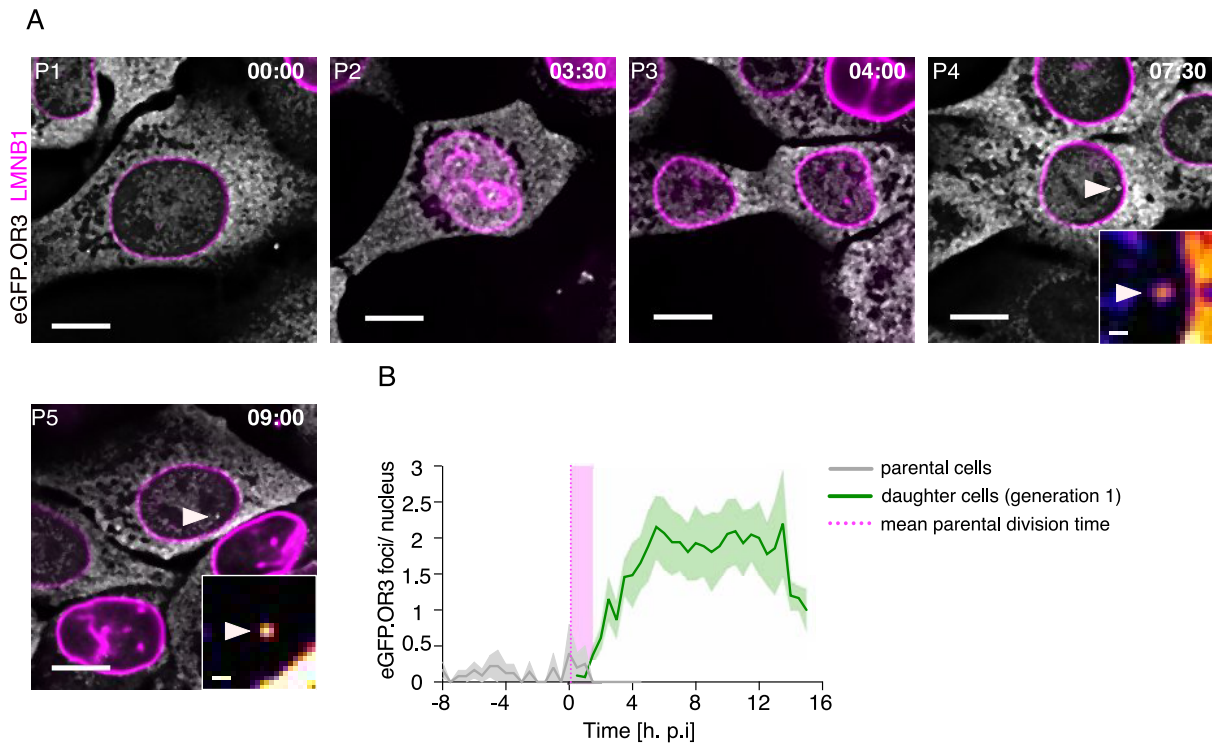


**Figure 28. Appearance of OR3 signal in the nucleus of daughter cells requires cellular division of the infected parent cell.** A. Live SC-1 expressing eGFP.OR3 eBFP2.mLMNB1 cells were infected with MLV ANCH VSV-G (2000  $\mu$ U RT/cell, 19.5 MOI) and imaged by SDCM. 3D stack acquisition by SDCM was initiated every 30 min for 48 h. Five panels numbered as P1-P5 depicted a cellular division with the following events: P1= identified parent cell, P2= parent cell undergoing mitosis, P3= daughter cells arising from the division event and P4-5= nuclear foci formation in the daughter cells. Representative images of one out of three independent experiments are shown as single z-slices. Enlargements are presented of nuclear foci with background contrast adjustment for better visualization. Scale bars: 10  $\mu$ m (overview) and 2  $\mu$ m (enlargement). B. Quantification of nuclear eGFP.OR3 foci from parent cells and the daughter cells arising from the first division event (1<sup>st</sup> generation) of images presented in A. The 0 h timepoint as well as the pink dotted line indicate the mean time of division measured of all parent cells. The hours prior of the 0 h timepoint are the imaged time of all tracked parent cells before their first division event. The pink shaded area arising from the line indicates the mean time needed to complete division (~30min). eGFP.OR3 foci arising in the parent cells are marked with a grey line and the foci arising in daughter cells are marked with a green line. Three independent experiments were performed. The error band represents the SD of the mean.

Subsequently, the OR3 signal arising from parent cells and each of the three consecutive daughter cell generations was analyzed individually (Figure 29A). In the first generation of daughter cells, I observed a lagging period of  $\sim 4$  h from the division event to the first foci appearance indicating that the nuclear viral cDNA requires time to either complete reverse transcription or is not accessible in the beginning but is revealed by the uncoating of the viral capsid (Figure 29B). Interestingly, this lagging period observed in the first generation (Figure 29B) could not be observed in the second and third generation, where an immediate appearance of OR3 signal was observed (Figure 29 C-D). Furthermore, the number of foci per cell remained steady over time in all generations (Figure 29 C-D). These data suggested that the signals arising in the first generation need time to be revealed or synthesized, whereas the signals in the subsequent generations were already present and accessible inside the nucleus. Furthermore, OR3 foci perseverance suggest integrated cDNA as unintegrated species would likely to be lost during mitosis or degraded over time.

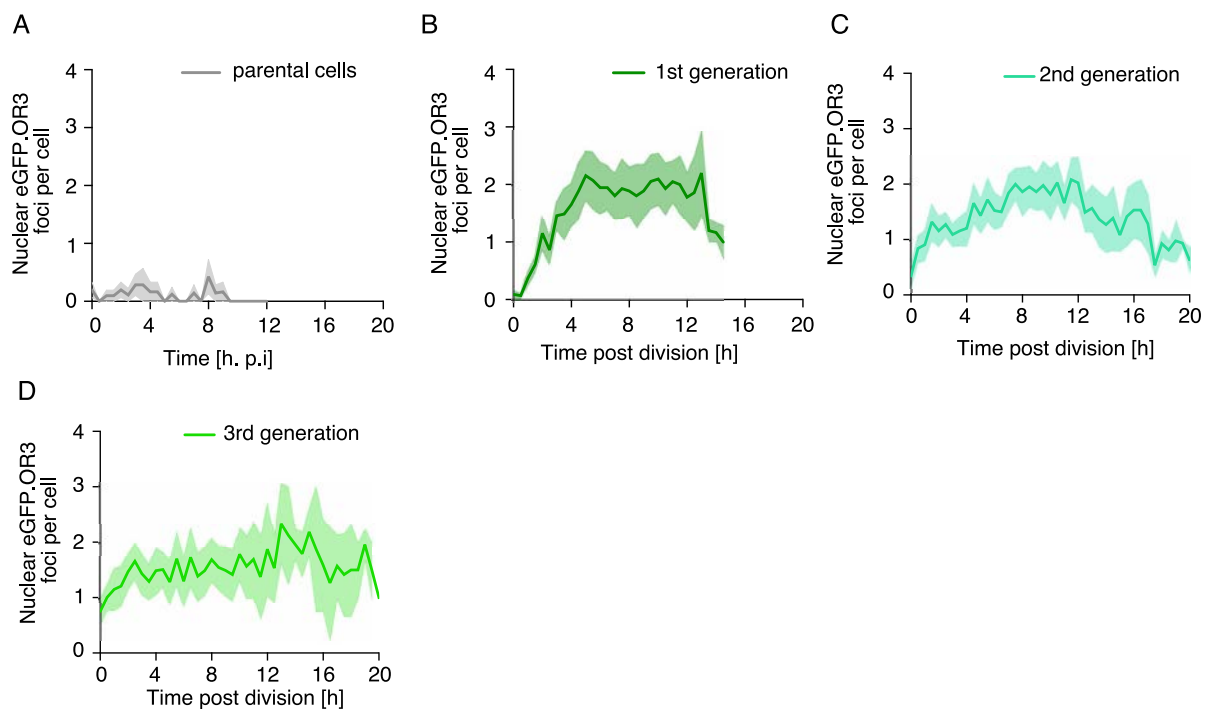


**Figure 29. Characterization of nuclear eGFP.OR3 signal dynamics post division in three generations of daughter cells.** A-D. Live cell-imaging in SC-1 eGFP.OR3 eBFP2.mLMNB1 infected with MLV ANCH VSV-G (2000  $\mu$ J RT/cell, 19.5 MOI) of viral cDNA. Every 30 min a 3D stack was acquired by SDCM for 48 h. The nuclear foci per cell were quantified in the parent cell (A) and daughter cells from the first (B), second (C) and third (D) generation. The error bands represent SD of mean. Three independent experiments were performed.

### 3.3.10 Characterization of nuclear OR3 foci dynamics and longevity in living MLV infected cells

In most daughter cells, the nuclear OR3 signals appeared and remained stable until the cell underwent a division (Figure 30A). The loss of signal during division may be explained by the condensation of chromatin, which may prevent OR3 binding to the viral cDNA. In addition, a sharp increase in background intensity of eGFP.OR3 was observed during division, which masked the weaker foci. Surprisingly, some nuclear OR3 signals had shorter lifetime and disappeared from the cells regardless of their division status (Figure 30B). Therefore, 161 OR3 signals in 57 infected cells were examined and documented for their longevity in the nucleus. The signals were then assigned to two groups depending on their lifetime: long-lived foci that were present longer than 2 h and short-lived foci that were present less than 2 h (Figure 30C). I also observed signals that were present in a single frame only, which were characterized in Figure 26, and subsequently excluded from the analysis (Figure 30C, magenta dotted line). The long-lived foci had a mean duration of detection of  $\sim 9$  h and made up  $78 \pm 36$  % of the total number of foci detected in the nuclei of infected cells (Figure 30D). One of the possible factors influencing the longevity of foci is cell division, therefore I investigated how many foci disappeared due to cells undergoing division. It was observed that  $\sim 55\%$  of detected eGFP.OR3 foci per cell are lost shortly before cell division (Figure 30E). Lastly, a graphical depiction of the OR3 signal dynamic nature in the nucleus of ten daughter cells is shown (Figure 30F). The aim is to demonstrate the heterogeneity of eGFP.OR3 appearance and loss, which was present in all cells except for daughter cells four and ten where one long-lived signal was observed up to the division event (Figure 30F)

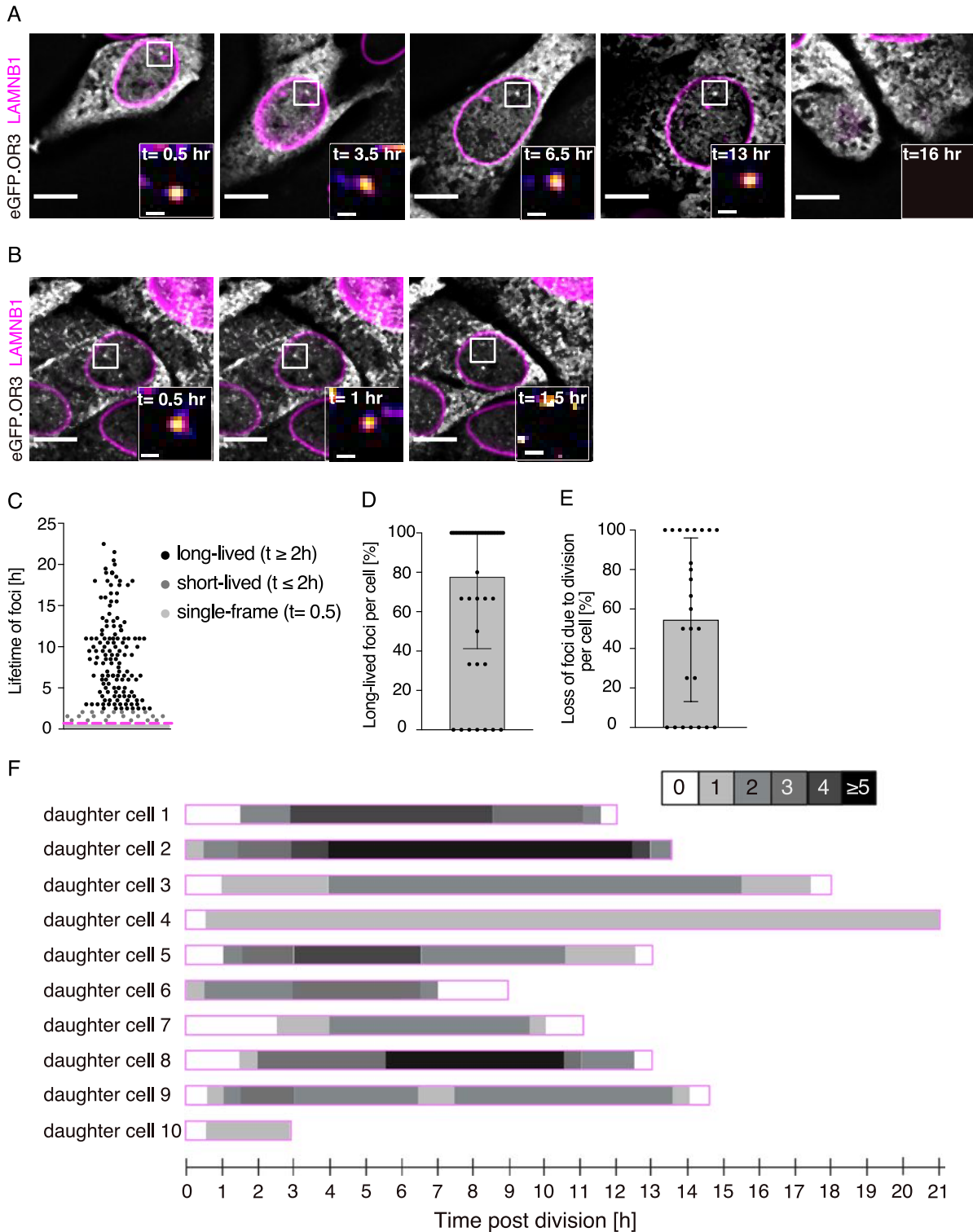


**Figure 30. Real-time characterization of nuclear OR3 signal dynamics and lifetimes.** A-B. Live cell imaging of eGFP.ORG3 foci in SC-1 cells infected with MLV ANCH VSV-G (2000  $\mu$ U RT/cell, 19.5 MOI). Representative images of one long-lived (A) and short-lived nuclear foci (B) are shown as single z-slice images. The images were picked from one out of three independent experiments performed. Scale bars: 10  $\mu$ m (overview) and 2  $\mu$ m (enlargement). Enlargements are presented of nuclear foci with background contrast adjustment for better visualization. White boxes indicate a detected eGFP.ORG3 foci. C-E.

Quantification of nuclear eGFP.OR3 foci from images presented in A-B. The duration of the eGFP.OR3 foci in h (C), the prevalence of long-lived foci in percentages per cell (single frame detections were excluded from the total number of foci) (D) and the loss of foci due to division (E) were quantified. Data presented from three independent experiments (n= 57 cells and 161 foci). Error bars represent SD of the mean. F. Graphical representation of daughter cells and the dynamic appearance of eGFP.OR3 foci in the nucleus. Each daughter cell is normalized to their division event. The lifetime of each daughter cell is represented with a pink rectangle from their creation to their own division event. Each box signifies time of 30 min and the grey gradient color indicates the number of nuclear foci detected at that timepoint.

### 3.3.11 The ANCHOR system enables detection and tracking of OR3 signal through division events and for up to three generations of infected daughter cells

Following the observations of long-lived versus short lived foci, I examined the appearance of the OR3 signals and their propagation in 12 lineages of cells in a total of 107 cells; each lineage underwent multiple division events reaching up to 3 generations per lineage. After cell division of an OR3 signal containing parent cell, a reappearance of OR3 signals were detected in 34 out of 96 daughter cells; however, these cells contained multiple OR3 signals, which made it difficult to trace the propagation of a possible integrated event. Therefore, the analysis was focused on cells propagating one or maximum of two foci. In four out of the twelve analyzed lineages, one or two OR3 signals were traced from the parent to the third-generation daughter cell (Figure 31 A-B, grey shaded boxes). In total, 20 out of 96 eGFP.OR3 signal positive daughter cells showed a traceable focus after further division (~21 %). For the single OR3 foci which were present through multiple cell division events it can be speculated that they represent integrated MLV proviruses (Figure 31 A-B, grey shaded box). Specifically in cases where a parent cell with one focus gives rise to two daughter cells each containing one focus themselves, which appeared instantaneously with the formation of the nuclear envelopes (Figure 31). In contrast, for cells in which a single OR3 focus could be observed in the first generation but not in the second generation of daughter cells, it seems likely that the respective MLV cDNA was not integrated and lost upon division (Figure 31B, pink shaded box). Interestingly, in rare cases I observed an asymmetric distribution of the viral cDNA in the daughter cells (Figure 31A, pink shaded), probably due to the *de novo* infection with viral particles that had remained in the medium or replication complexes that had previously remained in the cytoplasm.

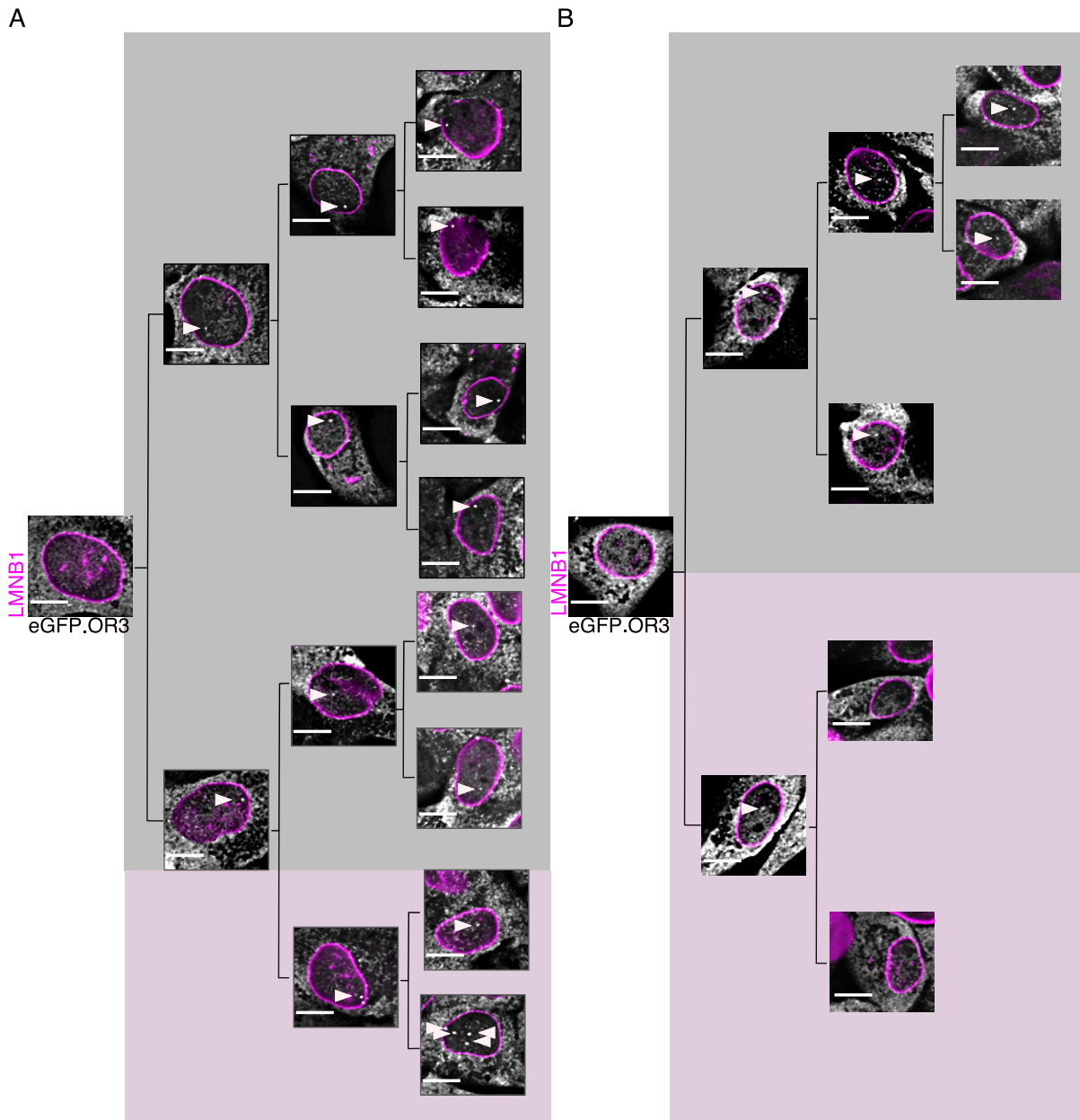
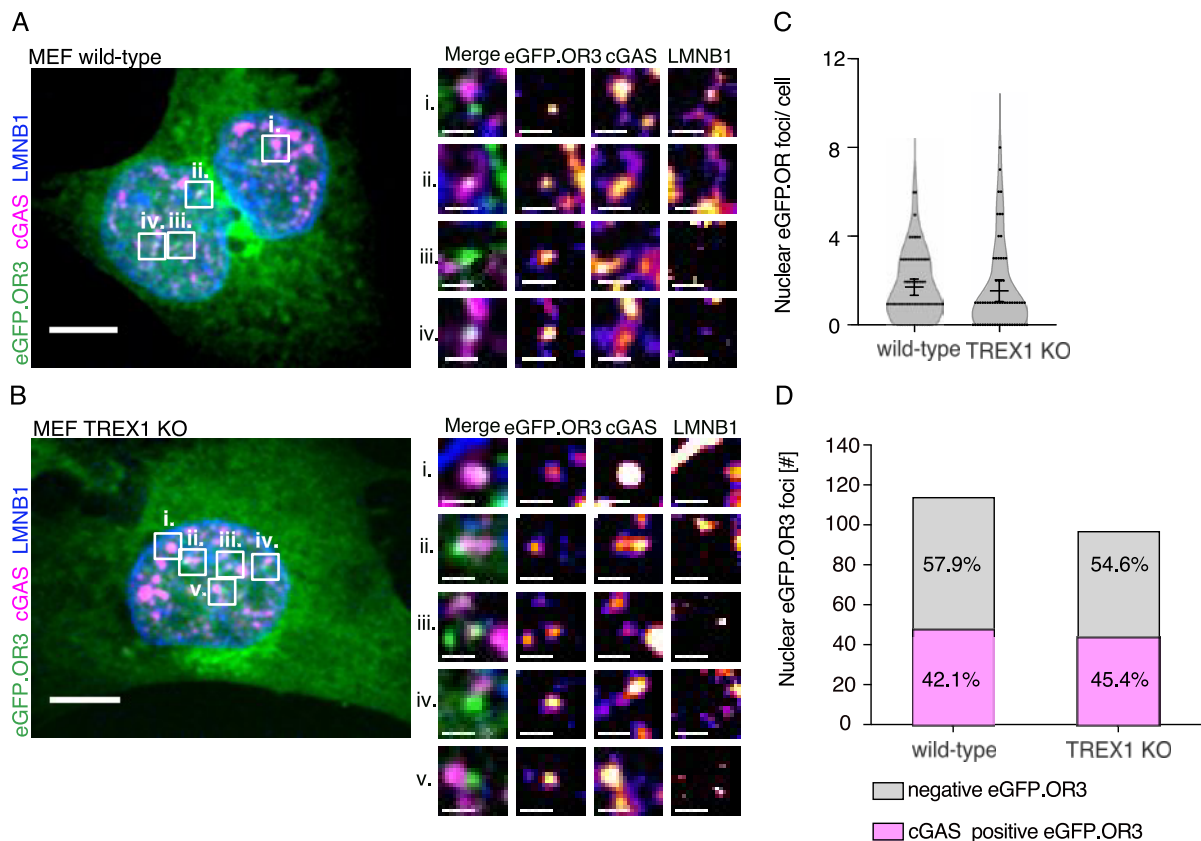


Figure 31. An OR3 signal was tracked through several generations of infected daughter cells. A-B. Representative single z-slice images of the different phenotypes characterized in the live SC-1 eGFP.OR3 eBFP2.mLMNB1 cells infected with 2000  $\mu$ U RT/cell (MOI= 19.5) MLV ANCH VSV-G. Two lineages are shown from one out of three performed experiments. The black lines indicate division events and the resulting daughter cells. The grey shaded boxes indicate cells in which a single focus was present in both daughter cells throughout the observation period of 3 generations (i.e. possible integration events). The pink shaded boxes indicate cells that showed an asymmetric distribution (i.e. likely de novo entry of MLV subviral particles into the nucleus post division) (A) or loss of eGFP.OR3 foci (i.e. likely non-integrated MLV cDNA) (B). Scale bars: 10  $\mu$ m.

### 3.3.12 The nuclear viral cDNA interacts with cGAS in the presence and/or absence of TREX1

To investigate the difference in lifetime of the nuclear eGFP.OR3 signals (*cf.* 3.3.10, Figure 30), possible interactions with host factors such as cGAS and TREX1 were examined. It has been described that viral MLV cDNA can be detected by nucleic acid sensors cGAS and DDX41 (Bhat and Fitzgerald, 2014; Gao et al., 2013; Moran and Ross, 2020; Stavrou et al., 2018, 2015). This detection depended on the depletion of TREX1, a cytosolic exonuclease that degrades reverse transcripts and dampens immune response (Gao et al., 2013; Kumar et al., 2018; Stavrou et al., 2018; Yan et al., 2010). Thus, it appeared possible that TREX1 may degrade some of the MLV cDNA and lead to disappearance of eGFP.OR3 spots over time. Accordingly, MEF eGFP.OR3 eBFP2.mLMNB1 expressing cells with a knockout of TREX1 were infected with VSV-G pseudotyped MLV ANCH (Figure 32 A, B). If TREX1 degrades a subset of cDNA, then TREX1 depleted MEF cells should result in higher numbers of total eGFP.OR3 foci compared to TREX1 competent cells. However, there was no difference detected in the number of nuclear foci between MEF wild-type (1.7 foci/cell) and TREX1 KO cells (1.53 foci/cell) (Figure 32C). Moreover, the samples were extracted with MeOH and immunostained with antibody raised against cGAS (Figure 32A, B). Strikingly, nuclear OR3 signals were co-localizing with cGAS in wild-type MEF in ~42 % of all spots and in TREX1 KO MEF in ~45 % of all spots (Figure 32D). These data indicated that TREX1 does not appear to be responsible for the transient nature of a subset of eGFP.OR3 foci. The recruitment of cGAS to eGFP.OR3 foci appeared to be independent of TREX1. Further experiments need to be performed to investigate the effect of the minus-glycoGag variant, which is more sensitive to nucleic acid sensors than the wild-type MLV.



**Figure 32. Number of eGFP.OR3 foci and association with cGAS is not dependent on TREX1.** A-B. MEF eGFP.OR3 eBFP2.mLMNB1 cells with (A) and without TREX1(B) were infected with MLV ANCH VSV-G (822  $\mu$ U RT/cell, MOI 6.3). The cells were then fixed at 24 h p.i. and IF stained using antibodies against cGAS. Representative images from one out of two performed experiments are shown as MIP overviews and single z-slices enlargements of nuclear eGFP.OR3 foci. Enlargements are presented of nuclear foci with background contrast adjustment for better visualization. Scale bars: 10  $\mu$ m (overview) and 2  $\mu$ m (enlargements). C. Quantification of nuclear eGFP.OR3 foci per cell at 24 h p.i. from images shown in A-B. Data presented from two independent experiments (with mean and error bars representing 95 % CI, n = 63-67 cells analyzed). D. Co-localization of nuclear eGFP.OR3 foci with cGAS from images shown in A-B. Total number of OR3 foci analyzed were 114 from infected MEF cells and 97 OR3 foci from infected MEF KO TREX1 cells. Percentage of co-localization of eGFP.OR3 foci with cGAS was calculated and shown. Data presented from two independent experiments (n = 40-51 cells analyzed).

### 3.3.13 Association of $\gamma$ H2AX with viral DNA in retroviral and lentiviral infected cells

In order to investigate early chromatinization of MLV viral cDNA, possible host cell proteins that could be involved in the integration process were explored. The DNA damage response (DDR) components were found to be involved in post-integration repair, generation of viral DNA species and cause for HIV-1 infected CD4<sup>+</sup> T-cells death

(Anisenko and Gottikh, 2019; Cooper et al., 2013; Sloan and Wainberg, 2011). Upon DNA damage, the histone H2AX becomes phosphorylated at serine 139 (γH2AX), which is highly visible as strong foci at sites of DNA damage by microscopy (Daniel et al., 2004). Furthermore, our lab recently observed that the DDR markers γH2AX and p53bp1 were co-localizing with integrated and unintegrated HIV-1 cDNA (Thorsten Müller, 2021). Therefore, it was tested if γH2AX was recruited to MLV viral cDNA as well.

MEF cells were infected with VSV-G pseudotyped NNHIV ANCH (integration incompetent virus), pWPI ANCH (integration competent HIV-1 based lentiviral vector) and MLV ANCH prior to fixation and immunostaining against γH2AX (Figure 33). To prevent integration of MLV, some samples were treated with 10 μM raltegravir during infection. First, it was validated that the antibody recognizes murine γH2AX by the increase of specific pattern that could be observed in infected NNHIV MEF cells (Figure 33A). Moreover, it was observed that the majority of unintegrated viral NNHIV cDNA co-localize with the γH2AX accumulations (Figure 33C) with ~ 71 % (Figure 33B). In contrast, upon infection with the HIV-1 based vector pWPI (Figure 33D), the co-localization percentage of viral cDNA with γH2AX decreased to ~ 47 % (Figure 33B). This is in line with previous experiments performed in human cell lines comparing integration competent versus non-competent HIV-1 viruses (Thorsten Müller, 2021). In the case of MLV ANCH infection (Figure 33E), viral cDNA co-localization with γH2AX accumulations was seen in 17 % and 34 % of all cases in the DMSO and raltegravir treated samples, respectively (Figure 33B).

In conclusion, MLV cDNA does not - in contrast to HIV-1 – co-localize with γH2AX in most cases. Blocking integration seems to slightly elevate these values, but more experiments are needed for a clear result.

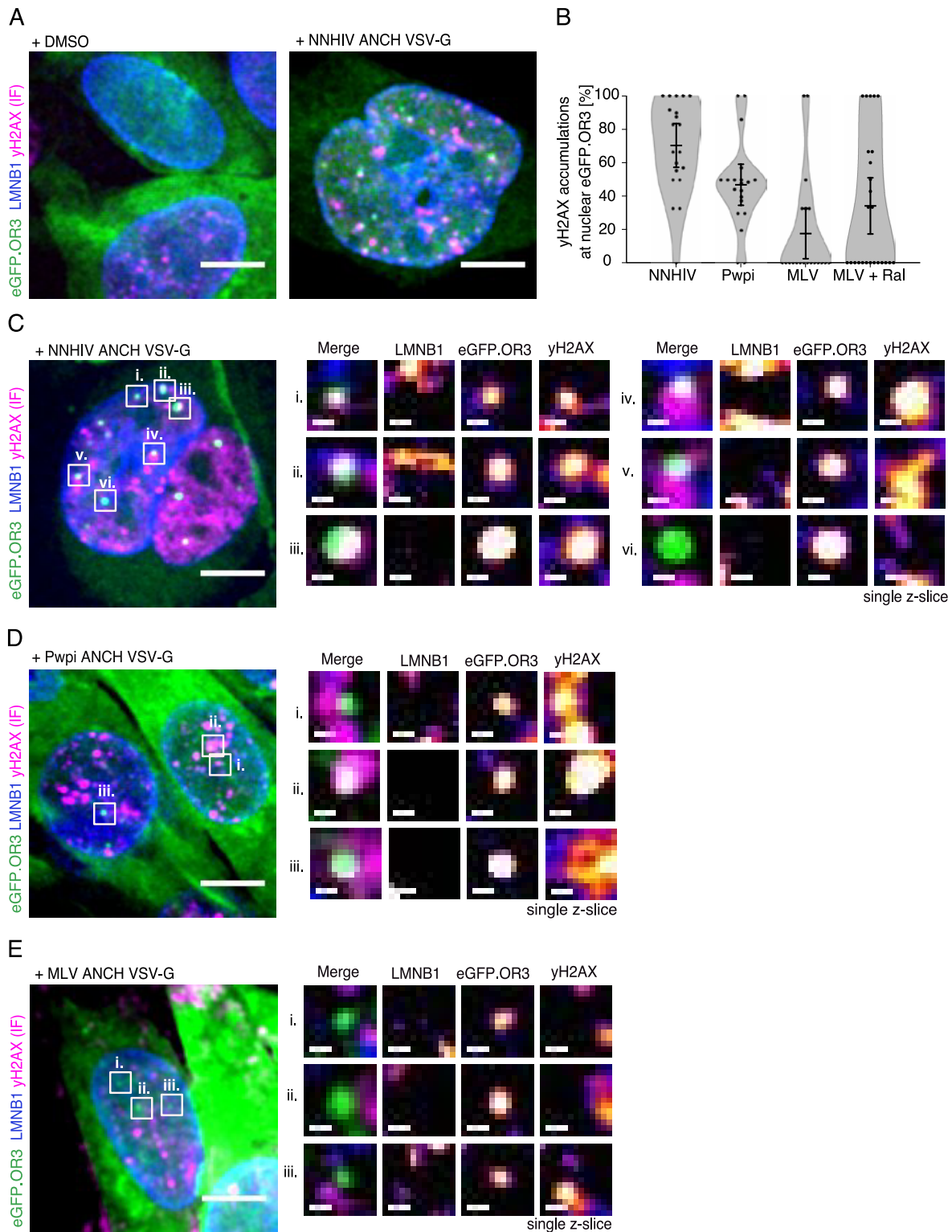


**Figure 33. Association of viral DNA with yH2AX.** MEF eGFP.OR3 eBFP2.mLMNB1 cells were infected with VSV-G pseudotyped NNHIV ANCH (30 $\mu$ U RT/cell; A, C), pWPI ANCH (30 $\mu$ U RT/cell; D), and MLV ANCH (822  $\mu$ U RT/cell; E) and uninfected cells (A). The cells were fixed at 24 h p.i. and IF stained using antibodies against yH2AX. Representative images from one performed experiment were shown as MIP overview and single z-slice enlargements of nuclear eGFP.OR3 foci. Enlargements are presented of nuclear foci with background contrast adjustment for better visualization. Scale bars: 10  $\mu$ m (overview)

and 2 $\mu$ m (enlargements). B. Co-localization percentages of nuclear eGFP.OR3 foci with  $\gamma$ H2AX per cell from images shown in C-E. Data presented from one independent experiment (mean and error bars representing 95 % CI, n = 20-25 cells analyzed per sample).

## 4 Discussion

In this thesis, a labeling system for visualization of single dsDNA molecules (the ANCHOR system) was adapted to investigate MLV cDNA synthesis, and its associations with viral and host cell proteins in a spatio-temporal context. The system allows the investigation of MLV capsid presence in relation to reverse transcription, which was complemented by infectivity experiments performed with a destabilized capsid variant lacking glycoGag.

This thesis additionally explored several different imaging-based strategies for visualizing MLV genomes. The application of the ANCHOR system represents the first successful approach for visualizing MLV dsDNA in living cells that have undergone division. Utilizing this method, it was shown that OR3 signals unambiguously emerge in the nucleus of MLV infected cells after cellular division. Furthermore, this thesis offers information about the viral protein composition of MLV subviral particles in the cytoplasm as well as nucleus. Destabilized capsid MLV particles showed diminished infectivity, attributed to early replication events in immunocompetent cells. These data are consistent with the hypothesis that intact MLV capsids are necessary in the cytoplasm to protect the viral cDNA. Furthermore, confocal microscopy of fixed subviral complexes in the nucleus revealed, that the majority of CA signals were found in complex with p12 after division, but not associated with viral cDNA. Taken in consideration data from this thesis and literature, the process of uncoating likely occurs during or shortly after cellular division with separation of the majority of detectable CA and p12 proteins from the viral cDNA (Wanaguru et al., 2018; Wang et al., 2016). The trigger as well as mechanism for uncoating, with a potential mediating cellular protein, are not known yet.

Importantly, the ANCHOR system, allowed real-time tracking of propagated cDNA signals from parent cell to up to three generations of daughter cells which likely

represents integrated retroviral genomes. Lastly, in this thesis, it was observed that the majority of MLV integrated and unintegrated cDNA, in contrast to HIV-1, does not associate with the  $\gamma$ H2AX component of the DDR pathway. Instead, a subset of MLV cDNA associates with the host cell factor cGAS independently from TREX1 activity, suggesting a possible bottleneck posed by the immune system on the unintegrated viral DNA.

#### 4.1 The spatio-temporal dynamics of MLV reverse transcription

The duration of reverse transcription is different depending on cell lines and retrovirus, which is mainly conditional on the dNTP abundance in the target cells (Bejarano et al., 2018). Generally, 6-12h was observed for retroviral dsDNA synthesis in dividing cells (Telesnitsky and Goff, 1997). Imaging MLV infected cells with the ANCHOR system revealed distinct OR3 signals in the nucleus with onset detected after  $\sim$ 8 h p.i. in fixed as well as real-time conditions (*cf* 3.3.1., Figure 16; *cf*. 3.3.7., Figure 25), meaning double-stranded MLV DNA is synthesized and accessible in the nucleus after that timepoint. Interestingly, this seemed to be similar to measurements in HIV-1 infected human cells (Müller et al., 2021). In contrast, the MLV late reverse transcription product *gag* reached half maximal signal levels at 4 h p.i., measured by ddPCR (*cf*. 3.3.7., Figure 25). Knowing that ddPCR detects both ssDNA and dsDNA, while the ANCHOR system detects only dsDNA, there are two ways to interpret the data. First interpretation proposes that the onset detected between *gag* and OR3 signal detection ( $\sim$ 4h) is the time needed for overcoming the 2<sup>nd</sup> strong stop encountered in reverse transcription and finishing synthesis of the dsDNA. Second interpretation is that the dsDNA is already synthesized but shielded by the capsid core and the  $\sim$ 4h difference between *gag* and OR3 signals is used for uncoating. The finished dsDNA genome may also be stalled in the cytoplasm waiting for cell division to access the nucleus where uncoating occurs.

The data raises the question of where exactly in the cell reverse transcription is completed. While it was believed that retroviruses complete synthesis of their viral dsDNA in the cytoplasm, recent evidence showed that for HIV-1 the completion occurs in the nucleus. Reports using inhibitor time of addition assays (Burdick et al., 2020; Dharan et al., 2020; Francis et al., 2020b) or strand-specific DNA labeling (Dharan et al.,

2020) were the first to propose that HIV-1 DNA genomes are only completed in the nucleus. Quantitative analysis using EdU metabolic labeling of viral DNA and the ANCHOR system confirmed these results (Müller et al., 2021). Uncoated nuclear HIV-1 complexes had higher relative EdU signals than cytoplasmic complexes, or nuclear complexes that did not recruit the OR3 marker. This demonstrates that reverse transcription of HIV-1 genomes starts in the cytoplasm but is completed in the nucleus. The current proposed model of HIV-1 reverse transcription suggests that cDNA synthesis is stalled in the cytoplasm after synthesis of ssDNA or incomplete dsDNA, and continues in the nucleus where it completes plus strand cDNA (Dharan et al., 2020; Müller et al., 2022, 2021). In the case for MLV, several studies have proposed that linear dsDNA is completed and contained in the capsid core in the cytoplasm of infected cells (Bowerman et al., 1989; Brown et al., 1987; Fassati and Goff, 1999; Wang et al., 2016). Brown et al., (1987) used an in vitro assay to show that cytoplasmic MLV linear DNA can integrate in vitro and Bowerman et al., (1989) complemented this study with co-precipitation experiments showing that cytoplasmic linear DNA is associated with MLV CA protein. However, both studies did not control for the presence of reverse transcriptase that could possibly complete the reaction in the test tube. Furthermore, Fasatti and Goff (1999) using co-sedimentation analysis, PCRs and immunoblots showed that cytoplasmic viral cDNA was associated with CA, RT, and IN. In this thesis, apart from the clear nuclear OR3 signals, a slight increase in the number of cytoplasmic signals above the background were detected in MLV infected samples (*cf.* 3.3.2., Figure 17). The cytoplasmic detections prompted increased scrutiny using aphidicolin treatment to block mitosis and therefore potentially increase cytoplasmic OR3 detections, but the treatment led to increased background detections of OR3 spots in uninfected cells likely due to cellular stress (*cf.* 3.3.4., Figure 21). It is certainly possible that a subset of MLV subviral structures uncoat inside the cytoplasm, however, due to the afore mentioned issues, I cannot make any conclusive statements about these events but will instead focus on the nuclear signals (section 4.4).

To conclude, the evidence collected from current literature and this thesis does not formally prove completion of reverse transcription of MLV dsDNA either in the cytoplasm or in the nucleus. Combining metabolic DNA labeling with the ANCHOR system (Müller et al., 2021) or application of plus- and minus-strand specific FISH

(Dharan et al., 2020) may allow to solve this issue. In the next section, I will discuss my attempts to achieve this goal using the incorporation of modified nucleosides and nucleotides.

## 4.2 Metabolic labeling of MLV genomes is hampered by nucleotide incorporation into host chromatin

Stochastic incorporation of modified nucleosides for labeling viral genomes has been extensively used to investigate early and late viral replication events. An advantage of using this method is the ability to quantify the relative cDNA content in infected fixed cells, which cannot be achieved with the ANCHOR system, and provide vital information of relative cDNA amounts during reverse transcription of viral genomes. Several studies have already adapted and utilized metabolic labeling of HIV-1 genomes with the incorporation of EdU into newly synthesized cDNA with the purpose to investigate capsid uncoating and reverse transcription in aphidicolin treated cells or terminally differentiated macrophages (Bejarano et al., 2019, 2018; Francis et al., 2020b; Peng et al., 2014; Rensen et al., 2021; Stultz et al., 2017; Zila et al., 2019). This demonstrated that retroviruses, which reverse transcribe their RNA genomes to DNA, can incorporate the modified nucleosides and this incorporation does not inhibit viral cDNA synthesis. Therefore, in this thesis I attempted to adapt metabolic labeling using differently modified nucleosides, with the aim to label MLV cDNA and provide quantitative analysis of the cDNA content.

MLV RT (*cf.* 1.4.2.) was able to successfully incorporate EdUTP in isolated particles *in vitro* with comparable levels as HIV-1 measured in the ERT assay (*cf.* 3.2.2., Figure 11). This experiment showed for the first-time application of metabolic labeling for MLV genomes (~8.3kb), which are ~ 1 kb smaller than HIV-1 (~9.2 kb). The lowest limit tested for successful metabolic labeling and signal generation above background was a genome size of ~3.75 kb with ~1800 possible insertion slots for the thymidine analogue EdU (Peng et al., 2014). However, the labeling of MLV viral genomes, in contrast to HIV-1, was not achieved with bulky modified nucleotide triphosphates like Alexa647-aha-dUTP (*cf.* 3.2.2., Figure 11). This limitation could be attributed to the higher reported fidelity of MLV compared to HIV-1 RT, which discriminates more

rigorously the larger modification on nucleosides (Oscorbin and Filipenko, 2021). Since misincorporation rates of MLV RT are similar to HIV-1 (Oscorbin and Filipenko, 2021), the issue might lie in the lower affinity of the MLV RT to the mismatched template (Skasko et al., 2005) resulting in slower or no extension of the labeled viral DNA. Alternatively, the tightly closed capsid core of MLV might present a challenge for penetration of larger modified nucleotides. In contrast, the HIV-1 capsid cores have a pore sitting in the middle of their hexamers, which is closing and opening (Jacques et al., 2016). This pore was shown to attract dNTPs and enhance reverse transcription (Jacques et al., 2016). Such pore or similar opening was not observed on MLV capsid cores (Qu et al., 2018), thus the differences in access could also explain the successful labeling using bulkier nucleotides of HIV-1 and not MLV genomes.

Application of the method in MLV infected cells resulted in detection of rare EdU positive subviral particles in the cytoplasm (*cf.* 3.2.2., Figure 12). Only particles that fuse and release the capsid into the cytoplasm will start reverse transcription. Thus, this result may be explained if the majority of particles reside in the endosomal system. However, this was not further tested as these experiments were complicated due to the bright signal coming from the nucleus, which precludes detection of the dimmer viral cDNA signals in the vicinity. Inhibiting the cellular DNA polymerase activity using APC could not completely eradicate signals from the nucleus (*cf.* 3.2.2., Figure 12). Most importantly, APC treatment blocks cell division and therefore prevents the detection of nuclear events for MLV as well.

Accordingly, the EdU click labeling method is mainly useful for lentiviruses infecting non-dividing cells (with no nuclear DNA synthesis) and was not used for further investigation of early and late replication steps of MLV particles due to the described limitations.

### 4.3 Subviral particles with a full subset of CA molecules enter the nucleus during mitosis

This thesis provided extensive evaluation of different extraction conditions and performed a semi-automated quantitative analysis of the CA immunostaining efficiency in cells and immobilized MLV particles (*cf.* 3.3.5., Figure 22). MLV subviral particles were identified by staining against p12, because this viral protein was found to interact and stabilize the CA core and it is a vital component of the RTC/PIC in both cytoplasm and upon translocation in the nucleus. There were inconclusive results concerning the IF detection of CA and p12 proteins in the nucleus (Elis et al., 2012; Wanaguru et al., 2018), which may be due to differences in treatment of the samples such as fixation time and extraction procedures with MeOH. Elis et al. (2012) reported ~ 80 % co-localization of p12 with CA proteins in the cytoplasm and a decrease to ~30 % upon nuclear entry. In contrast, Wanaguru et al. (2018) extracted the samples with MeOH prior to IF staining and observed ~60% of co-localization of p12 with CA in the nucleus of MLV infected cells. The experiments performed in this thesis, showed that MeOH mediated extraction is necessary to expose the CA epitopes in cells reaching the same degree of staining intensity as in the particles immobilized on imaging slides (*cf.* 3.3.5., Figure 22). Furthermore, in MeOH extracted samples, no major difference in CA staining of cytoplasmic and nuclear subviral particles was detected with ~60 % and ~80 % co-localization with p12, respectively. Interestingly, also in the non-extracted samples there was no major difference between staining of cytoplasmic vs nuclear particles, indicating that the accessibility of CA epitopes for staining is caused by host cell factors present in the cytoplasm and retained in the nucleus (*cf.* 3.3.5., Figure 22).

In contrast, the staining of the HIV-1 capsid in the nucleus but not in the cytoplasm is heavily dependent upon sample fixation and extraction. It was shown that non-specific MeOH extraction in HeLa-based cell lines resulted in strong nuclear CA signals. Moreover, competitively displacing the capsid binding CPSF6 protein with the PF74 inhibitor achieved similar results in T-cells and HeLa-based cells, indicating that CPSF6 acts as a shield in the nucleus and prevents access of the CA epitopes to antibodies (Müller et al., 2021). Possible host cell proteins which bind to MLV CA and may similarly shield epitopes as CPSF6, could be TRIM proteins (Tripartite motif proteins) and Fv1

(Goff, 2004; Uchil et al., 2008). The tropism of naturally circulating MLVs can be determined by pair of adjacent amino acids at position 110 in the CA, thus classifying them as N- or B-tropic capsids (Stevens et al., 2004). According to their tropism, the MLV capsids are targeted by the protein products of the *Fv1* gene in mice, subsequently blocking infection after reverse transcription and before the integration of the viral cDNA (Rein, 2011; Stevens et al., 2004). However, laboratory isolates such as Moloney Murine Leukemia virus (MuLV), termed NB tropic, have lost the sensitivity to Fv1 (Rein, 2011). Since in the experiments from this thesis, only MuLV based viruses were used, the Fv1 proteins were excluded from consideration. The TRIM protein family, E3 ubiquitin ligases, with over 70 members have both enhancing and restricting functions on retroviruses (Uchil et al., 2008). For example, the TRIM5 $\alpha$  protein binds to N-tropic MLV and HIV-1 capsid which results in disassembly of the capsids and activation of the NF- $\kappa$ b and MAPK signaling (Fletcher et al., 2018; Kutluay et al., 2013; Yap et al., 2004). Moreover, a screening study has identified mouse TRIM11 and TRIM30 to have enhancing effects on N-tropic MLV infection (Uchil et al., 2008). So far, no TRIM protein was identified that binds to the NB-tropic MLV capsids, like the ones used in this thesis. However, there is the possibility of not yet discovered host proteins that interact and shield MLV CA epitopes from detection like CPSF6 does for HIV-1.

The results presented here show that upon nuclear entry the MLV subviral complexes continue to consist of p12 and CA. Moreover, the quantification of CA staining intensities of subviral complexes in the nucleus compared to cytoplasm was similar, therefore it is possible that intact capsids enter the nucleus.

#### 4.4 MLV likely uncoats in the nucleus

Analysis of OR3 signals and the IF-stained viral proteins CA and p12 in the nucleus of infected cells showed no detectable co-localizations (*cf.* 3.3.5., Figure 23). Therefore, the imaging data indicated that subviral complexes containing a largely complete set of CA and p12 proteins enter the nucleus (*cf.* 3.3.5., Figure 22), upon which the viral cDNA appears to be separated from the p12/CA subviral complex and become accessible for the OR3 protein to bind (*cf.* 3.3.5., Figure 23). The appearance of nuclear foci is not only dependent on the cDNA synthesis completion but its accessibility to the OR3 protein

that is outside of the subviral replication complex and may not access viral cDNA inside the capsids shell.

The location, manner and timing of capsid uncoating is not well understood in the field of retroviruses in general. Based upon co-sedimentation analysis followed by immunoblot of viral proteins, the gradual capsid uncoating model was proposed for MLV particles (Fassati and Goff, 1999). Fassati and Goff (1999) have shown steady decrease of sedimentation properties of the RTC species over time, showing the maximum quantity of CA co-fractioning with strong stop DNA in the cytoplasm and only trace CA proteins in the nuclear fraction. The gradual uncoating model suggests non-synchronized uncoating events leaving particles in different states of undress and CA protein content, which may be sufficient for CA/p12 mediated nuclear entry during cell division and attachment of the viral cDNA to chromatin.

More recent literature and data from this thesis proposes a different model of MLV capsid uncoating. Wang et al. (2016) using CHIP analysis of MLV infected cells, showed a steady drop in CA association levels with MLV DNA, which corresponded to the time of nuclear entry and histone loading. Furthermore, this study utilized aphidicolin to exclude the viral DNA from the nucleus, which resulted in increased association of CA levels on the viral DNA in the cytoplasm (Wang et al., 2016). Moreover, it was found that binding of p12 protein with the N-terminus to the MLV CA not only stabilizes the capsid core but is necessary for p12 mediated nuclear entry (Wight et al., 2014). Next, the C-terminus of p12 during mitosis is anchored to the cell chromatin and ensures the nuclear retention of the CA containing subviral particle after division is completed (Wanaguru et al., 2018). In my co-localization analysis of nuclear subviral complexes in Figure 22, in agreement with results from Wanaguru et al. (2018), it was observed that after nuclear entry viral CA and p12 proteins remain together in a subviral complex. Along the same lines, using CHIP analysis of p12 mutants, it was found that CA loss and histone loading on viral DNA is dependent on the ability of p12 to tether on chromatin (Wang and Goff, 2021). Using the ANCHOR system in infected MLV cells allowed to investigate only largely completed and accessible dsDNA in relation with CA and p12. Previous reports of MLV cDNA FISH signals, which detected both ssDNA and dsDNA species, were found to co-localize with p12 signals inside the nucleus at 12 h p.i. Given

that CA and p12 signals showed a high degree of nuclear co-localization in this and other studies the presence of these p12 co-localizing DNA species are likely encased inside the capsid core and not accessible to external nuclear proteins (i.e. the 66 kDa OR3 marker). In addition, or alternatively, only single stranded DNA species could be present inside the capsid while the capsid may be permeable to the OR3 marker. Taken together, recent literature and this thesis, it is likely that the nuclear entry of capsid cores mediated by cellular division and p12 anchoring to host chromatin may play a role in the uncoating process.

Debating against gradual cytoplasmic uncoating are destabilized CA mutants, like the minus-glycoGag variant that is sensed by cGAS and elicits innate immune response thus maintaining that the capsid integrity is vital until integration (Moran and Ross, 2020; Pizzato, 2010; Stavrou et al., 2015). In addition, this thesis revealed that largely complete set of CA proteins enter the nucleus (*cf.* 3.3.5., Figure 22) suggesting that it is highly likely that intact cores enter the nucleus. However, these nuclear CA cores could be altered in their shape and conformation and could possibly have defects. In future experiments, CLEM analysis would be needed to investigate cytoplasmic and nuclear capsids in relation to the OR3 signals and to examine the integrity of these capsid structures. Lastly, the OR3 signal onset in the first generation of daughter cells showed a ~4h lag after division (*cf.* 3.3.9., Figure 29; discussed in *cf.* 4.6), which would be highly unlikely if completion of cDNA synthesis and uncoating had occurred in the cytoplasm and accessible viral cDNA entered the nucleus.

Taking together results from this thesis and the literature, the following model of uncoating is proposed; the capsid core gains access to the nucleus during nuclear envelope breakdown mediated by p12 tethering to chromatin. Once in the nucleus, the capsid still in complex to p12 either releases the viral genome, or cooperatively disassembles. Should the first assumption be true, then the spiral capsid structure of MLV needs to be peeled off or crack-open to release the genome for integration. Lastly, the released viral cDNA by uncoating is rapidly chromatinized via histone loading (Wang et al., 2016; Wang and Goff, 2021).

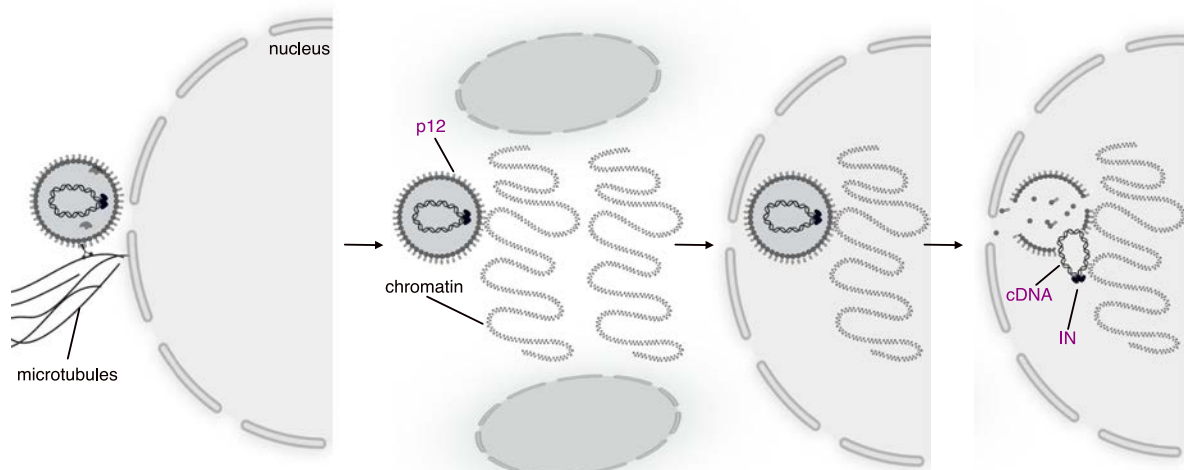


**Figure 34. Model of MLV capsid core uncoating.** The MLV subviral complex with the intact capsid core is waiting for nuclear envelope disintegration during mitosis to gain access to the nucleus. During mitosis, the viral protein p12 is anchoring the MLV capsid to the cell host chromatin and ensures retention of the subviral particle inside the nucleus of the daughter cells. The capsid core still attached to p12 cracks open and releases the viral cDNA in the nucleus. The IN together with the viral cDNA separates and is guided by BET proteins to sites of integration. Viral cDNA is rapidly chromatinized by histone loading prior to integration.

Interestingly, the MLV capsid uncoating model is reminiscent of the model proposed for HIV-1 capsids. Recent reports have shown that morphologically intact HIV-1 capsids enter the nucleus through the nuclear pore (Zila et al., 2021) and the translocation is mediated by binding Nup153 of the nuclear pore complex. Nuclear CPSF6 in turn displaces Nup153 and releases the capsid from the nuclear pore complex into the nucleoplasm (Bejarano et al., 2019; Müller et al., 2022; Zila et al., 2019). Next, the capsid core is cracked open to release the now completed dsDNA near active chromatin regions (Müller et al., 2022, 2021). Despite differences in cell tropism, nuclear entry, and capsid structure between MLV and HIV-1, there may be resemblances of the uncoating process perhaps attributed to the main function of the capsid, to protect the viral cDNA until integration.

#### 4.5 IN.FP remains associated with a subset of uncoated MLV cDNA molecules

To investigate the dynamics of viral cDNA in relation to another component of the PIC complex, namely the IN, imaging experiments using IN.SNAP labeled particles were performed. Initially, the focus was to visualize what occurs after nuclear entry and capsid uncoating, and analysis of IN.SNAP with MLV cDNA objects in the nucleus of fixed cells showed ~40% of co-localization (*cf.* 3.3.6., Figure 24). The observed co-localization may underestimate the true IN association with viral cDNA since IN.FP may shed more easily from the complex than the native IN, therefore the detection sensitivity may be insufficient to detect small amounts of IN retained on the viral cDNA.

In the same experiment, it was striking to observe that the IN.SNAP marker partially remained associated with the viral cDNA (*cf.* 3.3.6., Figure 24), despite p12/CA complex separation (*cf.* 3.3.5., Figure 23). The separation of MLV IN from the CA core in the nucleus was already documented by immunoblot analysis (Fassati and Goff, 1999) and more recently in a co-localization study using IN.FP labeled viral particles and IF stained CA (Borrenberghs et al., 2019). The imaging based study made IN.FP labeled MLV particles with the same plasmid vector that was used in this thesis (MLV-gag-pol-IN.FP), reporting co-localization of ~70 % and ~7% of IN.Venus with CA in cytoplasm and nucleus, respectively (Borrenberghs et al., 2019). Using single-molecule Förster resonance energy transfer (FRET) analysis, it was shown that the content and quaternary structure of the MLV intasome was not altered upon nuclear entry. However a structural reshaping of the intasome to an active state was observed in the nucleus after BET mediated interaction with the chromatin, which were independent of p12 mediated chromatin tethering (Borrenberghs et al., 2019). Moreover, the direct interaction of MLV IN and Brd4 was resolved in a crystal structure (reviewed in *cf.* 1.4.5., Figure 6). Taken together, the data from this thesis and literature, it can be proposed that during uncoating the viral cDNA and IN separate from the p12/CA complex, although the fate of native IN was not analyzed here. Then the MLV cDNA is likely translocated to integration sites through IN and BET interaction, where integration occurs.

This is different for HIV-1 infection, where during uncoating and release of the viral cDNA, the IN.FP marker remains with the CA core (Müller et al., 2021). However, the native HIV-1 IN is likely to remain with the viral cDNA until integration since productive infection was scored for IN.FP labeled virus. Therefore, the loss of IN.FP from HIV-1 cDNA most likely means that the overexpressed and over incorporated fusion protein does not actually form the true intasome (Müller et al., 2021). Accordingly in the case of MLV, the IN.FP might “stick “ more strongly to the PIC than for HIV-1, but in both cases this is an artificial protein which might not reflect the native IN.

To validate the observations made for MLV cDNA and IN.FP with focus on uncoating, more experiments need to be performed under real-time conditions. Due to the low particle yield such live imaging experiments using the IN.SNAP virus could not yet be performed and require optimization in future work. Lastly, to evaluate the association of the native MLV IN to viral cDNA and the CA core, future work needs to be done using different experimental setup.

#### 4.6 Visualization of integrated and non-integrated MLV cDNA in dividing cells

A prerequisite for integration and life cycle of viruses like MLV, PFV and PV is nuclear access achieved through the division of the target cells. Specifically, the investigation of bulk infectivity as well as cDNA nuclear entry in relation to the cell cycle of MLV infected cells has been based upon cell cycle inhibitors that either synchronize or block infection (*cf.* 3.3.4., Figure 19) (Elis et al., 2015, 2012; Hagino-Yamagishi et al., 1981; Roe et al., 1993; Wang et al., 2016). Use of APC blocks the normal progression of the cell cycle through S phase. The ANCHOR system allowed, for the first time without the use of cell cycle inhibitors, to relate the appearance of uncoated MLV cDNA in the nucleus of infected cells to the cellular division status in real time (*cf.* 3.3.9., Figure 28). In line with current knowledge, nuclear MLV cDNA appeared only in mitotic cells (*cf.* 3.3.9., Figure 28). Remarkably, the ANCHOR system complemented with the fluorescently labeled nuclear envelope enabled tracking of propagating OR3 signals in multiple cell-lineages up to three generations of daughter cells (*cf.* 3.3.7., Figure 25; *cf.* 3.3.8., Figure 27). OR3 signals which were present in the parent cell before and both

daughter cells after division, likely represent integrated MLV genomes (*cf.* 3.3.11., Figure 31) since DNA replication would also duplicate the integrated ANCH containing MLV provirus. On the other hand, an OR3 signal that was detected in the parent cell and after division only in one or no daughter cell did not represent an integrated genome (*cf.* 3.3.11., Figure 31). Moreover, when the timing of appearance of OR3 signals in daughter cells are grouped depending on cell generation, there was immediate onset of OR3 signal detection post division in the second and third generation, but not in the first generation of daughter cell where a delay of ~4 h was observed (*cf.* 3.3.9., Figure 29). These data indicate that the majority of signals appearing in the second and third generations represent complete MLV cDNA with immediate accessibility after division, whereas the lag in the first generation of daughter cells is potentially the time needed for cDNA completion and/or CA uncoating. To validate potentially integrated viral cDNA, future work is planned to identify lineages with stably transmitting OR3 signals in real-time microscopy, followed by fixation and immunostaining for Gag expression of the last daughter cell carrying the OR3 signal.

In conclusion, this thesis provides a promising imaging-based method to study the behavior of integrated and non-integrated MLV cDNA in dividing living cells. More in depth analysis of the integration status of the OR3 signals is planned in future work.

#### 4.7 Protection of MLV nucleic acids by capsid is important in immunocompetent cells.

Studies have reported that minus-glycoGag mutants with destabilized capsids are more likely to activate cytoplasmic DNA sensors because of increased accessibility of viral nucleic acids (Stavrou et al., 2015, 2013). Wild-type MLV on the other hand proved to be more resistant due to intact capsid integrity (Stavrou et al., 2015, 2013). Additionally, an increase of IFN- $\beta$  production mediated by cGAS was detected in both wild-type and minus-glycoGag variants upon TREG1 depletion, with enhanced effect observed in the minus-glycoGag mutant (Gao et al., 2013; Stavrou et al., 2013).

In this thesis, a reduction in infectivity and amount of reverse transcripts of minus-glycoGag particles was only observed when tested in immunocompetent MEF cells (*cf.*

3.1.2., Figure 9), which is in line with data obtained by Pizzato (2010). These results suggested that an innate immune sensing pathway may be responsible for the observed effect. Therefore, the potential degradation of reverse transcripts by TREX1 and the effect it has on infectivity in immunocompetent cells was evaluated. The result showed that infectivity of both wild-type and minus-glycoGag mutant in MEF cells was independent of TREX1 (*cf.* 3.1.2., Figure 9). This result could be explained if integration competent full-length transcripts are not a target of TREX1 degradation. This has been indeed observed for HIV-1, where the degradation activity of TREX1 is limited to abortive reverse transcripts and the loss of TREX1 did not result in increased proviral integration (Kumar et al., 2018). Thus, for MLV might be possible that TREX1 targets specifically abortive DNA products which do not have influence on overall infectivity of wild-type and minus-glycoGag variant in single round infection *in vitro*. To entangle the extent of TREX1 involvement in degradation of reverse transcripts products and innate immune sensing, further investigation beyond infectivity analysis is required.

Alternatively, the infection phenotype of minus-glycoGag variant may be attributed to the endogenous APOBEC3 expressed protein in the target MEF cells. APOBEC3 are cytidine deaminases which induce G to A hypermutation in viral DNA, by acting directly on the minus-strand DNA during synthesis and effectively reducing productive infection (Harris and Dudley, 2015; Moran and Ross, 2020). Remarkably, APOBEC3 can also block viral cDNA synthesis by binding to RT directly (Pollpeter et al., 2018), which is the primary mode of action used for blocking murine retroviruses like mouse mammary tumor virus (MMTV) and MLV (Moran and Ross, 2020). This could explain the decrease in reverse transcripts, detected by ddPCR, during infection of MEFs with the minus-glycoGag particles (*cf.* 3.1.2., Figure 9). The minus-glycoGag destabilized capsids are more sensitive to APOBEC3 mediated block of viral cDNA synthesis due to increased accessibility, which is not the case for wild-type intact capsids (Rosales Gerpe et al., 2015; Stavrou et al., 2015, 2013). Most commonly, APOBEC3 are packaged into virions in the producer cell lines and inhibit reverse transcription once the virions infect target cells (Harris and Dudley, 2015). The production of the particles in this thesis used HEK293T cells, which do not express APOBEC3 mRNA or protein (Thul et al., 2017). Nonetheless, the activity of APOBEC3 could still play a role in this experiment, since it was found that APOBEC3 expressed in the target cells blocks incoming minus-

glycoGag particles effectively and restricts infection (Low et al., 2009; Stavrou et al., 2013).

#### 4.8 Nuclear environment and host cell factors interacting with MLV cDNA after the uncoating event

Imaging the nuclear OR3 signals in real-time revealed a distinct loss of signal during division (*cf.* 3.3.10., Figure 30), partly due to condensation of chromatin which prevents OR3 binding and/or the sharp increase in background intensity of eGFP.OR3 during division which can conceal the weaker viral cDNA signals. Surprisingly, the analysis of OR3 signals in the nucleus revealed heterogenous lifetimes where some OR3 signals were completely lost over time (*cf.* 3.3.10., Figure 30). Possible explanations for loss of signals are viral cDNA degradation or displacement of the OR3 protein from the viral cDNA.

Recent studies have expanded cGAS function beyond its cytoplasmic location, reporting detection of HIV-2 viral DNA by cGAS in the nucleus (Lahaye et al., 2018). Given the possibility of MLV cDNA mediated cGAS sensing in the nucleus, the association of OR3 signals and IF stained cGAS was evaluated in a co-localization analysis. Almost half of the observed nuclear OR3 signals were co-localizing to IF detectable cGAS (*cf.* 3.3.12., Figure 32). It is possible that cGAS targets unintegrated MLV cDNA due to its prolonged accessibility in the nucleus, whereas viral DNA that is rapidly integrated in the host genome is rendered inaccessible and considered as a part of the host DNA. However, the exact role of nuclear cGAS as well as its interaction to unintegrated and integrated viral cDNA is at this point speculative. In the end, MLV viral DNA can successfully integrate and result in productive infection, thus this cannot be so well controlled by the innate immune sensing mediated *via* nuclear cGAS. Alternatively, it can be considered that cGAS can recognize and bind viral DNA but is inactive. A recent study revealed that nuclear cGAS is inhibited by chromatin through interactions with histone 2A-histone 2B, which bury one out of the three DNA-binding sites of cGAS, thus blocking the formation of active cGAS dimers (Michalski et al., 2020). Since both unintegrated and integrated MLV cDNA is rapidly loaded with histones upon nuclear entry (Wang et al., 2016; Wang and Goff, 2021), it may well be that the

associated cGAS is rendered inactive due to the close proximity of chromatin. Therefore, to identify the origin of OR3 signal loss and the possible host and viral components involved, further investigation needs to be done.

Upon nuclear entry, the MLV intasome structure of the unintegrated PIC with the two dsDNA LTR ends in close vicinity resembles a double strand break and may recruit components of the DDR pathway. The first component recruited upon DNA damage is the histone variant H2AX, which is then phosphorylated by checkpoint kinases ( e.g. protein kinase catalytic subunits DNA-PKcs) and is named  $\gamma$ H2AX (Daniel et al., 2004; Panier and Boulton, 2014). The  $\gamma$ H2AX mediates the recruitment and docking of other factors belonging to the DDR pathway, which mediate the DNA damage resolution through homologous recombination (HR) or non-homologous end-joining (NHEJ). Recently, our lab has found that  $\gamma$ H2AX is recruited to uncoated nuclear HIV-1 cDNA, which was also confirmed by the co-localization analysis performed in this thesis where the majority of HIV-1 OR3 signals co-localized with  $\gamma$ H2AX independent of their ability to be integrated (*cf.* 3.3.13., Figure 33; Thorsten Müller, 2021). However, a comparable co-localization was not found for MLV cDNA where the majority of OR3 signals did not co-localize with  $\gamma$ H2AX (*cf.* 3.3.13., Figure 33), implying no interaction with the DDR pathway.

Interestingly, a component of the DDR pathway named Ku70 was found to associate with MLV IN (Studamire and Goff, 2008) and to be the first protein binding at each DNA end of the double stranded breaks (Lieber et al., 2006). The Ku heterodimer normally participates in the NHEJ pathway of DNA repair by binding to the double stranded ends together with DNA-PK<sub>cs</sub> (Hartley et al., 1995; Lieber et al., 2006, 2003) and this may also be the case for MLV. Therefore, it may well be that the DDR is involved in MLV cDNA genome recognition and integration with different entry points and pathway than HIV-1. Moreover, only one timepoint was used to examine the co-localization of  $\gamma$ H2AX with viral cDNA, it may well be that it is an early timepoint where not many molecules can be detected by IF staining. Hence the DDR components and their attachment to MLV cDNA is still not completely clear. For more conclusive results, to validate the possible binding of DDR pathway components like  $\gamma$ H2AX and Ku70, the experiments need to be

replicated in fixed and real-time conditions where transient contacts could as well be detected.

## 4.9 Outlook

The current understanding of reverse transcription and capsid uncoating of MLV is not complete, which can partly be attributed to a lack of appropriate experimental systems. The newly adapted ANCHOR labeling system from this thesis is well suited to investigate this process following MLV subviral particles containing viral cDNA in real-time, which was not possible before.

Future work should focus on correlating the long-lived OR3 signals from real time imaging with productive infection to prove that they are indeed integrated proviruses. Propagating OR3 signals would be tracked from parent through several generations of daughter cells in real-time conditions, after which the last generation of daughter cells may be stained for CA expression to identify productive infection; or, alternatively, a fluorescent infection marker may be added to the MLV genome to enable live imaging. The data will be complemented with real-time trafficking of IN.SNAP marker from the cytoplasm to nucleus and its association with the OR3 marker and other cellular factors, revealing viral cDNA dynamics in relation to IN.FP and subsequent integration.

A disadvantage of the ANCHOR system is the ambiguity of whether the appearance of the OR3 signals is due to completion of viral cDNA synthesis or accessibility due to uncoating. To disentangle these possibilities, the ANCHOR method needs to be combined with a quantitative experimental system assessing viral cDNA content in single subviral particles in dividing cells and/or experimental systems which are able to differentiate specific steps of reverse transcription. Therefore, specific metabolic labeling of MLV genomes without the use of aphidicolin is required and/or hybridization probes specific for each DNA strand formed during reverse transcription, similar to those utilized in the study for HIV-1 (Dharan et al., 2020). To avoid cellular incorporation of modified nucleosides and aphidicolin treatment, reverse-transcriptase specific nucleosides could be envisioned in metabolic labeling of MLV. First results for developing nucleosides with enhanced incorporation efficiency for HIV-1 RT over DNA

polymerases have been described (De Wit et al., 2019). The ANCHOR system could explore the possibility of (transient) cytoplasmic cDNA detection with the destabilized minus-glycoGag capsid mutant. These modified particles should then be compared to wildtype MLV regarding longevity, localization but also the association with factors such as cGAS, Brd2, γH2AX and Ku70 should be analyzed.

To characterize the ultrastructure of subviral particles, a CLEM and electron tomography (CLEM-ET) workflow should shed light on the presence of capsid cores and their degree of disassembly or rupture, similar to analysis with HIV-1 (Müller et al., 2021). In order to investigate capsid uncoating dynamics of MLV, a live compatible direct label of CA is necessary. One promising technique to achieve this in highly fragile viral capsid structures is minimally invasive genetic code expansion combined with click labeling, as has been shown for HIV-1 CA (Schifferdecker et al., 2022).

#### 4.10 Conclusion

This thesis was able to expand the toolbox for labeling retroviral genomes in order to study MLV replication steps. Moreover, the ANCHOR labeling system is the first approach that allows continuous visualization of MLV genomes from nuclear entry through cellular division up to the propagation of integrated viral DNA throughout multiple generations of daughter cells.

In the cytoplasm, the capsid serves as enclosed compartment needed for efficient reverse transcription as well as for protection of the viral nucleic acids from the innate immune response. Data presented here confirms that nuclear entry of the PIC requires cellular division. During division, p12 mediates the attachment and retention of the PIC to chromatin (Elis et al., 2012; Wanaguru et al., 2018). Results from this thesis and others (Wanaguru et al., 2018) indicate that also a full set of CA proteins is retained on the nuclear subviral particles, indicative of the capsid core entering the nucleus together with the PIC. Once in the nucleus, MLV cDNA labeled with OR3 can be found separated from the CA/p12 protein complexes. This implies that uncoating could occur during the mitotic division step, or inside the nucleus after reformation of the nuclear envelope. The exact mechanism of uncoating is still unknown and needs to be studied with

ultrastructural analysis. It can only be speculated that uncoating for MLV may occur by unraveling the layer like capsid structure by cracking open similarly as a hatching eggshell, or by disassembly into the individual components and thus releasing the viral cDNA in the nucleus.

## 5 Summary

---

MLV productively only infects proliferating cells such as T cells and B cells but cannot enter the nucleus and integrate its genome in non-dividing cells, in contrast to HIV-1. Reverse transcription of the viral single-stranded RNA (ssRNA) genome into double-stranded DNA (dsDNA) starts inside the cytoplasm after delivery of the capsid core. The viral nucleic acids are protected from host cell factors by the capsid this process. The capsid is then transported to the nuclear envelope, where the subviral particles wait for cellular division to access the nucleus. Nuclear entry and retention upon mitosis is mediated by p12, a cleavage product of the main structural protein Gag, which anchors the reverse transcription and pre-integration complex (RTC/PIC) to chromatin and retains the viral genome in the nucleus once the nuclear envelope reforms. For integration to occur, the MLV capsid needs to release the viral copy DNA (cDNA) in a process called uncoating. Despite being extensively studied, the exact location, mechanism, and spatio-temporal nature of uncoating as well as its relationship to viral cDNA synthesis and integration have not been completely elucidated. Due to the absence of experimental systems able to visualize MLV cDNA in living and dividing cells, the understanding of early replication events is hindered.

To overcome this issue, this thesis, adapted a system (ANCHOR) to visualize single molecules of accessible MLV dsDNA genomes in living and dividing cells and to investigate the dynamics of viral dsDNA synthesis using fluorescence microscopy. The ANCHOR system is based on a DNA binding fluorescently tagged protein (OR3) binding its cognate sequence (ANCH) engineered into the envelope region of the MLV genome. Nuclear viral dsDNA was unambiguously detected in daughter cells after cellular division using both fixed and live cell conditions. Notably, subviral complexes comprised of largely complete sets of CA and p12 proteins entered the nucleus, whereas the viral cDNA was devoid of detectable CA and p12 proteins. In contrast to HIV-1, a fluorescently tagged integrase fusion protein (IN.FP) additionally incorporated into the particle was not retained at positions of the CA/p12 complex but accompanied MLV cDNA, likely to integration sites. These data suggest, that MLV capsids remain largely intact until nuclear envelope breakdown and subsequent chromatin attachment. Afterwards, the viral genome moves away from the CA protein shell. The uncoated viral

cDNA associated with IN.FP is then likely translocated to integration sites of the host genome. Importantly, this thesis achieved, for the first time, tracking of living cell lineages together with visualization of MLV genomes within the nuclei of multiple cell generations. Using this approach allowed the observation of long lived single nuclear signals that are propagated from a single parent to both daughter cells; these cDNA signals likely represent integrated proviruses.

Further experiments utilizing a destabilized MLV capsid mutant revealed infectivity reduction only in immunocompetent MEF and not in SC1 cell lines, indicating a link between capsid stability, cDNA accessibility and activation of immune sensing pathways. Furthermore, association of the uncoated viral cDNA with the DNA sensor cyclic GMP-AMP synthase (cGAS) inside the nucleus suggested a possible nuclear innate sensing pathway and warrants further investigation into the activity of these complexes.

In conclusion, the adaptation and validation of the ANCHOR system for the visualization of MLV dsDNA provided a versatile tool for single particle investigation of productive early replication events and shed light on the relation of capsid uncoating and reverse transcription. Finally, this tool may enable future studies to gain additional insights into retroviral replication.

## 6 Zusammenfassung

---

MLV infiziert nur proliferierende Zellen wie T-Zellen und B-Zellen, da es im Gegensatz zu HIV-1 nicht in den Kern von sich nicht teilenden Zellen eindringen kann. Die Reverse Transkription des viralen Einzelstrang RNA-Genoms (ssRNA) in Doppelstrang DNA (dsDNA) beginnt im Zytoplasma nach Eindringen des Kapsids, welches die viralen Nukleinsäuren vor Wirtszellfaktoren schützt. Anschließend wird es zur Kernhülle transportiert, wo die subviralen Partikel auf die Zellteilung warten, um in den Zellkern zu gelangen. Der Kernimport wird durch p12 vermittelt, ein Spaltprodukt des Hauptstrukturproteins Gag, das den Reverse Transkriptions- und Prä-integrationskomplex (RTC/PIC) am Chromatin verankert und dadurch das virale Genom während der Mitose im Zellkern hält. Damit die Integration stattfinden kann, muss das MLV-Kapsid die virale copy DNA (cDNA) in einem als Uncoating bezeichneten Prozess freisetzen. Trotz umfangreicher Untersuchungen sind der genaue Ort, der Mechanismus, und die räumliche und zeitliche Beziehung des Uncoating zur viralen cDNA-Synthese und Integration noch nicht vollständig geklärt. Unser Verständnis der frühen Replikationsvorgänge ist limitiert, weil es keine experimentellen Systeme gibt um MLV-cDNA in lebenden Zellen zu visualisieren.

Als Lösung für dieses Problem wurde in der vorliegenden Arbeit eine Methode (ANCHOR) zur Visualisierung von MLV-dsDNA mittels Fluoreszenzmikroskopie adaptiert und validiert. Mit diesem System konnten einzelne Moleküle zugänglicher MLV-dsDNA-Genome in lebenden und sich teilenden Zellen visualisiert werden und die Dynamik der viralen dsDNA-Synthese untersucht werden. Das ANCHOR-System basiert auf einem DNA-bindenden, fluoreszent markierten Protein (OR3). Dieses bindet seine entsprechende Sequenz (ANCH), die in das Env Gen des MLV-Genoms eingebaut wurde. In Tochterzellen wurde nach der Zellteilung, sowohl in fixierten Zellen als auch unter Lebendzellbedingungen, virale dsDNA im Zellkern eindeutig nachgewiesen. Bemerkenswert ist, dass subvirale Komplexe im Zellkern aus einer weitgehend vollständigen Anzahl von CA- und p12-Proteinen bestanden. Die virale cDNA hatte jedoch keine nachweisbaren CA- und p12 – Signale und wurde separiert von diesen detektiert. Im Gegensatz zu HIV-1 wurde ein fluoreszenzmarkiertes Integrase-

Fusionsprotein (IN.FP), das zusätzlich in das Partikel eingebaut wurde, nicht an Positionen des CA/p12-Komplexes gefunden. Stattdessen begleitete es die MLV-cDNA, wahrscheinlich bis zu deren Integrationsstellen. Diese Daten deuten darauf hin, dass MLV-Kapside innerhalb der Zelle weitgehend intakt bleiben bis es zum Zusammenbruch der Kernhülle und der Assoziation mit dem Chromatin der Wirtszelle kommt. Anschließend entfernt sich das virale Genom von der CA-Proteinhülle. Es kann davon ausgegangen werden, dass die nicht umhüllte virale cDNA, die nun mit IN.FP assoziiert ist, dann zu Integrationsstellen des Wirtsgenoms transportiert wird. In dieser Arbeit ist es zum ersten Mal gelungen, MLV-Genome in den Kernen mehrerer lebender Zellgenerationen zu verfolgen. Dieser Ansatz ermöglichte die Beobachtung von langlebigen einzelnen cDNA-Signalen, die von einem Elternteil auf beide Tochterzellen übertragen werden; diese cDNA-Signale stellen wahrscheinlich integrierte Proviren dar.

Weitere Experimente mit einer destabilisierten MLV-Kapsidmutante zeigten eine Verringerung der Infektiosität nur in immunkompetenten MEF und nicht in SC1-Zelllinien, was auf einen Zusammenhang zwischen Kapsidstabilität, cDNA-Zugänglichkeit und Aktivierung des angeborenen Immunsystems hinweist. Darüber hinaus deutet die Assoziation der viralen cDNA mit dem DNA-Sensor cyclic GMP-AMP synthase (cGAS) im Zellkern mechanistisch auf einen möglichen Erkennungsweg im Zellkern hin und rechtfertigt weitere Untersuchungen zur Aktivität dieser Komplexe.

Zusammenfassend lässt sich sagen, dass die Anpassung und Validierung des ANCHOR-Systems für die Visualisierung von MLV-dsDNA ein vielseitiges Werkzeug für die Untersuchung von produktiven frühen Replikationsereignissen auf der Ebene einzelner Partikel darstellt und Licht auf die Beziehung zwischen Capsid-Uncoating und Reverser Transkription geworfen hat. Schließlich wird dieses Werkzeug zukünftigen Studien weitere Einblicke in die retrovirale Replikation ermöglichen.

## 7 Reference List

- Aiyer, S., Swapna, G.V.T., Malani, N., Aramini, J.M., Schneider, W.M., Plumb, M.R., Ghanem, M., Larue, R.C., Sharma, A., Studamire, B., Kvaratskhelia, M., Bushman, F.D., Montelione, G.T., Roth, M.J., 2014. Altering murine leukemia virus integration through disruption of the integrase and BET protein family interaction. *Nucleic Acids Res* 42, 5917–5928. <https://doi.org/10.1093/nar/gku175>
- Albanese, A., Arosio, D., Terreni, M., Cereseto, A., 2008. HIV-1 Pre-Integration Complexes Selectively Target Decondensed Chromatin in the Nuclear Periphery. *PLOS ONE* 3, e2413. <https://doi.org/10.1371/journal.pone.0002413>
- Ambrose, Z., Aiken, C., 2014. HIV-1 uncoating: connection to nuclear entry and regulation by host proteins. *Virology* 454–455, 371–379. <https://doi.org/10.1016/j.virol.2014.02.004>
- Anisenko, A.N., Gottikh, M.B., 2019. Role of Cellular DNA Repair Systems in HIV-1 Replication. *Mol Biol* 53, 313–322. <https://doi.org/10.1134/S0026893319030026>
- Aydin, I., Schelhaas, M., 2016. Viral Genome Tethering to Host Cell Chromatin: Cause and Consequences. *Traffic* 17, 327–340. <https://doi.org/10.1111/tra.12378>
- Bachrach, E., Marin, M., Pelegrin, M., Karavanas, G., Piechaczyk, M., 2000. Efficient Cell Infection by Moloney Murine Leukemia Virus-Derived Particles Requires Minimal Amounts of Envelope Glycoprotein. *J Virol* 74, 8480–8486.
- Bakhanashvili, M., Hizi, A., 1992. Fidelity of the RNA-dependent DNA synthesis exhibited by the reverse transcriptases of human immunodeficiency virus types 1 and 2 and of murine leukemia virus: mispair extension frequencies. *Biochemistry* 31, 9393–9398. <https://doi.org/10.1021/bi00154a010>
- Baltimore, D., 1971. Expression of animal virus genomes. *Bacteriol Rev* 35, 235–241.
- Barnett, A.L., Cunningham, J.M., 2001. Receptor Binding Transforms the Surface Subunit of the Mammalian C-Type Retrovirus Envelope Protein from an Inhibitor to an Activator of Fusion. *J Virol* 75, 9096–9105. <https://doi.org/10.1128/JVI.75.19.9096-9105.2001>
- Bejarano, D.A., Peng, K., Laketa, V., Börner, K., Jost, K.L., Lucic, B., Glass, B., Lusic, M., Müller, B., Kräusslich, H.-G., 2019. HIV-1 nuclear import in macrophages is regulated by CPSF6-capsid interactions at the nuclear pore complex. *eLife* 8, e41800. <https://doi.org/10.7554/eLife.41800>
- Bejarano, D.A., Puertas, M.C., Börner, K., Martinez-Picado, J., Müller, B., Kräusslich, H.-G., 2018. Detailed Characterization of Early HIV-1 Replication Dynamics in Primary Human Macrophages. *Viruses* 10, 620. <https://doi.org/10.3390/v10110620>
- Belmont, A.S., Straight, A.F., 1998. In vivo visualization of chromosomes using lac operator-repressor binding. *Trends Cell Biol* 8, 121–124. [https://doi.org/10.1016/s0962-8924\(97\)01211-7](https://doi.org/10.1016/s0962-8924(97)01211-7)

- Bhat, N., Fitzgerald, K.A., 2014. Recognition of Cytosolic DNA by cGAS and other STING-dependent sensors. *Eur J Immunol* 44, 634–640. <https://doi.org/10.1002/eji.201344127>
- Bieniasz, P.D., Weiss, R.A., McClure, M.O., 1995. Cell cycle dependence of foamy retrovirus infection. *J Virol* 69, 7295–7299.
- Blanco-Rodriguez, G., Gazi, A., Monel, B., Frabetti, S., Scoca, V., Mueller, F., Schwartz, O., Krijnse-Locker, J., Charneau, P., Di Nunzio, F., 2020. Remodeling of the Core Leads HIV-1 Preintegration Complex into the Nucleus of Human Lymphocytes. *Journal of Virology* 94, e00135-20. <https://doi.org/10.1128/JVI.00135-20>
- Börner, K., Hermle, J., Sommer, C., Brown, N.P., Knapp, B., Glass, B., Kunkel, J., Torralba, G., Reymann, J., Beil, N., Beneke, J., Pepperkok, R., Schneider, R., Ludwig, T., Hausmann, M., Hamprecht, F., Erfle, H., Kaderali, L., Kräusslich, H.-G., Lehmann, M.J., 2010. From experimental setup to bioinformatics: an RNAi screening platform to identify host factors involved in HIV-1 replication. *Biotechnol J* 5, 39–49. <https://doi.org/10.1002/biot.200900226>
- Borrenberghs, D., Zurnic, I., De Wit, F., Acke, A., Dirix, L., Cereseto, A., Debyser, Z., Hendrix, J., 2019. Post-mitotic BET-induced reshaping of integrase quaternary structure supports wild-type MLV integration. *Nucleic Acids Research* 47, 1195–1210. <https://doi.org/10.1093/nar/gky1157>
- Bowerman, B., Brown, P.O., Bishop, J.M., Varmus, H.E., 1989. A nucleoprotein complex mediates the integration of retroviral DNA. *Genes Dev.* 3, 469–478. <https://doi.org/10.1101/gad.3.4.469>
- Briggs, J.A.G., Simon, M.N., Gross, I., Kräusslich, H.-G., Fuller, S.D., Vogt, V.M., Johnson, M.C., 2004. The stoichiometry of Gag protein in HIV-1. *Nat Struct Mol Biol* 11, 672–675. <https://doi.org/10.1038/nsmb785>
- Brockhurst, M.A., Chapman, T., King, K.C., Mank, J.E., Paterson, S., Hurst, G.D.D., 2014. Running with the Red Queen: the role of biotic conflicts in evolution. *Proceedings of the Royal Society B: Biological Sciences* 281, 20141382. <https://doi.org/10.1098/rspb.2014.1382>
- Brown, P.O., Bowerman, B., Varmus, H.E., Bishop, J.M., 1987. Correct integration of retroviral DNA in vitro. *Cell* 49, 347–356. [https://doi.org/10.1016/0092-8674\(87\)90287-X](https://doi.org/10.1016/0092-8674(87)90287-X)
- Buffett, R.F., Grace, J.T., DiBerardino, L.A., Mirand, E.A., 1969. Vertical transmission of murine leukemia virus through successive generations. *Cancer Res* 29, 596–602.
- Burdick, R.C., Li, C., Munshi, M., Rawson, J.M.O., Nagashima, K., Hu, W.-S., Pathak, V.K., 2020. HIV-1 uncoats in the nucleus near sites of integration. *Proceedings of the National Academy of Sciences* 117, 5486–5493. <https://doi.org/10.1073/pnas.1920631117>
- Cai, X., Chiu, Y.-H., Chen, Z.J., 2014. The cGAS-cGAMP-STING pathway of cytosolic DNA sensing and signaling. *Mol Cell* 54, 289–296. <https://doi.org/10.1016/j.molcel.2014.03.040>

- Caly, L., Jans, D.A., Piller, S.C., 2009. Proteolytic cleavage of HIV-1 GFP-Vpr fusions at novel sites within virions and living cells: concerns for intracellular trafficking studies. *J Fluoresc* 19, 567–573. <https://doi.org/10.1007/s10895-008-0445-8>
- Campbell, E.M., Hope, T.J., 2015. HIV-1 capsid: the multifaceted key player in HIV-1 infection. *Nat Rev Microbiol* 13, 471–483. <https://doi.org/10.1038/nrmicro3503>
- Campbell, E.M., Perez, O., Melar, M., Hope, T.J., 2007. Labeling HIV-1 virions with two fluorescent proteins allows identification of virions that have productively entered the target cell. *Virology* 360, 286–293. <https://doi.org/10.1016/j.virol.2006.10.025>
- Carlson, L.-A., Briggs, J.A.G., Glass, B., Riches, J.D., Simon, M.N., Johnson, M.C., Müller, B., Grünewald, K., Kräusslich, H.-G., 2008. Three-dimensional analysis of budding sites and released virus suggests a revised model for HIV-1 morphogenesis. *Cell Host Microbe* 4, 592–599. <https://doi.org/10.1016/j.chom.2008.10.013>
- Carnes, S.K., Zhou, J., Aiken, C., 2018. HIV-1 Engages a Dynein-Dynactin-BICD2 Complex for Infection and Transport to the Nucleus. *Journal of Virology* 92, e00358-18. <https://doi.org/10.1128/JVI.00358-18>
- Cherepanov, P., Maertens, G., Proost, P., Devreese, B., Van Beeumen, J., Engelborghs, Y., De Clercq, E., Debyser, Z., 2003. HIV-1 integrase forms stable tetramers and associates with LEDGF/p75 protein in human cells. *J Biol Chem* 278, 372–381. <https://doi.org/10.1074/jbc.M209278200>
- Chesebro, B., Britt, W., Evans, L., Wehrly, K., Nishio, J., Cloyd, M., 1983. Characterization of monoclonal antibodies reactive with murine leukemia viruses: use in analysis of strains of friend MCF and Friend ecotropic murine leukemia virus. *Virology* 127, 134–148. [https://doi.org/10.1016/0042-6822\(83\)90378-1](https://doi.org/10.1016/0042-6822(83)90378-1)
- Chin, C.R., Perreira, J.M., Savidis, G., Portmann, J.M., Aker, A.M., Feeley, E.M., Smith, M.C., Brass, A.L., 2015. Direct Visualization of HIV-1 Replication Intermediates Shows that Capsid and CPSF6 Modulate HIV-1 Intra-nuclear Invasion and Integration. *Cell Reports* 13, 1717–1731. <https://doi.org/10.1016/j.celrep.2015.10.036>
- Chuck, A.S., Clarke, M.F., Palsson, B.O., 1996. Retroviral infection is limited by Brownian motion. *Hum Gene Ther* 7, 1527–1534. <https://doi.org/10.1089/hum.1996.7.13-1527>
- Chun, R., Fan, H., 1994. Recovery of Glycosylated gag Virus from Mice Infected with a Glycosylated gag-Negative Mutant of Moloney Murine Leukemia Virus. *J Biomed Sci* 1, 218–223. <https://doi.org/10.1007/BF02253305>
- Ciuffi, A., Llano, M., Poeschla, E., Hoffmann, C., Leipzig, J., Shinn, P., Ecker, J.R., Bushman, F., 2005. A role for LEDGF/p75 in targeting HIV DNA integration. *Nat Med* 11, 1287–1289. <https://doi.org/10.1038/nm1329>
- Coffin, J.M., Fan, H., 2016. The Discovery of Reverse Transcriptase. *Annu. Rev. Virol.* 3, 29–51. <https://doi.org/10.1146/annurev-virology-110615-035556>
- Coffin, J.M., Hughes, S.H., Varmus, H.E. (Eds.), 1997. *Retroviruses*. Cold Spring Harbor Laboratory Press, Cold Spring Harbor (NY).

- Colicelli, J., Goff, S.P., 1988. Sequence and spacing requirements of a retrovirus integration site. *J Mol Biol* 199, 47–59. [https://doi.org/10.1016/0022-2836\(88\)90378-6](https://doi.org/10.1016/0022-2836(88)90378-6)
- Cooper, A., García, M., Petrovas, C., Yamamoto, T., Koup, R.A., Nabel, G.J., 2013. HIV-1 causes CD4 cell death through DNA-dependent protein kinase during viral integration. *Nature* 498, 376–379. <https://doi.org/10.1038/nature12274>
- Corbin, A., Prats, A.C., Darlix, J.L., Sitbon, M., 1994. A nonstructural gag-encoded glycoprotein precursor is necessary for efficient spreading and pathogenesis of murine leukemia viruses. *J Virol* 68, 3857–3867. <https://doi.org/10.1128/JVI.68.6.3857-3867.1994>
- Coté, M.L., Roth, M.J., 2008. Murine Leukemia Virus Reverse Transcriptase: Structural Comparison with HIV-1 Reverse Transcriptase. *Virus Res* 134, 186–202. <https://doi.org/10.1016/j.virusres.2008.01.001>
- Craigie, R., Fujiwara, T., Bushman, F., 1990. The IN protein of Moloney murine leukemia virus processes the viral DNA ends and accomplishes their integration in vitro. *Cell* 62, 829–837. [https://doi.org/10.1016/0092-8674\(90\)90126-y](https://doi.org/10.1016/0092-8674(90)90126-y)
- Cui, S., Yu, Q., Chu, L., Cui, Y., Ding, M., Wang, Q., Wang, H., Chen, Y., Liu, X., Wang, C., 2020. Nuclear cGAS Functions Non-canonically to Enhance Antiviral Immunity via Recruiting Methyltransferase Prmt5. *Cell Rep* 33, 108490. <https://doi.org/10.1016/j.celrep.2020.108490>
- Daniel, R., Ramcharan, J., Rogakou, E., Taganov, K.D., Greger, J.G., Bonner, W., Nussenzweig, A., Katz, R.A., Skalka, A.M., 2004. Histone H2AX is phosphorylated at sites of retroviral DNA integration but is dispensable for postintegration repair. *J Biol Chem* 279, 45810–45814. <https://doi.org/10.1074/jbc.M407886200>
- Das, D., Georgiadis, M.M., 2004. The Crystal Structure of the Monomeric Reverse Transcriptase from Moloney Murine Leukemia Virus. *Structure* 12, 819–829. <https://doi.org/10.1016/j.str.2004.02.032>
- de Chaumont, F., Dallongeville, S., Chenouard, N., Hervé, N., Pop, S., Provoost, T., Meas-Yedid, V., Pankajakshan, P., Lecomte, T., Le Montagner, Y., Lagache, T., Dufour, A., Olivo-Marin, J.-C., 2012. Icy: an open bioimage informatics platform for extended reproducible research. *Nat Methods* 9, 690–696. <https://doi.org/10.1038/nmeth.2075>
- De Rijck, J., de Kogel, C., Demeulemeester, J., Vets, S., El Ashkar, S., Malani, N., Bushman, F.D., Landuyt, B., Husson, S.J., Busschots, K., Gijssbers, R., Debyser, Z., 2013. The BET family of proteins targets moloney murine leukemia virus integration near transcription start sites. *Cell Rep* 5, 886–894. <https://doi.org/10.1016/j.celrep.2013.09.040>
- Desai, T.M., Marin, M., Sood, C., Shi, J., Nawaz, F., Aiken, C., Melikyan, G.B., 2015. Fluorescent protein-tagged Vpr dissociates from HIV-1 core after viral fusion and rapidly enters the cell nucleus. *Retrovirology* 12, 88. <https://doi.org/10.1186/s12977-015-0215-z>
- Dharan, A., Bachmann, N., Talley, S., Zwickelmaier, V., Campbell, E.M., 2020. Nuclear pore blockade reveals that HIV-1 completes reverse transcription and uncoating in the

- nucleus. *Nat Microbiol* 5, 1088–1095. <https://doi.org/10.1038/s41564-020-0735-8>
- Dharan, A., Opp, S., Abdel-Rahim, O., Keceli, S.K., Imam, S., Diaz-Griffero, F., Campbell, E.M., 2017. Bicaudal D2 facilitates the cytoplasmic trafficking and nuclear import of HIV-1 genomes during infection. *Proc Natl Acad Sci U S A* 114, E10707–E10716. <https://doi.org/10.1073/pnas.1712033114>
- Diehl, W.E., Stansell, E., Kaiser, S.M., Emerman, M., Hunter, E., 2008. Identification of Postentry Restrictions to Mason-Pfizer Monkey Virus Infection in New World Monkey Cells. *Journal of Virology* 82, 11140–11151. <https://doi.org/10.1128/JVI.00269-08>
- Dudek, H., Ghosh, A., Greenberg, M.E., 2001. Calcium phosphate transfection of DNA into neurons in primary culture. *Curr Protoc Neurosci Chapter 3, Unit 3.11*. <https://doi.org/10.1002/0471142301.ns0311s03>
- Edwards, S.A., Fan, H., 1979. gag-Related polyproteins of Moloney murine leukemia virus: evidence for independent synthesis of glycosylated and unglycosylated forms. *J Virol* 30, 551–563. <https://doi.org/10.1128/JVI.30.2.551-563.1979>
- Elis, E., Ehrlich, M., Bacharach, E., 2015. Dynamics and restriction of murine leukemia virus cores in mitotic and interphase cells. *Retrovirology* 12, 95. <https://doi.org/10.1186/s12977-015-0220-2>
- Elis, E., Ehrlich, M., Prizan-Ravid, A., Laham-Karam, N., Bacharach, E., 2012. p12 Tethers the Murine Leukemia Virus Pre-integration Complex to Mitotic Chromosomes. *PLOS Pathogens* 8, e1003103. <https://doi.org/10.1371/journal.ppat.1003103>
- Engelman, A., Bushman, F.D., Craigie, R., 1993. Identification of discrete functional domains of HIV-1 integrase and their organization within an active multimeric complex. *EMBO J* 12, 3269–3275. <https://doi.org/10.1002/j.1460-2075.1993.tb05996.x>
- Engelman, A., Cherepanov, P., 2008. The lentiviral integrase binding protein LEDGF/p75 and HIV-1 replication. *PLoS Pathog* 4, e1000046. <https://doi.org/10.1371/journal.ppat.1000046>
- Engelman, A., Mizuuchi, K., Craigie, R., 1991. HIV-1 DNA integration: Mechanism of viral DNA cleavage and DNA strand transfer. *Cell* 67, 1211–1221. [https://doi.org/10.1016/0092-8674\(91\)90297-C](https://doi.org/10.1016/0092-8674(91)90297-C)
- Fan, H., Chute, H., Chao, E., Feuerman, M., 1983. Construction and characterization of Moloney murine leukemia virus mutants unable to synthesize glycosylated gag polyprotein. *Proceedings of the National Academy of Sciences* 80, 5965–5969. <https://doi.org/10.1073/pnas.80.19.5965>
- Fassati, A., Goff, S.P., 1999. Characterization of Intracellular Reverse Transcription Complexes of Moloney Murine Leukemia Virus. *Journal of Virology* 73, 8919–8925. <https://doi.org/10.1128/JVI.73.11.8919-8925.1999>
- Faure, A., Calmels, C., Desjobert, C., Castroviejo, M., Caumont-Sarcos, A., Tarrago-Litvak, L., Litvak, S., Parissi, V., 2005. HIV-1 integrase crosslinked oligomers are active in vitro. *Nucleic Acids Res* 33, 977–986. <https://doi.org/10.1093/nar/gki241>

- Fletcher, A.J., Vaysburd, M., Maslen, S., Zeng, J., Skehel, J.M., Towers, G.J., James, L.C., 2018. Trivalent RING Assembly on Retroviral Capsids Activates TRIM5 Ubiquitination and Innate Immune Signaling. *Cell Host & Microbe* 24, 761-775.e6. <https://doi.org/10.1016/j.chom.2018.10.007>
- Francis, A.C., Marin, M., Prellberg, M.J., Palermino-Rowland, K., Melikyan, G.B., 2020a. HIV-1 Uncoating and Nuclear Import Precede the Completion of Reverse Transcription in Cell Lines and in Primary Macrophages. *Viruses* 12, E1234. <https://doi.org/10.3390/v12111234>
- Francis, A.C., Marin, M., Shi, J., Aiken, C., Melikyan, G.B., 2016. Time-Resolved Imaging of Single HIV-1 Uncoating In Vitro and in Living Cells. *PLoS Pathog* 12, e1005709. <https://doi.org/10.1371/journal.ppat.1005709>
- Francis, A.C., Marin, M., Singh, P.K., Achuthan, V., Prellberg, M.J., Palermino-Rowland, K., Lan, S., Tedbury, P.R., Sarafianos, S.G., Engelman, A.N., Melikyan, G.B., 2020b. HIV-1 replication complexes accumulate in nuclear speckles and integrate into speckle-associated genomic domains. *Nat Commun* 11, 3505. <https://doi.org/10.1038/s41467-020-17256-8>
- Francis, A.C., Melikyan, G.B., 2018. Single HIV-1 Imaging Reveals Progression of Infection through CA-Dependent Steps of Docking at the Nuclear Pore, Uncoating, and Nuclear Transport. *Cell Host Microbe* 23, 536-548.e6. <https://doi.org/10.1016/j.chom.2018.03.009>
- Gao, D., Wu, J., Wu, Y.-T., Du, F., Aroh, C., Yan, N., Sun, L., Chen, Z.J., 2013. Cyclic GMP-AMP synthase is an innate immune sensor of HIV and other retroviruses. *Science* 341, 903–906. <https://doi.org/10.1126/science.1240933>
- Georgiadis, M.M., Jessen, S.M., Ogata, C.M., Telesnitsky, A., Goff, S.P., Hendrickson, W.A., 1995. Mechanistic implications from the structure of a catalytic fragment of Moloney murine leukemia virus reverse transcriptase. *Structure* 3, 879–892. [https://doi.org/10.1016/S0969-2126\(01\)00223-4](https://doi.org/10.1016/S0969-2126(01)00223-4)
- Germier, T., Kocanova, S., Walther, N., Bancaud, A., Shaban, H.A., Sellou, H., Politi, A.Z., Ellenberg, J., Gallardo, F., Bystricky, K., 2017. Real-Time Imaging of a Single Gene Reveals Transcription-Initiated Local Confinement. *Biophysical Journal* 113, 1383–1394. <https://doi.org/10.1016/j.bpj.2017.08.014>
- Goff, S.P., 2021. Silencing of Unintegrated Retroviral DNAs. *Viruses* 13, 2248. <https://doi.org/10.3390/v13112248>
- Goff, S.P., 2004. Retrovirus Restriction Factors. *Molecular Cell* 16, 849–859. <https://doi.org/10.1016/j.molcel.2004.12.001>
- Graham, F.L., van der Eb, A.J., 1973. A new technique for the assay of infectivity of human adenovirus 5 DNA. *Virology* 52, 456–467. [https://doi.org/10.1016/0042-6822\(73\)90341-3](https://doi.org/10.1016/0042-6822(73)90341-3)
- Gross, L., 1957. Filterable agent causing leukemia following inoculation into newborn mice. *Tex Rep Biol Med* 15, 603–616; discussion 616-626.
- Guiot, E., Carayon, K., Delelis, O., Simon, F., Tauc, P., Zubin, E., Gottikh, M., Mouscadet, J.-F., Brochon, J.-C., Deprez, E., 2006. Relationship between the oligomeric status

- of HIV-1 integrase on DNA and enzymatic activity. *J Biol Chem* 281, 22707–22719. <https://doi.org/10.1074/jbc.M602198200>
- Gupta, S.S., Maetzig, T., Maertens, G.N., Sharif, A., Rothe, M., Weidner-Glunde, M., Galla, M., Schambach, A., Cherepanov, P., Schulz, T.F., 2013. Bromo- and extraterminal domain chromatin regulators serve as cofactors for murine leukemia virus integration. *J Virol* 87, 12721–12736. <https://doi.org/10.1128/JVI.01942-13>
- Hacein-Bey-Abina, S., Pai, S.-Y., Gaspar, H.B., Armant, M., Berry, C.C., Blanche, S., Bleesing, J., Blondeau, J., de Boer, H., Buckland, K.F., Caccavelli, L., Cros, G., De Oliveira, S., Fernández, K.S., Guo, D., Harris, C.E., Hopkins, G., Lehmann, L.E., Lim, A., London, W.B., van der Loo, J.C.M., Malani, N., Male, F., Malik, P., Marinovic, M.A., McNicol, A.-M., Moshous, D., Neven, B., Oleastro, M., Picard, C., Ritz, J., Rivat, C., Schambach, A., Shaw, K.L., Sherman, E.A., Silberstein, L.E., Six, E., Touzot, F., Tsytsykova, A., Xu-Bayford, J., Baum, C., Bushman, F.D., Fischer, A., Kohn, D.B., Filipovich, A.H., Notarangelo, L.D., Cavazzana, M., Williams, D.A., Thrasher, A.J., 2014. A Modified  $\gamma$ -Retrovirus Vector for X-Linked Severe Combined Immunodeficiency. *N Engl J Med* 371, 1407–1417. <https://doi.org/10.1056/NEJMoa1404588>
- Hadravová, R., de Marco, A., Ulbrich, P., Stokrová, J., Dolezal, M., Pichová, I., Ruml, T., Briggs, J.A.G., Rumlová, M., 2012. In vitro assembly of virus-like particles of a gammaretrovirus, the murine leukemia virus XMRV. *J Virol* 86, 1297–1306. <https://doi.org/10.1128/JVI.05564-11>
- Hagino-Yamagishi, K., Kano, K., Mano, Y., 1981. Effects of aphidicolin on retrovirus DNA synthesis in vivo. *Biochemical and Biophysical Research Communications* 102, 1372–1378. [https://doi.org/10.1016/S0006-291X\(81\)80163-5](https://doi.org/10.1016/S0006-291X(81)80163-5)
- Han, J.Y., Zhao, Y., Anderson, W.F., Cannon, P.M., 1998. Role of variable regions A and B in receptor binding domain of amphotropic murine leukemia virus envelope protein. *J Virol* 72, 9101–9108. <https://doi.org/10.1128/JVI.72.11.9101-9108.1998>
- Harris, R.S., Dudley, J.P., 2015. APOBECs and virus restriction. *Virology*, 60th Anniversary Issue 479–480, 131–145. <https://doi.org/10.1016/j.virol.2015.03.012>
- Hartley, J.W., Rowe, W.P., 1975. Clonal cells lines from a feral mouse embryo which lack host-range restrictions for murine leukemia viruses. *Virology* 65, 128–134. [https://doi.org/10.1016/0042-6822\(75\)90013-6](https://doi.org/10.1016/0042-6822(75)90013-6)
- Hartley, K.O., Gell, D., Smith, G.C., Zhang, H., Divecha, N., Connelly, M.A., Admon, A., Lees-Miller, S.P., Anderson, C.W., Jackson, S.P., 1995. DNA-dependent protein kinase catalytic subunit: a relative of phosphatidylinositol 3-kinase and the ataxia telangiectasia gene product. *Cell* 82, 849–856. [https://doi.org/10.1016/0092-8674\(95\)90482-4](https://doi.org/10.1016/0092-8674(95)90482-4)
- Hatfield, D.L., Levin, J.G., Rein, A., Oroszlan, S., 1992. Translational Suppression in Retroviral GENE Expression. *Adv Virus Res* 41, 193–239. [https://doi.org/10.1016/S0065-3527\(08\)60037-8](https://doi.org/10.1016/S0065-3527(08)60037-8)

- Higashikawa, F., Chang, L., 2001. Kinetic analyses of stability of simple and complex retroviral vectors. *Virology* 280, 124–131. <https://doi.org/10.1006/viro.2000.0743>
- Hinsberger, A., Graillot, B., Blachère Lopez, C., Juliant, S., Cerutti, M., King, L.A., Possee, R.D., Gallardo, F., Lopez Ferber, M., 2020. Tracing Baculovirus AcMNPV Infection Using a Real-Time Method Based on ANCHORTM DNA Labeling Technology. *Viruses* 12, 50. <https://doi.org/10.3390/v12010050>
- Hulme, A.E., Perez, O., Hope, T.J., 2011. Complementary assays reveal a relationship between HIV-1 uncoating and reverse transcription. *Proc Natl Acad Sci U S A* 108, 9975–9980. <https://doi.org/10.1073/pnas.1014522108>
- Jacques, D.A., McEwan, W.A., Hilditch, L., Price, A.J., Towers, G.J., James, L.C., 2016. HIV-1 uses dynamic capsid pores to import nucleotides and fuel encapsidated DNA synthesis. *Nature* 536, 349–353. <https://doi.org/10.1038/nature19098>
- Jones, K.S., Coleman, J., Merkel, G.W., Laue, T.M., Skalka, A.M., 1992. Retroviral integrase functions as a multimer and can turn over catalytically. *J Biol Chem* 267, 16037–16040.
- Jonsson, C.B., Donzella, G.A., Gaucan, E., Smith, C.M., Roth, M.J., 1996. Functional domains of Moloney murine leukemia virus integrase defined by mutation and complementation analysis. *J Virol* 70, 4585–4597. <https://doi.org/10.1128/JVI.70.7.4585-4597.1996>
- Joop, G., Vilcinskis, A., 2016. Coevolution of parasitic fungi and insect hosts. *Zoology, SI: Host-Parasite Coevolution* 119, 350–358. <https://doi.org/10.1016/j.zool.2016.06.005>
- Kamiyama, H., Kakoki, K., Yoshii, H., Iwao, M., Igawa, T., Sakai, H., Hayashi, H., Matsuyama, T., Yamamoto, N., Kubo, Y., 2011. Infection of XC Cells by MLVs and Ebola Virus Is Endosome-Dependent but Acidification-Independent. *PLoS One* 6, e26180. <https://doi.org/10.1371/journal.pone.0026180>
- Klasse, P.J., 2015. Chapter Ten - Molecular Determinants of the Ratio of Inert to Infectious Virus Particles, in: Klasse, P.J. (Ed.), *Progress in Molecular Biology and Translational Science, The Molecular Basis of Viral Infection*. Academic Press, pp. 285–326. <https://doi.org/10.1016/bs.pmbts.2014.10.012>
- Kohn, D.B., 2017. Historical Perspective on the Current Renaissance for Hematopoietic Stem Cell Gene Therapy. *Hematol Oncol Clin North Am* 31, 721–735. <https://doi.org/10.1016/j.hoc.2017.06.006>
- Kohn, D.B., Sadelain, M., Glorioso, J.C., 2003. Occurrence of leukaemia following gene therapy of X-linked SCID. *Nat Rev Cancer* 3, 477–488. <https://doi.org/10.1038/nrc1122>
- Kolokithas, A., Rosenke, K., Malik, F., Hendrick, D., Swanson, L., Santiago, M.L., Portis, J.L., Hasenkrug, K.J., Evans, L.H., 2010. The glycosylated Gag protein of a murine leukemia virus inhibits the antiretroviral function of APOBEC3. *J Virol* 84, 10933–10936. <https://doi.org/10.1128/JVI.01023-10>
- Komatsu, T., Quentin-Froignant, C., Carlon-Andres, I., Lagadec, F., Rayne, F., Ragues, J., Kehlenbach, R.H., Zhang, W., Ehrhardt, A., Bystricky, K., Morin, R., Lagarde, J.-M.,

- Gallardo, F., Wodrich, H., 2018. In Vivo Labelling of Adenovirus DNA Identifies Chromatin Anchoring and Biphasic Genome Replication. *J Virol* 92, e00795-18. <https://doi.org/10.1128/JVI.00795-18>
- Kumar, P., Nachagari, D., Fields, C., Franks, J., Albritton, L.M., 2007. Host Cell Cathepsins Potentiate Moloney Murine Leukemia Virus Infection. *J Virol* 81, 10506–10514. <https://doi.org/10.1128/JVI.02853-06>
- Kumar, S., Morrison, J.H., Dingli, D., Poeschla, E., 2018. HIV-1 Activation of Innate Immunity Depends Strongly on the Intracellular Level of TREX1 and Sensing of Incomplete Reverse Transcription Products. *Journal of Virology* 92, e00001-18. <https://doi.org/10.1128/JVI.00001-18>
- Kutluay, S.B., Perez-Caballero, D., Bieniasz, P.D., 2013. Fates of Retroviral Core Components during Unrestricted and TRIM5-Restricted Infection. *PLOS Pathogens* 9, e1003214. <https://doi.org/10.1371/journal.ppat.1003214>
- Kwon, M., Firestein, B.L., 2013. DNA Transfection: Calcium Phosphate Method, in: Zhou, R., Mei, L. (Eds.), *Neural Development: Methods and Protocols*, Methods in Molecular Biology. Humana Press, Totowa, NJ, pp. 107–110. [https://doi.org/10.1007/978-1-62703-444-9\\_10](https://doi.org/10.1007/978-1-62703-444-9_10)
- Lahaye, X., Gentili, M., Silvin, A., Conrad, C., Picard, L., Jouve, M., Zueva, E., Maurin, M., Nadalin, F., Knott, G.J., Zhao, B., Du, F., Rio, M., Amiel, J., Fox, A.H., Li, P., Etienne, L., Bond, C.S., Colleaux, L., Manel, N., 2018. NONO Detects the Nuclear HIV Capsid to Promote cGAS-Mediated Innate Immune Activation. *Cell* 175, 488-501.e22. <https://doi.org/10.1016/j.cell.2018.08.062>
- Lahaye, X., Satoh, T., Gentili, M., Cerboni, S., Conrad, C., Hurbain, I., El Marjou, A., Lacabaratz, C., Lelièvre, J.-D., Manel, N., 2013. The capsids of HIV-1 and HIV-2 determine immune detection of the viral cDNA by the innate sensor cGAS in dendritic cells. *Immunity* 39, 1132–1142. <https://doi.org/10.1016/j.immuni.2013.11.002>
- Landau, N.R., Littman, D.R., 1992. Packaging system for rapid production of murine leukemia virus vectors with variable tropism. *J Virol* 66, 5110–5113. <https://doi.org/10.1128/jvi.66.8.5110-5113.1992>
- Larue, R.C., Plumb, M.R., Crowe, B.L., Shkriabai, N., Sharma, A., DiFiore, J., Malani, N., Aiyer, S.S., Roth, M.J., Bushman, F.D., Foster, M.P., Kvaratskhelia, M., 2014. Bimodal high-affinity association of Brd4 with murine leukemia virus integrase and mononucleosomes. *Nucleic Acids Res* 42, 4868–4881. <https://doi.org/10.1093/nar/gku135>
- LeRoy, G., Chepelev, I., DiMaggio, P.A., Blanco, M.A., Zee, B.M., Zhao, K., Garcia, B.A., 2012. Proteogenomic characterization and mapping of nucleosomes decoded by Brd and HP1 proteins. *Genome Biol* 13, R68. <https://doi.org/10.1186/gb-2012-13-8-r68>
- Lesbats, P., Serrao, E., Maskell, D.P., Pye, V.E., O'Reilly, N., Lindemann, D., Engelman, A.N., Cherepanov, P., 2017. Structural basis for spumavirus GAG tethering to chromatin. *Proc Natl Acad Sci U S A* 114, 5509–5514. <https://doi.org/10.1073/pnas.1621159114>

- Lewinski, M.K., Yamashita, M., Emerman, M., Ciuffi, A., Marshall, H., Crawford, G., Collins, F., Shinn, P., Leipzig, J., Hannenhalli, S., Berry, C.C., Ecker, J.R., Bushman, F.D., 2006. Retroviral DNA integration: viral and cellular determinants of target-site selection. *PLoS Pathog* 2, e60. <https://doi.org/10.1371/journal.ppat.0020060>
- Lewis, P.F., Emerman, M., 1994. Passage through mitosis is required for oncoretroviruses but not for the human immunodeficiency virus. *J Virol* 68, 510–516.
- Li, M., Mizuuchi, M., Burke, T.R., Craigie, R., 2006. Retroviral DNA integration: reaction pathway and critical intermediates. *EMBO J* 25, 1295–1304. <https://doi.org/10.1038/sj.emboj.7601005>
- Li, S., Ahmad, I., Shi, J., Wang, B., Yu, C., Zhang, L., Zheng, Y.-H., 2019. Murine Leukemia Virus Glycosylated Gag Reduces Murine SERINC5 Protein Expression at Steady-State Levels via the Endosome/Lysosome Pathway to Counteract SERINC5 Antiretroviral Activity. *J Virol* 93, e01651-18. <https://doi.org/10.1128/JVI.01651-18>
- Lieber, M.R., Ma, Y., Pannicke, U., Schwarz, K., 2003. Mechanism and regulation of human non-homologous DNA end-joining. *Nat Rev Mol Cell Biol* 4, 712–720. <https://doi.org/10.1038/nrm1202>
- Lieber, M.R., Yu, K., Raghavan, S.C., 2006. Roles of nonhomologous DNA end joining, V(D)J recombination, and class switch recombination in chromosomal translocations. *DNA Repair (Amst)* 5, 1234–1245. <https://doi.org/10.1016/j.dnarep.2006.05.013>
- Ligasová, A., Koberna, K., 2021. Strengths and Weaknesses of Cell Synchronization Protocols Based on Inhibition of DNA Synthesis. *International Journal of Molecular Sciences* 22, 10759. <https://doi.org/10.3390/ijms221910759>
- Low, A., Datta, S., Kuznetsov, Y., Jahid, S., Kothari, N., McPherson, A., Fan, H., 2007. Mutation in the glycosylated gag protein of murine leukemia virus results in reduced in vivo infectivity and a novel defect in viral budding or release. *J Virol* 81, 3685–3692. <https://doi.org/10.1128/JVI.01538-06>
- Low, A., Okeoma, C.M., Lovsin, N., de las Heras, M., Taylor, T.H., Peterlin, B.M., Ross, S.R., Fan, H., 2009. Enhanced replication and pathogenesis of Moloney murine leukemia virus in mice defective in the murine APOBEC3 gene. *Virology* 385, 455–463. <https://doi.org/10.1016/j.virol.2008.11.051>
- Luby-Phelps, K., 1999. Cytoarchitecture and Physical Properties of Cytoplasm: Volume, Viscosity, Diffusion, Intracellular Surface Area, in: Walter, H., Brooks, D.E., Sreer, P.A. (Eds.), *International Review of Cytology, Microcompartmentation and Phase Separation in Cytoplasm*. Academic Press, pp. 189–221. [https://doi.org/10.1016/S0074-7696\(08\)60527-6](https://doi.org/10.1016/S0074-7696(08)60527-6)
- Lucas, J.S., Zhang, Y., Dudko, O.K., Murre, C., 2014. 3D trajectories adopted by coding and regulatory DNA elements: first-passage times for genomic interactions. *Cell* 158, 339–352. <https://doi.org/10.1016/j.cell.2014.05.036>

- Luecke, S., Paludan, S.R., 2017. Molecular requirements for sensing of intracellular microbial nucleic acids by the innate immune system. *Cytokine* 98, 4–14. <https://doi.org/10.1016/j.cyto.2016.10.003>
- Mamede, J.I., Cianci, G.C., Anderson, M.R., Hope, T.J., 2017. Early cytoplasmic uncoating is associated with infectivity of HIV-1. *Proc Natl Acad Sci U S A* 114, E7169–E7178. <https://doi.org/10.1073/pnas.1706245114>
- Manel, N., Hogstad, B., Wang, Y., Levy, D.E., Unutmaz, D., Littman, D.R., 2010. A cryptic sensor for HIV-1 activates antiviral innate immunity in dendritic cells. *Nature* 467, 214–217. <https://doi.org/10.1038/nature09337>
- Mariamé, B., Kappler-Gratias, S., Kappler, M., Balor, S., Gallardo, F., Bystricky, K., 2018. Real-Time Visualization and Quantification of Human Cytomegalovirus Replication in Living Cells Using the ANCHOR DNA Labeling Technology. *Journal of Virology* 92, e00571-18. <https://doi.org/10.1128/JVI.00571-18>
- Marini, B., Kertesz-Farkas, A., Ali, H., Lucic, B., Lisek, K., Manganaro, L., Pongor, S., Luzzati, R., Recchia, A., Mavilio, F., Giacca, M., Lusic, M., 2015. Nuclear architecture dictates HIV-1 integration site selection. *Nature* 521, 227–231. <https://doi.org/10.1038/nature14226>
- Mattei, S., Glass, B., Hagen, W.J.H., Kräusslich, H.-G., Briggs, J.A.G., 2016. The structure and flexibility of conical HIV-1 capsids determined within intact virions. *Science* 354, 1434–1437. <https://doi.org/10.1126/science.aah4972>
- McDonald, D., Vodicka, M.A., Lucero, G., Svitkina, T.M., Borisy, G.G., Emerman, M., Hope, T.J., 2002. Visualization of the intracellular behavior of HIV in living cells. *J Cell Biol* 159, 441–452. <https://doi.org/10.1083/jcb.200203150>
- Michalski, S., de Oliveira Mann, C.C., Stafford, C.A., Witte, G., Bartho, J., Lammens, K., Hornung, V., Hopfner, K.-P., 2020. Structural basis for sequestration and autoinhibition of cGAS by chromatin. *Nature* 587, 678–682. <https://doi.org/10.1038/s41586-020-2748-0>
- Miller, M.D., Farnet, C.M., Bushman, F.D., 1997. Human immunodeficiency virus type 1 preintegration complexes: studies of organization and composition. *J Virol* 71, 5382–5390. <https://doi.org/10.1128/JVI.71.7.5382-5390.1997>
- Milone, M.C., Bhoj, V.G., 2018. The Pharmacology of T Cell Therapies. *Mol Ther Methods Clin Dev* 8, 210–221. <https://doi.org/10.1016/j.omtm.2018.01.010>
- Mitchell, R.S., Beitzel, B.F., Schroder, A.R.W., Shinn, P., Chen, H., Berry, C.C., Ecker, J.R., Bushman, F.D., 2004. Retroviral DNA integration: ASLV, HIV, and MLV show distinct target site preferences. *PLoS Biol* 2, E234. <https://doi.org/10.1371/journal.pbio.0020234>
- Miyazaki, Y., Garcia, E.L., King, S.R., Iyalla, K., Loeliger, K., Starck, P., Syed, S., Telesnitsky, A., Summers, M.F., 2010. An RNA structural switch regulates diploid genome packaging by Moloney murine leukemia virus. *J Mol Biol* 396, 141–152. <https://doi.org/10.1016/j.jmb.2009.11.033>
- Moloney, J.B., 1966. A virus-induced rhabdomyosarcoma of mice. *Natl Cancer Inst Monogr* 22, 139–142.

- Moran, E.A., Ross, S.R., 2020. Insights into Sensing of Murine Retroviruses. *Viruses* 12, 836. <https://doi.org/10.3390/v12080836>
- Mukherjee, S., Boutant, E., Réal, E., Mély, Y., Anton, H., 2021. Imaging Viral Infection by Fluorescence Microscopy: Focus on HIV-1 Early Stage. *Viruses* 13, 213. <https://doi.org/10.3390/v13020213>
- Müller, T.G., Zila, V., Müller, B., Kräusslich, H.-G., 2022. Nuclear Capsid Uncoating and Reverse Transcription of HIV-1. *Annu Rev Virol* 9, 261–284. <https://doi.org/10.1146/annurev-virology-020922-110929>
- Müller, T.G., Zila, V., Peters, K., Schifferdecker, S., Stanic, M., Lucic, B., Laketa, V., Lusic, M., Müller, B., Kräusslich, H.-G., 2021. HIV-1 uncoating by release of viral cDNA from capsid-like structures in the nucleus of infected cells. *eLife* 10, e64776. <https://doi.org/10.7554/eLife.64776>
- Müllers, E., Stirrnagel, K., Kaulfuss, S., Lindemann, D., 2011. Prototype Foamy Virus Gag Nuclear Localization: a Novel Pathway among Retroviruses. *J Virol* 85, 9276–9285. <https://doi.org/10.1128/JVI.00663-11>
- Muthumani, K., Montaner, L.J., Ayyavoo, V., Weiner, D.B., 2000. Vpr-GFP virion particle identifies HIV-infected targets and preserves HIV-1Vpr function in macrophages and T-cells. *DNA Cell Biol* 19, 179–188. <https://doi.org/10.1089/104454900314564>
- Nitta, T., Kuznetsov, Y., McPherson, A., Fan, H., 2010. Murine leukemia virus glycosylated Gag (gPr80gag) facilitates interferon-sensitive virus release through lipid rafts. *Proceedings of the National Academy of Sciences* 107, 1190–1195. <https://doi.org/10.1073/pnas.0908660107>
- Opazo, T., Garcés, A., Tapia, D., Barraza, F., Bravo, A., Schwenke, T., Cancino, J., Arriagada, G., 2017. Functional Evidence of the Involvement of the Dynein Light Chain DYNLRB2 in Murine Leukemia Virus Infection. *J Virol* 91, e00129-17. <https://doi.org/10.1128/JVI.00129-17>
- Oscorbin, I.P., Filipenko, M.L., 2021. M-MuLV reverse transcriptase: Selected properties and improved mutants. *Computational and Structural Biotechnology Journal* 19, 6315–6327. <https://doi.org/10.1016/j.csbj.2021.11.030>
- Overbaugh, J., Miller, A.D., Eiden, M.V., 2001. Receptors and Entry Cofactors for Retroviruses Include Single and Multiple Transmembrane-Spanning Proteins as well as Newly Described Glycophosphatidylinositol-Anchored and Secreted Proteins. *Microbiol Mol Biol Rev* 65, 371–389. <https://doi.org/10.1128/MMBR.65.3.371-389.2001>
- Panier, S., Boulton, S.J., 2014. Double-strand break repair: 53BP1 comes into focus. *Nat Rev Mol Cell Biol* 15, 7–18. <https://doi.org/10.1038/nrm3719>
- Pear, W.S., Nolan, G.P., Scott, M.L., Baltimore, D., 1993. Production of high-titer helper-free retroviruses by transient transfection. *Proc Natl Acad Sci U S A* 90, 8392–8396. <https://doi.org/10.1073/pnas.90.18.8392>
- Peng, K., Muranyi, W., Glass, B., Laketa, V., Yant, S.R., Tsai, L., Cihlar, T., Müller, B., Kräusslich, H.-G., 2014. Quantitative microscopy of functional HIV post-entry

- complexes reveals association of replication with the viral capsid. *eLife* 3, e04114. <https://doi.org/10.7554/eLife.04114>
- Pettersen, E.F., Goddard, T.D., Huang, C.C., Meng, E.C., Couch, G.S., Croll, T.I., Morris, J.H., Ferrin, T.E., 2021. UCSF ChimeraX: Structure visualization for researchers, educators, and developers. *Protein Sci* 30, 70–82. <https://doi.org/10.1002/pro.3943>
- Pfisterer, U., Kirkeby, A., Torper, O., Wood, J., Nelander, J., Dufour, A., Björklund, A., Lindvall, O., Jakobsson, J., Parmar, M., 2011. Direct conversion of human fibroblasts to dopaminergic neurons. *Proc Natl Acad Sci U S A* 108, 10343–10348. <https://doi.org/10.1073/pnas.1105135108>
- Pietrantonì, G., Gaete-Argel, A., Herrera-Rojo, D., Ibarra-Karmy, R., Bustos, F.J., Valiente-Echeverría, F., Arriagada, G., 2021. Dynein Light-Chain Dynlrb2 Is Essential for Murine Leukemia Virus Traffic and Nuclear Entry. *J Virol* 95, e0017021. <https://doi.org/10.1128/JVI.00170-21>
- Pietrantonì, G., Ibarra-Karmy, R., Arriagada, G., 2020. Microtubule Retrograde Motors and Their Role in Retroviral Transport. *Viruses* 12, 483. <https://doi.org/10.3390/v12040483>
- Pizzato, M., 2010. MLV glycosylated-Gag is an infectivity factor that rescues Nef-deficient HIV-1. *Proceedings of the National Academy of Sciences* 107, 9364–9369. <https://doi.org/10.1073/pnas.1001554107>
- Pizzato, M., Erlwein, O., Bonsall, D., Kaye, S., Muir, D., McClure, M.O., 2009. A one-step SYBR Green I-based product-enhanced reverse transcriptase assay for the quantitation of retroviruses in cell culture supernatants. *J Virol Methods* 156, 1–7. <https://doi.org/10.1016/j.jviromet.2008.10.012>
- Pizzato, M., Marlow, S.A., Blair, E.D., Takeuchi, Y., 1999. Initial binding of murine leukemia virus particles to cells does not require specific Env-receptor interaction. *J Virol* 73, 8599–8611. <https://doi.org/10.1128/JVI.73.10.8599-8611.1999>
- Pollpeter, D., Parsons, M., Sobala, A.E., Coxhead, S., Lang, R.D., Bruns, A.M., Papaioannou, S., McDonnell, J.M., Apolonia, L., Chowdhury, J.A., Horvath, C.M., Malim, M.H., 2018. Deep sequencing of HIV-1 reverse transcripts reveals the multifaceted antiviral functions of APOBEC3G. *Nat Microbiol* 3, 220–233. <https://doi.org/10.1038/s41564-017-0063-9>
- Portis, J.L., McAtee, F.J., Hayes, S.F., 1987. Horizontal transmission of murine retroviruses. *Journal of Virology* 61, 1037–1044. <https://doi.org/10.1128/jvi.61.4.1037-1044.1987>
- Portis, J.L., Spangrude, G.J., McAtee, F.J., 1994. Identification of a sequence in the unique 5' open reading frame of the gene encoding glycosylated Gag which influences the incubation period of neurodegenerative disease induced by a murine retrovirus. *J Virol* 68, 3879–3887. <https://doi.org/10.1128/JVI.68.6.3879-3887.1994>
- Prats, A.C., De Billy, G., Wang, P., Darlix, J.L., 1989. CUG initiation codon used for the synthesis of a cell surface antigen coded by the murine leukemia virus. *J Mol Biol* 205, 363–372. [https://doi.org/10.1016/0022-2836\(89\)90347-1](https://doi.org/10.1016/0022-2836(89)90347-1)

- Prizan-Ravid, A., Elis, E., Laham-Karam, N., Selig, S., Ehrlich, M., Bacharach, E., 2010. The Gag cleavage product, p12, is a functional constituent of the murine leukemia virus pre-integration complex. *PLoS Pathog* 6, e1001183. <https://doi.org/10.1371/journal.ppat.1001183>
- Qu, K., Glass, B., Doležal, M., Schur, F.K.M., Murciano, B., Rein, A., Rumlová, M., Ruml, T., Kräusslich, H.-G., Briggs, J.A.G., 2018. Structure and architecture of immature and mature murine leukemia virus capsids. *Proceedings of the National Academy of Sciences* 115, E11751–E11760. <https://doi.org/10.1073/pnas.1811580115>
- Quentin-Froignant, C., Kappler-Gratias, S., Top, S., Bertagnoli, S., Gallardo, F., 2021. ANCHOR-tagged equine herpesvirus 1: A new tool for monitoring viral infection and discovering new antiviral compounds. *J Virol Methods* 294, 114194. <https://doi.org/10.1016/j.jviromet.2021.114194>
- Quercioli, V., Di Primio, C., Casini, A., Mulder, L.C.F., Vranckx, L.S., Borrenberghs, D., Gijssbers, R., Debyser, Z., Cereseto, A., 2016. Comparative Analysis of HIV-1 and Murine Leukemia Virus Three-Dimensional Nuclear Distributions. *Journal of Virology* 90, 5205–5209. <https://doi.org/10.1128/JVI.03188-15>
- Rein, A., 2011. Murine leukemia viruses: objects and organisms. *Adv Virol* 2011, 403419. <https://doi.org/10.1155/2011/403419>
- Renner, T.M., Bélanger, K., Lam, C., Gerpe, M.C.R., McBane, J.E., Langlois, M.-A., 2018. Full-Length Glycosylated Gag of Murine Leukemia Virus Can Associate with the Viral Envelope as a Type I Integral Membrane Protein. *J Virol* 92, e01530-17. <https://doi.org/10.1128/JVI.01530-17>
- Renner, T.M., Tang, V.A., Burger, D., Langlois, M.-A., 2020. Intact Viral Particle Counts Measured by Flow Virometry Provide Insight into the Infectivity and Genome Packaging Efficiency of Moloney Murine Leukemia Virus. *J Virol* 94, e01600-19. <https://doi.org/10.1128/JVI.01600-19>
- Rensen, E., Mueller, F., Scoca, V., Parmar, J.J., Souque, P., Zimmer, C., Di Nunzio, F., 2021. Clustering and reverse transcription of HIV-1 genomes in nuclear niches of macrophages. *The EMBO Journal* 40, e105247. <https://doi.org/10.15252/embj.2020105247>
- Robinett, C.C., Straight, A., Li, G., Wilhelm, C., Sudlow, G., Murray, A., Belmont, A.S., 1996. In vivo localization of DNA sequences and visualization of large-scale chromatin organization using lac operator/repressor recognition. *Journal of Cell Biology* 135, 1685–1700. <https://doi.org/10.1083/jcb.135.6.1685>
- Roe, T., Reynolds, T.C., Yu, G., Brown, P.O., 1993. Integration of murine leukemia virus DNA depends on mitosis. *The EMBO Journal* 12, 2099–2108. <https://doi.org/10.1002/j.1460-2075.1993.tb05858.x>
- Rosales Gerpe, M.C., Renner, T.M., Bélanger, K., Lam, C., Aydin, H., Langlois, M.-A., 2015. N-Linked Glycosylation Protects Gammaretroviruses against Deamination by APOBEC3 Proteins. *Journal of Virology* 89, 2342–2357. <https://doi.org/10.1128/JVI.03330-14>

- Roth, M.J., Schwartzberg, P.L., Goff, S.P., 1989. Structure of the termini of DNA intermediates in the integration of retroviral DNA: dependence on IN function and terminal DNA sequence. *Cell* 58, 47–54. [https://doi.org/10.1016/0092-8674\(89\)90401-7](https://doi.org/10.1016/0092-8674(89)90401-7)
- Roth, M.J., Tanese, N., Goff, S.P., 1985. Purification and characterization of murine retroviral reverse transcriptase expressed in *Escherichia coli*. *Journal of Biological Chemistry* 260, 9326–9335. [https://doi.org/10.1016/S0021-9258\(17\)39369-9](https://doi.org/10.1016/S0021-9258(17)39369-9)
- Roukos, V., Voss, T.C., Schmidt, C.K., Lee, S., Wangsa, D., Misteli, T., 2013. Spatial dynamics of chromosome translocations in living cells. *Science* 341, 660–664. <https://doi.org/10.1126/science.1237150>
- Saad, H., Gallardo, F., Dalvai, M., Tanguy-le-Gac, N., Lane, D., Bystricky, K., 2014. DNA Dynamics during Early Double-Strand Break Processing Revealed by Non-Intrusive Imaging of Living Cells. *PLOS Genetics* 10, e1004187. <https://doi.org/10.1371/journal.pgen.1004187>
- Salic, A., Mitchison, T.J., 2008. A chemical method for fast and sensitive detection of DNA synthesis in vivo. *Proceedings of the National Academy of Sciences* 105, 2415–2420. <https://doi.org/10.1073/pnas.0712168105>
- Schifferdecker, S., Zila, V., Müller, T.G., Sakin, V., Anders-Össwein, M., Laketa, V., Kräusslich, H.-G., Müller, B., 2022. Direct Capsid Labeling of Infectious HIV-1 by Genetic Code Expansion Allows Detection of Largely Complete Nuclear Capsids and Suggests Nuclear Entry of HIV-1 Complexes via Common Routes. *mBio* 13, e01959-22. <https://doi.org/10.1128/mbio.01959-22>
- Schindelin, J., Arganda-Carreras, I., Frise, E., Kaynig, V., Longair, M., Pietzsch, T., Preibisch, S., Rueden, C., Saalfeld, S., Schmid, B., Tinevez, J.-Y., White, D.J., Hartenstein, V., Eliceiri, K., Tomancak, P., Cardona, A., 2012. Fiji: an open-source platform for biological-image analysis. *Nat Methods* 9, 676–682. <https://doi.org/10.1038/nmeth.2019>
- Schneider, W.M., Brzezinski, J.D., Aiyer, S., Malani, N., Gyuricza, M., Bushman, F.D., Roth, M.J., 2013. Viral DNA tethering domains complement replication-defective mutations in the p12 protein of MuLV Gag. *Proc Natl Acad Sci U S A* 110, 9487–9492. <https://doi.org/10.1073/pnas.1221736110>
- Schwartzberg, P., Colicelli, J., Goff, S.P., 1983. Deletion mutants of Moloney murine leukemia virus which lack glycosylated gag protein are replication competent. *J Virol* 46, 538–546. <https://doi.org/10.1128/JVI.46.2.538-546.1983>
- Sharma, A., Larue, R.C., Plumb, M.R., Malani, N., Male, F., Slaughter, A., Kessler, J.J., Shkriabai, N., Coward, E., Aiyer, S.S., Green, P.L., Wu, L., Roth, M.J., Bushman, F.D., Kvaratskhelia, M., 2013. BET proteins promote efficient murine leukemia virus integration at transcription start sites. *Proc Natl Acad Sci U S A* 110, 12036–12041. <https://doi.org/10.1073/pnas.1307157110>
- Sharma, S., Murai, F., Miyanochara, A., Friedmann, T., 1997. Noninfectious virus-like particles produced by Moloney murine leukemia virus-based retrovirus packaging cells deficient in viral envelope become infectious in the presence

- of lipofection reagents. *Proceedings of the National Academy of Sciences* 94, 10803–10808. <https://doi.org/10.1073/pnas.94.20.10803>
- Singh, P.K., Plumb, M.R., Ferris, A.L., Iben, J.R., Wu, X., Fadel, H.J., Luke, B.T., Esnault, C., Poeschla, E.M., Hughes, S.H., Kvaratskhelia, M., Levin, H.L., 2015. LEDGF/p75 interacts with mRNA splicing factors and targets HIV-1 integration to highly spliced genes. *Genes Dev.* 29, 2287–2297. <https://doi.org/10.1101/gad.267609.115>
- Skasko, M., Weiss, K.K., Reynolds, H.M., Jamburuthugoda, V., Lee, K., Kim, B., 2005. Mechanistic Differences in RNA-dependent DNA Polymerization and Fidelity between Murine Leukemia Virus and HIV-1 Reverse Transcriptases\*. *Journal of Biological Chemistry* 280, 12190–12200. <https://doi.org/10.1074/jbc.M412859200>
- Sloan, R.D., Wainberg, M.A., 2011. The role of unintegrated DNA in HIV infection. *Retrovirology* 8, 52. <https://doi.org/10.1186/1742-4690-8-52>
- Sowd, G.A., Serrao, E., Wang, H., Wang, W., Fadel, H.J., Poeschla, E.M., Engelman, A.N., 2016. A critical role for alternative polyadenylation factor CPSF6 in targeting HIV-1 integration to transcriptionally active chromatin. *Proc Natl Acad Sci U S A* 113, E1054-1063. <https://doi.org/10.1073/pnas.1524213113>
- Stavrou, S., Aguilera, A.N., Blouch, K., Ross, S.R., 2018. DDX41 Recognizes RNA/DNA Retroviral Reverse Transcripts and Is Critical for In Vivo Control of Murine Leukemia Virus Infection. *mBio* 9, e00923-18. <https://doi.org/10.1128/mBio.00923-18>
- Stavrou, S., Blouch, K., Kotla, S., Bass, A., Ross, S.R., 2015. Nucleic acid recognition orchestrates the anti-viral response to retroviruses. *Cell Host Microbe* 17, 478–488. <https://doi.org/10.1016/j.chom.2015.02.021>
- Stavrou, S., Nitta, T., Kotla, S., Ha, D., Nagashima, K., Rein, A.R., Fan, H., Ross, S.R., 2013. Murine leukemia virus glycosylated Gag blocks apolipoprotein B editing complex 3 and cytosolic sensor access to the reverse transcription complex. *Proceedings of the National Academy of Sciences* 110, 9078–9083. <https://doi.org/10.1073/pnas.1217399110>
- Stevens, A., Bock, M., Ellis, S., LeTissier, P., Bishop, K.N., Yap, M.W., Taylor, W., Stoye, J.P., 2004. Retroviral Capsid Determinants of Fv1 NB and NR Tropism. *Journal of Virology* 78, 9592–9598. <https://doi.org/10.1128/JVI.78.18.9592-9598.2004>
- Stewart, S.A., Dykxhoorn, D.M., Palliser, D., Mizuno, H., Yu, E.Y., An, D.S., Sabatini, D.M., Chen, I.S.Y., Hahn, W.C., Sharp, P.A., Weinberg, R.A., Novina, C.D., 2003. Lentivirus-delivered stable gene silencing by RNAi in primary cells. *RNA* 9, 493–501. <https://doi.org/10.1261/rna.2192803>
- Studamire, B., Goff, S.P., 2008. Host proteins interacting with the Moloney murine leukemia virus integrase: Multiple transcriptional regulators and chromatin binding factors. *Retrovirology* 5, 48. <https://doi.org/10.1186/1742-4690-5-48>
- Stultz, R.D., Cenker, J.J., McDonald, D., 2017. Imaging HIV-1 Genomic DNA from Entry through Productive Infection. *Journal of Virology* 91, e00034-17. <https://doi.org/10.1128/JVI.00034-17>

- Sundquist, W.I., Kräusslich, H.-G., 2012. HIV-1 Assembly, Budding, and Maturation. *Cold Spring Harbor Perspect Med* 2, a006924. <https://doi.org/10.1101/cshperspect.a006924>
- Suzuki, Y., Craigie, R., 2007. The road to chromatin – nuclear entry of retroviruses. *Nat Rev Microbiol* 5, 187–196. <https://doi.org/10.1038/nrmicro1579>
- Telesnitsky, A., Goff, S.P., 1997. Reverse Transcriptase and the Generation of Retroviral DNA, Retroviruses. Cold Spring Harbor Laboratory Press.
- Thorsten Müller, 2021. Imaging of HIV-1 cDNA dynamics in living cells. Combined Faculty of Natural Sciences and Mathematics of the Ruperto Carola University Heidelberg, Heidelberg.
- Thul, P.J., Åkesson, L., Wiking, M., Mahdessian, D., Geladaki, A., Ait Blal, H., Alm, T., Asplund, A., Björk, L., Breckels, L.M., Bäckström, A., Danielsson, F., Fagerberg, L., Fall, J., Gatto, L., Gnann, C., Hober, S., Hjelmare, M., Johansson, F., Lee, S., Lindskog, C., Mulder, J., Mulvey, C.M., Nilsson, P., Oksvold, P., Rockberg, J., Schutten, R., Schwenk, J.M., Sivertsson, Å., Sjöstedt, E., Skogs, M., Stadler, C., Sullivan, D.P., Tegel, H., Winsnes, C., Zhang, C., Zwahlen, M., Mardinoglu, A., Pontén, F., von Feilitzen, K., Lilley, K.S., Uhlén, M., Lundberg, E., 2017. A subcellular map of the human proteome. *Science* 356, eaal3321. <https://doi.org/10.1126/science.aal3321>
- Tobaly-Tapiero, J., Bittoun, P., Lehmann-Che, J., Delelis, O., Giron, M.-L., De Thé, H., Saïb, A., 2008. Chromatin Tethering of Incoming Foamy Virus by the Structural Gag Protein. *Traffic* 9, 1717–1727. <https://doi.org/10.1111/j.1600-0854.2008.00792.x>
- Uchil, P.D., Quinlan, B.D., Chan, W.-T., Luna, J.M., Mothes, W., 2008. TRIM E3 Ligases Interfere with Early and Late Stages of the Retroviral Life Cycle. *PLOS Pathogens* 4, e16. <https://doi.org/10.1371/journal.ppat.0040016>
- Valle-Tenney, R., Opazo, T., Cancino, J., Goff, S.P., Arriagada, G., 2016. Dynein Regulators Are Important for Ecotropic Murine Leukemia Virus Infection. *J Virol* 90, 6896–6905. <https://doi.org/10.1128/JVI.00863-16>
- Van Valen, L., 1973. A new evolutionary law. *Evolutionary theory* 1, 1–30.
- Villanueva, R.A., Jonsson, C.B., Jones, J., Georgiadis, M.M., Roth, M.J., 2003. Differential multimerization of Moloney murine leukemia virus integrase purified under nondenaturing conditions. *Virology* 316, 146–160. [https://doi.org/10.1016/s0042-6822\(03\)00559-2](https://doi.org/10.1016/s0042-6822(03)00559-2)
- Volkman, H.E., Cambier, S., Gray, E.E., Stetson, D.B., 2019. Tight nuclear tethering of cGAS is essential for preventing autoreactivity. *eLife* 8, e47491. <https://doi.org/10.7554/eLife.47491>
- Wallin, M., Ekström, M., Garoff, H., 2005. The fusion-controlling disulfide bond isomerase in retrovirus Env is triggered by protein destabilization. *J Virol* 79, 1678–1685. <https://doi.org/10.1128/JVI.79.3.1678-1685.2005>
- Wanaguru, M., Barry, D.J., Benton, D.J., O'Reilly, N.J., Bishop, K.N., 2018. Murine leukemia virus p12 tethers the capsid-containing pre-integration complex to

- chromatin by binding directly to host nucleosomes in mitosis. *PLoS Pathogens* 14, e1007117. <https://doi.org/10.1371/journal.ppat.1007117>
- Wang, G.Z., Goff, S.P., 2021. Moloney Murine Leukemia Virus p12 Is Required for Histone Loading onto Retroviral DNAs. *J Virol* 95, e0049521. <https://doi.org/10.1128/JVI.00495-21>
- Wang, G.Z., Goff, S.P., 2015. Postentry Restriction of Mason-Pfizer Monkey Virus in Mouse Cells. *Journal of Virology* 89, 2813–2819. <https://doi.org/10.1128/JVI.03051-14>
- Wang, G.Z., Wang, Y., Goff, S.P., 2016. Histones Are Rapidly Loaded onto Unintegrated Retroviral DNAs Soon after Nuclear Entry. *Cell Host & Microbe* 20, 798–809. <https://doi.org/10.1016/j.chom.2016.10.009>
- Weigert, M., Schmidt, U., Boothe, T., Müller, A., Dibrov, A., Jain, A., Wilhelm, B., Schmidt, D., Broaddus, C., Culley, S., Rocha-Martins, M., Segovia-Miranda, F., Norden, C., Henriques, R., Zerial, M., Solimena, M., Rink, J., Tomancak, P., Royer, L., Jug, F., Myers, E.W., 2018. Content-aware image restoration: pushing the limits of fluorescence microscopy. *Nat Methods* 15, 1090–1097. <https://doi.org/10.1038/s41592-018-0216-7>
- Wight, D.J., Boucherit, V.C., Nader, M., Allen, D.J., Taylor, I.A., Bishop, K.N., 2012. The Gammaretroviral p12 protein has multiple domains that function during the early stages of replication. *Retrovirology* 9, 83. <https://doi.org/10.1186/1742-4690-9-83>
- Wight, D.J., Boucherit, V.C., Wanaguru, M., Elis, E., Hirst, E.M.A., Li, W., Ehrlich, M., Bacharach, E., Bishop, K.N., 2014. The N-Terminus of Murine Leukaemia Virus p12 Protein Is Required for Mature Core Stability. *PLoS Pathogens* 10, e1004474. <https://doi.org/10.1371/journal.ppat.1004474>
- Wilens, C.B., Tilton, J.C., Doms, R.W., 2012. HIV: Cell Binding and Entry. *Cold Spring Harb Perspect Med* 2, a006866. <https://doi.org/10.1101/cshperspect.a006866>
- Xu, H., Franks, T., Gibson, G., Huber, K., Rahm, N., Strambio De Castillia, C., Luban, J., Aiken, C., Watkins, S., Sluis-Cremer, N., Ambrose, Z., 2013. Evidence for biphasic uncoating during HIV-1 infection from a novel imaging assay. *Retrovirology* 10, 70. <https://doi.org/10.1186/1742-4690-10-70>
- Yamashita, M., Emerman, M., 2004. Capsid Is a Dominant Determinant of Retrovirus Infectivity in Nondividing Cells. *J Virol* 78, 5670–5678. <https://doi.org/10.1128/JVI.78.11.5670-5678.2004>
- Yan, N., Regalado-Magdos, A.D., Stiggelbout, B., Lee-Kirsch, M.A., Lieberman, J., 2010. The cytosolic exonuclease TREX1 inhibits the innate immune response to human immunodeficiency virus type 1. *Nat Immunol* 11, 1005–1013. <https://doi.org/10.1038/ni.1941>
- Yang, F., Leon, O., Greenfield, N.J., Roth, M.J., 1999. Functional interactions of the HHCC domain of moloney murine leukemia virus integrase revealed by nonoverlapping complementation and zinc-dependent dimerization. *J Virol* 73, 1809–1817. <https://doi.org/10.1128/JVI.73.3.1809-1817.1999>

- Yap, M.W., Nisole, S., Lynch, C., Stoye, J.P., 2004. Trim5α protein restricts both HIV-1 and murine leukemia virus. *Proceedings of the National Academy of Sciences* 101, 10786–10791. <https://doi.org/10.1073/pnas.0402876101>
- Yeager, M., Wilson-Kubalek, E.M., Weiner, S.G., Brown, P.O., Rein, A., 1998. Supramolecular organization of immature and mature murine leukemia virus revealed by electron cryo-microscopy: implications for retroviral assembly mechanisms. *Proc Natl Acad Sci U S A* 95, 7299–7304. <https://doi.org/10.1073/pnas.95.13.7299>
- Yoshii, H., Kamiyama, H., Minematsu, K., Goto, K., Mizota, T., Oishi, K., Katunuma, N., Yamamoto, N., Kubo, Y., 2009. Cathepsin L is required for ecotropic murine leukemia virus infection in NIH3T3 cells. *Virology* 394, 227–234. <https://doi.org/10.1016/j.virol.2009.08.045>
- Yuan, B., Fassati, A., Yueh, A., Goff, S.P., 2002. Characterization of Moloney murine leukemia virus p12 mutants blocked during early events of infection. *J Virol* 76, 10801–10810. <https://doi.org/10.1128/jvi.76.21.10801-10810.2002>
- Yuan, B., Li, X., Goff, S.P., 1999. Mutations altering the moloney murine leukemia virus p12 Gag protein affect virion production and early events of the virus life cycle. *EMBO J* 18, 4700–4710. <https://doi.org/10.1093/emboj/18.17.4700>
- Yueh, A., Goff, S.P., 2003. Phosphorylated serine residues and an arginine-rich domain of the moloney murine leukemia virus p12 protein are required for early events of viral infection. *J Virol* 77, 1820–1829. <https://doi.org/10.1128/jvi.77.3.1820-1829.2003>
- Zerbini, F.M., Kitajima, E.W., 2022. From Contagium vivum fluidum to Riboviria: A Tobacco Mosaic Virus-Centric History of Virus Taxonomy. *Biomolecules* 12, 1363. <https://doi.org/10.3390/biom12101363>
- Zila, V., Margiotta, E., Turoňová, B., Müller, T.G., Zimmerli, C.E., Mattei, S., Allegretti, M., Börner, K., Rada, J., Müller, B., Lusic, M., Kräusslich, H.-G., Beck, M., 2021. Cone-shaped HIV-1 capsids are transported through intact nuclear pores. *Cell* 184, 1032-1046.e18. <https://doi.org/10.1016/j.cell.2021.01.025>
- Zila, V., Müller, T.G., Laketa, V., Müller, B., Kräusslich, H.-G., 2019. Analysis of CA Content and CPSF6 Dependence of Early HIV-1 Replication Complexes in SupT1-R5 Cells. *mBio* 10, e02501-19. <https://doi.org/10.1128/mBio.02501-19>
- Zobell, C.E., Rittenberg, S.C., 2011. Microbiology by numbers. *Nat Rev Microbiol* 9, 628–628. <https://doi.org/10.1038/nrmicro2644>

## 8 Personal contribution to data acquisition / Assessment and Personal Publications

---

This project was conducted in the context of the SPP1923: "Innate sensing and Restriction of Retroviruses" DFG Priority Program. The data acquisition and analysis making up the majority of the main results for this dissertation was conducted by me, with certain exceptions that can be seen below.

The isolation and immortalization of the MEF wild-type and TREX1 KO cells were done entirely by our collaborating partners and were received as a gift. The work with mice and isolation of embryos were performed by Dr. Bettina Stop from University Hospital Heidelberg, Fackler research group. The MEF isolation from embryos and immortalization was done by Dr. Bruno Galy and Dr. Michael Bonadonna from the German Cancer Research Center, Galy research group. The wild-type and knockout status was confirmed by immunoblot analysis performed by Dr. Julia Welsch from University Hospital Heidelberg, Ruggieri research group. The organization and driving the progress of the immortalized MEF cell lines was done by group leader Dr. Alessia Ruggieri and Dr. Julia Welsch.

The visualization of MLV DNA using hybridizing probes were done in collaboration with Dr. Mia Stanic from University Hospital Heidelberg, Lusic research group. I have prepared the infected samples, whereas Dr. Mia Stanic generated the hybridizing probes and performed the FISH staining. The data acquisition and visualization were performed by me.

The ANCHOR technology was provided by NeoVirTech. For generation of ANCH containing viruses the ANCH3 sequence was initially amplified from pANCH3 provided by NeoVirTech. In addition, to create lentiviral transfer vectors with eGFP-OR3, the coding sequence was initially amplified from peGFP-OR3 provided by NeoVirTech.

The acquisition of the live imaging data with the SDCM (*cf.* 3.3.7.- *cf.* 3.3.11, Figure 25-31) was performed by Dr. Vibor Laketa from the Infectious Diseases Imaging Platform (IDIP), whereas the deconvolution of those images was performed equally by me and a student Charlotte Kamm. The analysis, data visualization and graphical representation of the data was performed solely by me.

The experiments quantifying reverse transcription products using ddPCR (*cf.* 3.3.7., Figure 25C) were performed equally by myself and our technical assistant Vera Sonntag-Buck (University Hospital Heidelberg, Kräusslich research group). The acquisitions, analysis and visualization of the data was performed by me.

Assistance in design of cloning strategies for the generated plasmids in this dissertation was given by Dr. Thorsten Müller from University Hospital Heidelberg, Kräusslich research group. Assistance in design of transduction and selection protocol for the generation of eGFP.OR3 and eBFP2.mLMNB1 expressing cell lines was also provided by Dr. Thorsten Müller.

Manuscript consisting of partial results from this thesis is in preparation but has not yet been finalized and submitted to be published.

## 9 Appendix

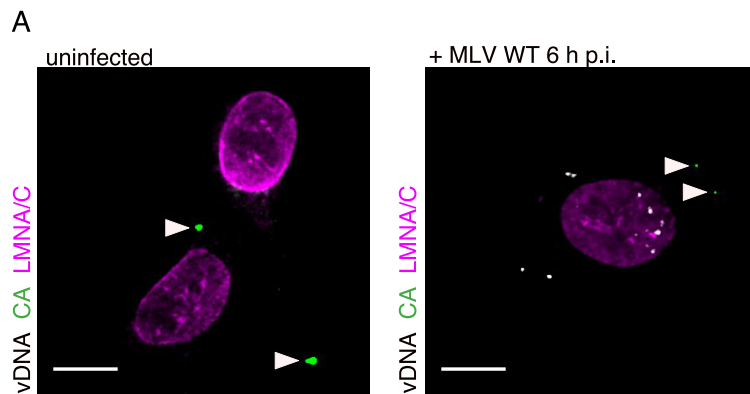


**Figure 35. IF staining of MLV CA under FISH hybridization conditions.** A. SC-1 cells were uninfected or infected with MLV wild-type (1000  $\mu$ U RT/cell) for 6h before fixation and FISH staining. The cells were also IF stained with antibodies raised against LMNA/C and CA. The hybridization probe generation and FISH staining were done by Mia Stanic (University Hospital Heidelberg). Scale bars: 10 $\mu$ m. White arrows point towards CA signals. Representative images from one experiment are shown.

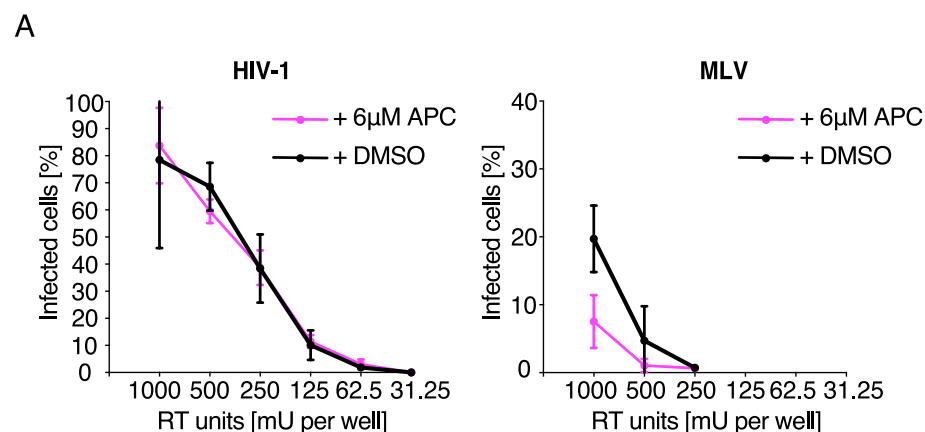


**Figure 36. Aphidicolin treatment prevents MLV, but not HIV-1 infection in SC-1 cells.** A. Infection of SC-1 with VSV-G pseudotyped HIV-1 and MLV treated with either DMSO or aphidicolin (6 $\mu$ M). The cells were treated prior and during infection with aphidicolin or DMSO. Cells were fixed, immunostained against MLV or HIV-1 CA and imaged after 48 h p.i. HIV-1 virus particles and infection followed by fixation performed in S3 was done by David Bejarano (University Hospital Heidelberg). The number of infected cells was quantified based on detected CA signal and total number of nuclei, based on the Hoechst stain, counted manually in Fiji. The graph shows mean values and SD from 6 FOV performed in one independent experiment.

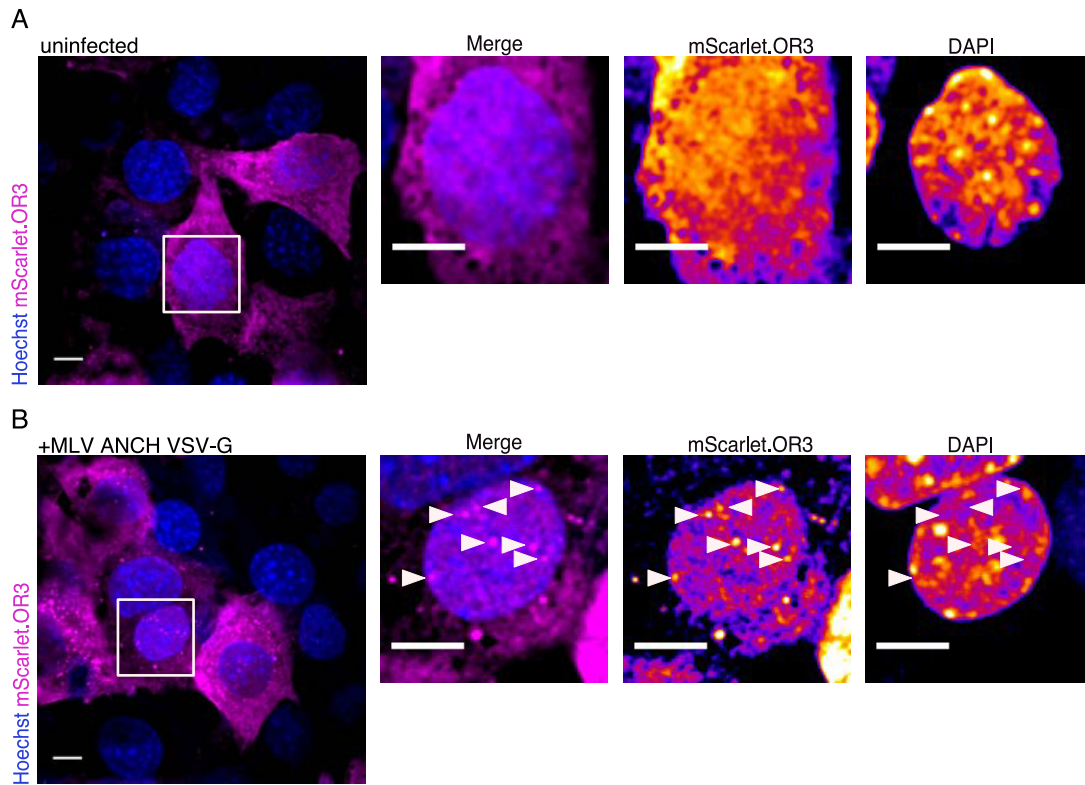


Figure 37. Visualization of MLV cDNA in infected murine cells expressing mScarlet.OR3. A-B. MEF expressing mScarlet.OR3 were infected with MLV ANCH VSV-G (822  $\mu$ U RT/cell). The cells were fixed, stained with Hoechst, and imaged by SDCM after 24 h p.i. Scale bars: 10  $\mu$ m. Representative MIPs are shown from the overview and enlargements as single z-slices. White arrows point to a detected eGFP.OR3 foci.

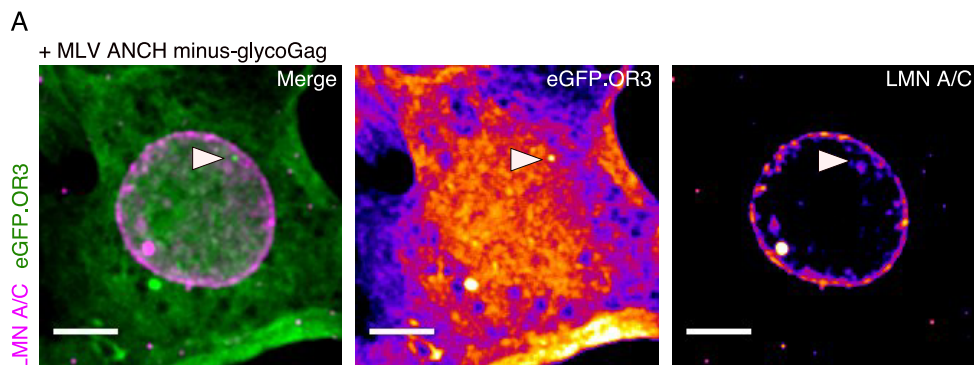


Figure 38. Infection with MLV ANCH minus-glycoGag induces formation of nuclear OR3 signals. A. MEF expressing eGFP.OR3 eBFP2.mLMNB1 were infected with MLV ANCH -gg VSV-G (1266  $\mu$ U RT/cell). The cells were fixed and imaged by SDCM after 72 h p.i. Scale bars: 10  $\mu$ m. Representative z-slice images are shown from one performed independent experiment.

## 10 Acknowledgments

---

Primarily, I would like to thank Prof. Dr. med. Dr. h. c. Hans-Georg Kräusslich for the opportunity to work on an exciting project with the freedom to develop and pursue different ideas. Moreover, the scientific guidance as well the encouragement to work independently and take responsibility for data presentation was highly appreciated. Due to your supervision, I have improved drastically as a scientist that is able to drive scientific ideas to completion and discuss acquired data in a critical way. Looking back on the last 6 years I can say that I have also grown on a personal level, which would have not been possible without the support of Hans-Georg!

I would also like to thank my TAC members and potential reviewers of my thesis for their guidance during the last years. I am grateful for the support of Dr. Alessia Ruggieri for allowing me to attend her lab meetings and the fruitful collaborations, which without I would have not been able to investigate capsid mutants in immunocompetent cell lines. I am also thankful for Prof. Dr Friedrich Frischknecht for joining my TAC committee on a short notice and agreeing to possibly be my second reviewer of this dissertation. Moreover, I would like to thank Prof. Dr. Stefan Bauer for taking the time to travel from Marburg to Heidelberg to discuss the progress of my project as well as agreeing to possibly be my third reviewer. Additionally, I would like to give special thanks to Prof. Dr. Barbara Müller for teaching me how to write and present my data in posters and presentations for conferences. She also provided valuable advice in choosing the right directions to pursue in this project. Of note, I would like to thank Dr. Vibor Laketa for technical support and incredible insight in scientific discussions. I appreciate his positive attitude and scientific curiosity which made me evaluate and rethink how I conduct my experiments and understand my data. This thesis gained value by his collaboration and helping me acquire data with the SDCM for this thesis.

I was lucky to work with colleagues that I can now call friends. I highly value the mental and scientific support of Thorsten Müller, Djordje Salaj, Sandra Schifferdecker, Mia Stanic, David Bejarano and honorary colleague Maike Petersen. Thank you for the coffee breaks, birthday parties, every shared glass of wine together. Most importantly

thank you for providing me with good advice when I was discouraged and helping me overcome many obstacles in my personal and professional life. I am very humbled that the last few years of work are finally leading to a doctoral dissertation and degree, but I am even more grateful for the meaningful human contacts I made. Much love and thanks to Anja, Andre, and Ashley for being my partners in crime and offering a helping hand and ear to listen when needed.

Finally, I would like to dedicate this dissertation to my parents Milosh and Natasha Naumoski, sister Teona Naumoska and my recently deceased grandmother Zorica Vujic, which is dearly missed. Thank you for always being there to give me support and motivation to keep going. I would not be who I am and where I am without them.

## 11 Eidesstattliche Versicherung (Affidavit)

---

1. Bei der eingereichten Dissertation zu dem Thema "Imaging of MLV cDNA dynamics and replication in living cells" handelt es sich um meine eigenständig erbrachte Leistung.

2. Ich habe nur die angegebenen Quellen und Hilfsmittel benutzt und mich keiner unzulässigen Hilfe Dritter bedient. Insbesondere habe ich wörtlich oder sinngemäß aus anderen Werken übernommene Inhalte als solche kenntlich gemacht.

3. Die Arbeit oder Teile davon habe ich bislang nicht an einer Hochschule des In- oder Auslands als Bestandteil einer Prüfungs- oder Qualifikationsleistung vorgelegt.

4. Die Richtigkeit der vorstehenden Erklärungen bestätige ich.

5. Die Bedeutung der eidesstattlichen Versicherung und die strafrechtlichen Folgen einer unrichtigen oder unvollständigen eidesstattlichen Versicherung sind mir bekannt. Ich versichere an Eides statt, dass ich nach bestem Wissen die reine Wahrheit erkläre und nichts verschwiegen habe.

Place, Date

Heidelberg,

doctoral candidate's signature